12-9-2020 1:30 PM

Coordination and Reactivity of a Structurally Responsive Phosphine-1-Azallyl Ligand

Meagan Kindervater, *The University of Western Ontario*

Supervisor: Blacquiere, Johanna M., *The University of Western Ontario*

A thesis submitted in partial fulfillment of the requirements for the Master of Science degree in Chemistry

Abstract

The reactivity and coordination of a phosphine-1-azaallyl (P^AzA) ligand was explored using palladium (Pd) and ruthenium (Ru) complexes. Small molecules, H_2, O_2, and organic acids were added to a Pd(II) dimer to explore small molecule activation with a complex bearing a structurally responsive ligand. Notably, the 1-azaallyl moiety of a Pd(II) dimer was proton-responsive toward H_2 and organic acids may be harnessed under catalytic conditions. The possible coordination modes of the P^AzA ligand were further explored by synthesising a Ru-P^AzA complex. The compound was proposed to exist in an equilibrium of three complexes that stabilise the Ru-center, suggesting a coordination site is easily accessible by a substrate. Preliminary experiments with pyridine or phenylacetylene and the Ru-P^AzA complex indicated a coordination site was accessible within seconds. Notably, reactivity studies suggested the Ru-P^AzA complex could be an active catalyst for alkyne cyclisation.

Key Terms:

Palladium; ruthenium; structurally responsive ligand; homogenous catalysis; small molecule activation; 1-azaallyl; phosphine-1-azaallyl

Summary for Lay Audience:

Catalysis describes the process of a compound (i.e., a catalyst) speeding up the rate of a chemical reaction. To do this, a catalyst must be highly reactive under the right conditions to facilitate a specific chemical reaction. Ideally, a catalyst can cleanly synthesise a product repeatedly, over long periods of time. This can be difficult to achieve for all catalysts because catalysts can decompose. Sometimes before the desired chemical transformation starts, a fast side reaction(s) can occur that renders the catalyst inactive. When this happens the amount of product achieved could be reduced or none observed. Chemists have thus been exploring methods of limiting catalyst decomposition throughout the years. One notable method has been the addition of an organic functionality to a metal to promote reactivity and/or stabilise the metal throughout the catalytic cycle. The main goal of my study was to expand upon such research; to address the issue of catalyst decomposition through the addition of a novel organic functionality to a metal that has been proposed to reversibly stabilise a metal centre. If the metal center was only partially and reversibly stabilised under catalytic conditions this could prevent undesired side reactions that lead to catalyst decomposition, while still keeping the catalyst reactive. To study this, two metal-organic compounds were explored that contained a novel partially stabilising organic functionality, nicknamed "P^AzA". Specifically, a sought-after ruthenium-P^AzA compound was made cleanly for the first time. The synthesis of this compound suggested the P^AzA was able to partially and reversibly stabilise ruthenium readily at room temperature. Additionally, the preliminary chemical reactivity of the ruthenium- and palladium-P^AzA compounds were explored to understand the implications of the P^AzA group on a chemical transformation. These reactivity studies suggested that the P^AzA group was able to promote desirable reactivity with some organic substrates (i.e., alkynes) and that acidic environments may be exploited for catalysis.

Co-authorship Statement

All chapters were written by Meagan Kindervater and were edited by Johanna Blacquiere.

All experimental work was conducted by Meagan Kindervater, with the exception of crystal data collection and structure refinement, which were performed and written by Paul Boyle.

Chapters and experimental work were reviewed and edited by committee members (Richard Puddephatt, Kim Baines, and Sheila MacFie).

Acknowledgements

Graduate studies have challenged me both professionally and personally throughout the last two years. Without the support and mentorship of Dr. Johanna Blacquiere I'm confident the world of research would have ended much earlier for me. Her perseverance and positive attitude were and always will be appreciated, so, thank you.

To my lab mates; Ben, Sofia, Devon, Matt, Nick, Kyle, and the Kerr boys (David and Shane); It's been a real pleasure to know all of you and to share a few beers, all the best to you in the future, keep me updated! In particular, big thank you to Ben for welcoming me with open arms and showing me the ropes. Devon and Matt I appreciate all the rides and I hope my NMR tubes found their way to you. Leanne, thank you for being a great friend the past two years.

Big thank you to Mat Willans for running a fine NMR facility, Paul Boyle for crystallography work, and to Kristina Juric for mass spec analysis.

To my friends and family, thank you for listening to me talk about stuff you did not understand for two years.

Table of Contents

List of Abbreviations

Atm	Standard atmosphere
CMD	Concerted metalation deprotonation
COD	1,5-Cyclooctadiene
COSY	Correlation spectroscopy
Cp*	1,2,3,4,5-Pentamethylcyclopentadienide
DME	1,2-Dimethoxyethane
DMT	Dimethyl terephthalate
h	Hours
H[DMF]	Protonated dimethylformamide
HMBC	Heteronuclear multiple bond correlation
HSQC	Heteronuclear single-quantum correlation
IR	Infared
MALDI	Matrix assisted laser desorption ionization
min	Minutes
MS	Mass spectrometry
NMR	Nuclear magnetic resonance
P^AzA	Phosphine-1-azaallyl
P^I	Phosphine-imine
py	Pyridine
s	Seconds
SRL	Structurally responsive ligand
TOF	Turnover frequency
TON	Turnover number

List of Tables

List of Figures

List of Schemes

Compound Guide

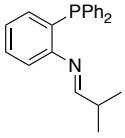

H[**L1**]

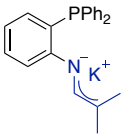

K[**L1**]

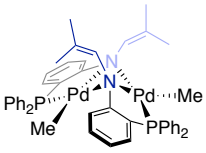

1

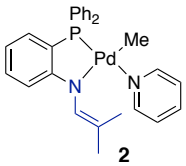

2

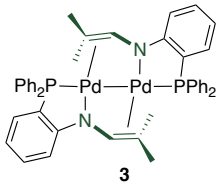

3

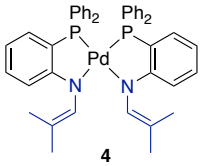

4

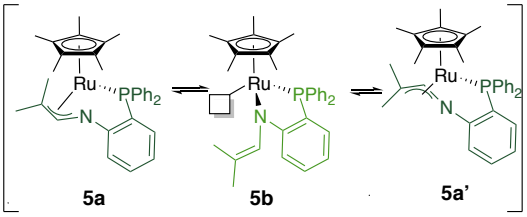

5a **5b** **5a'**

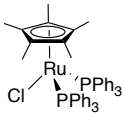

6

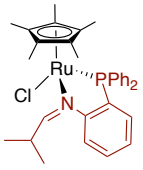

7

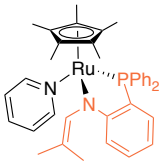

8

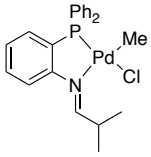

9

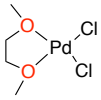

10

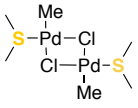

11

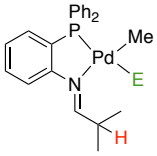

12

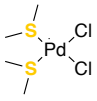

13

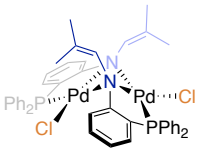

14

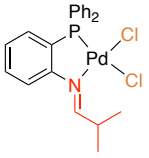

15

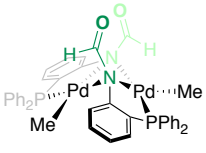

proposed structure
16a

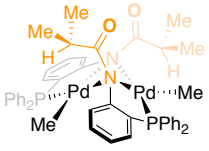

proposed structure
16b

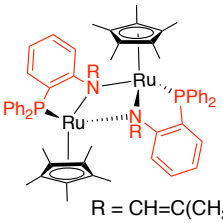

R = $CH{=}C(CH_3)_2$
17

1 Introduction

1.1 Homogenous Catalysis

Catalysts are advantageous in many chemical processes as they increase the rate of a chemical reaction by lowering the energy barrier of an chemical transformation without themselves being consumed.[1,2] Catalysts are required in small (sub-stoichiometric) amounts because they are regenerated during a catalytic cycle.[2] Two main types of catalysis are defined as homogenous and heterogenous and these terms signify the phase of the catalyst with respect to the reactants/products. A homogenous catalyst is in the same phase (e.g., liquid) as the reactants, whereas a heterogenous catalyst is in a separate phase (e.g., solid and liquid). Typically, heterogenous catalyst are used in industry for large-scale (e.g., > Mkg) processes in part because they are more easily separated from the product.[3,4] Homogenous catalysts have two main advantages over heterogenous catalysts, their selectivity and improved ease of mechanistic analysis. Improved selectivity of homogenous catalysts has been typically due to the influence of ligands that are bound to the metal by altering the electron density and steric pocket of that metal.[5] Different ligands possess different electronic and steric properties that can cause different selectivity and activity of the resulting complex. Notably, the ability to elucidate the steps of the catalytic cycle (or mechanism) has permitted the optimisation of homogenous catalysts for higher selectivity and faster activity by altering the steric and electronic properties of the ligand in favourable ways.[4] For example, Ru is widely known for its ability to perform olefin metathesis, a 2+2 transformation of two alkenes.[6] The knowledge of the mechanistic steps has led to immense catalyst improvement over the years through ligand design. A notable example of this is the faster initiation rates observed of Grubbs II compared to the first-generation Grubbs catalyst (Scheme 1.1).[7] Computational studies revealed that there was an increased affinity of the H_2IMes-substituted Ru center for π-acidic olefins relative to σ-donating phosphines that resulted in the increased activity observed. Replacing a PCy_3 ligand (Grubbs I) with a bulky *N*-heterocyclic carbene (H_2IMes) ligand (Grubbs II) can result in improved catalyst activity while maintaining a high functional group tolerance and thermal stability.

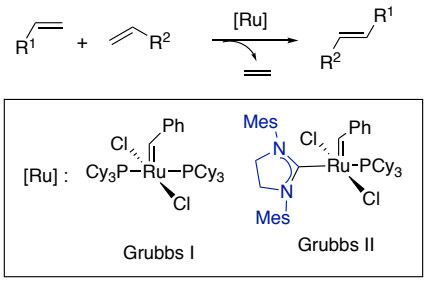

Scheme 1.1: Generic scheme of olefin metathesis using a Ru catalyst Grubbs I or II.[7]

In homogenous catalysis, a pre-catalyst (ML_4) typically undergoes a dissociative process to lose a ligand to become the active catalyst (ML_3; Scheme 1.2).[2] A substrate (Sub) can then bind to the open coordination site of the active catalyst and be converted to product (Prod). These active catalysts are typically unstable in solution as they are extremely reactive, which often can lead to decomposition product(s), limiting a catalyst's lifetime. Decomposition of an active catalyst would likely be caused by fast undesired side reactivity that could occur before substrate coordination. The mechanism of catalyst decomposition is highly case dependent and ligand design can aid in increasing catalyst lifetime.

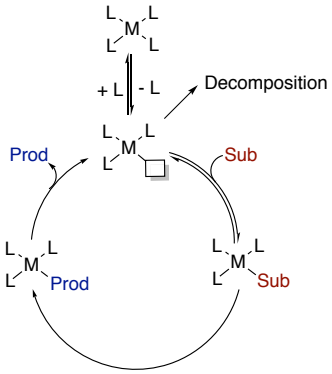

Scheme 1.2: Generic catalytic cycle of a homogenous catalyst.[2]

1.2 Small Molecule Activation

Activation of small molecules is an attractive area of research due their potential use as synthons (N_2, O_2, H_2O) in fine chemical synthesis, their environmental impact (CO_2), and their energy storage potential (H_2).[8-13] In particular, small molecule activation of O_2 for use as a stochiometric oxidant in catalysis still faces challenges of low turnover numbers

(TON) and/or turnover frequencies (TOF) that limit applications.[8] One strategy to improve small molecule activation has been harnessing the influence of ligand design to control reactivity of organometallic compounds and examples of such will be discussed within this section.

1.2.1 Dioxygen Activation by Organometallic Pd Species

Molecular oxygen (O_2) is the ideal oxidant since it is abundantly available, inexpensive, and on reduction it is converted to environmentally benign by-products (i.e., H_2O_2 or H_2O).[9,13-15] However, overoxidation, low selectivity, and low TONs are issues with utilizing O_2 as the sole oxidant in catalysis.[14,16] Combining the oxidizing power of O_2 and the selectivity of organometallic compounds could circumvent these issues. Molecular oxygen is thermodynamically capable of oxidizing reduced Pd under many conditions, but competitive oxidation of bound ligands has been an issue.[16,17] Regardless, Pd catalysts with O_2 as the oxidant have found success in C-H functionalization, alcohol oxidation, and oxidative C-C, C-O, or C-N coupling.[15-20] Advancements in Pd/O_2 systems have allowed for the use of O_2 as the sole oxidant to development of new ligands that promote aerobic oxidation.[16,17,20,21] An example is the Pd(II) catalyzed asymmetric oxidative annulation of *N*-alkoxy aryl amides and 1,3-dienes (generic representation in Scheme 1.3).[19] Under control conditions $Pd(OAc)_2$ was used as the catalyst with O_2 as the oxidant and a poor yield of product was observed (7%). Upon the addition of an N-based bulky ligand to the Pd catalyst an improved yield of 88% was gained. A major role of the ligand in this Pd aerobic oxidation reaction was to stabilise the Pd(0) catalysis intermediate, as without a ligand present Pd black was produced and a poor product yield was observed (7%). Additionally, by systematic ligand design and increased stereocontrol (due to bulky *t*-Butyl group), improved enantioselectivity (likely caused by the electron donating OMe group) was achieved. This Pd(II) catalysis study highlights how organometallic Pd(II) complexes and ligand design can greatly improve product yield.

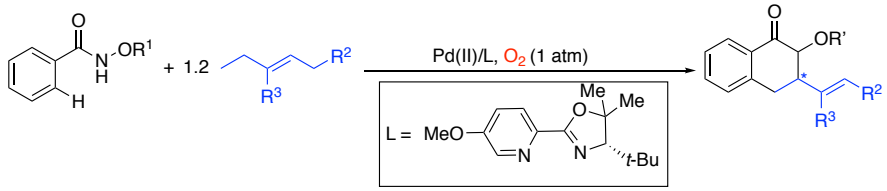

Scheme 1.3: Generic representation of a Pd(II)-catalyzed asymmetric oxidative annulation of *N*-alkoxyheteroaryl amides and 1,3-dienes.[19]

One main type of O_2 activation is described as an oxidase pathway. Oxidase reactions are more common and are pathways where O_2 regenerates the active catalyst by oxidation of Pd(0) to Pd(II) or by insertion into a Pd(II)-H bond to generate H_2O_2 or H_2O (Scheme 1.4A/B).[15,16,20,21] Three possible mechanistic pathways have been found and the operative route was always highly case dependent: (1) a mononuclear redox pathway involving Pd(0)/Pd(II) (Scheme 1.4C),[15,20,21] (2) a pathway involving a binuclear Pd(II)-Pd(II) complex with bridging hydroxyl groups (Scheme 1.4D),[16] or (3) the redox neutral O_2 insertion into Pd-H bond (Scheme 1.4E).[15,20,21] Mechanistic pathways (1) and (3) are the two main pathways for most Pd/O_2 catalytic systems.[15,20,21]

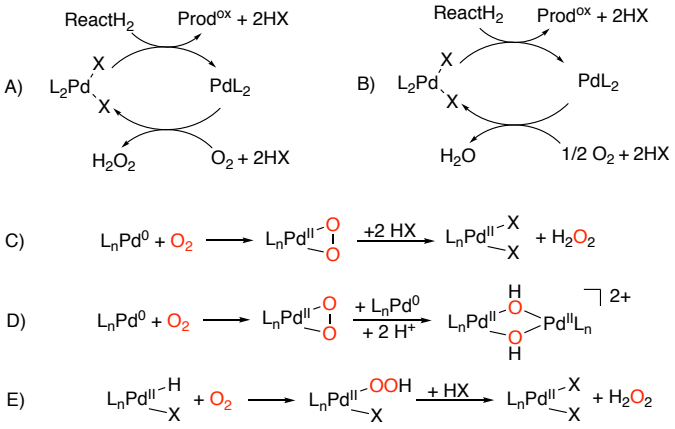

Scheme 1.4: Two reaction pathways in which O_2 oxidizes Pd(0) to Pd(II) in oxidase reactivity where O_2 is converted to environmentally benign products H_2O_2 (A)[15] or H_2O (B)[16,20]; Three possible mechanistic pathways for the oxidation of Pd by O_2 in oxidase type pathways: Pd(0)/Pd(II) redox cycle (C);[15,20,21] resulting in a Pd(II)-Pd(II) (D);[9] and insertion of O_2 into a Pd(II)-H bond (E).[15,20,21]

The direct oxidation of Pd(II) species are not common in comparison to aerobic C-H bond oxidations and only a few examples of clean O_2 reactivity towards Pd(II)-Me species are prevalent in the literature.[18,22-26] A notable example is the Pd(II)-Me species bearing a bulky N-based ligand reported by Vedernikov *et al* (Scheme 1.5A).[22,23] This

complex underwent the photochemical aerobic oxidation to form desirable products ethane (Me-Me), methanol (MeOH) or methylhydroperoxide (MeOOH). At high pH (14.0) the production of MeOH was favoured (54% selectivity); whereas, at low pH the release of ethane was preferred (94% selectivity). A minor reaction mechanism pathway was proposed to involve the insertion of O_2 into Pd-C bond of a photochemically excited Pd complex. When this mechanism was at play the O-source of MeOOH was proposed to be solely from O_2, and one equivalent of produced MeOH contained an O-atom from O_2. This type of O_2 reactivity is called an oxygenase pathway.[24] Oxygenase pathways of O_2 activation are processes where O_2 was both the oxidant and the O-atom source that was added to the substrate. The insertion of O_2 into Pd-R bonds to form alkyl peroxide or alkoxide complexes would allow for the direct functionalization of hydrocarbons by O_2.[14,25] In 2009 Goldberg published the first example of O_2 insertion via a proposed radical chain mechanism into a Pd-Me bond (**A**; Scheme 1.5B).[18] Since then, clean O_2 insertions into Pd(II)-Me bonds have been performed under different conditions and intermediates have been proposed to form by different mechanisms,[24,26] providing no distinct reactivity trend between Pd(II)-Me complexes and O_2.

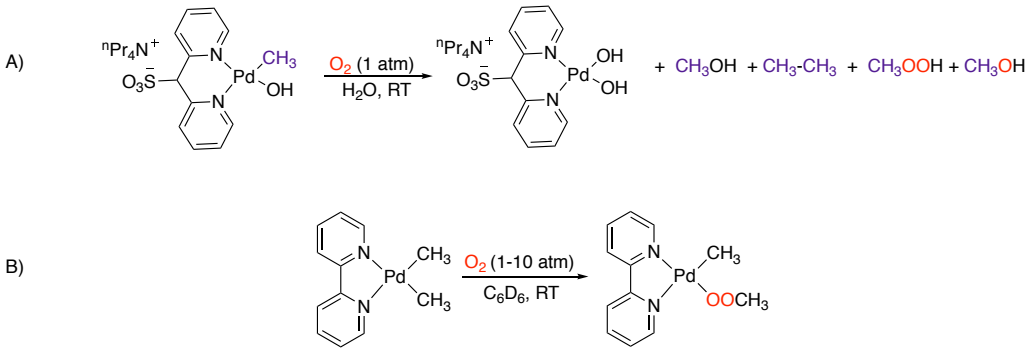

Scheme 1.5: The aerobic oxidative C-C bond formation from O_2 and Pd(II) reported by Vedernikov *et al* (A)[22] and the first example of O_2 insertion into a Pd(II)-Me bond reported by Goldberg *et al* (B).[18]

Bimetallic catalysis has gained interest by inorganic and organometallic chemists in part because of the unique substrate activation that can be achieved with multiple metal centers.[27-32] Bimetallic complexes have been shown to activate a variety of bonds, specifically Pd bimetallic complexes can activate C-H bonds or O_2.[28-32] An example is the Pd(II) dimer (Pd_2hpp_4; where hppH = hexahydro-2*H*-pyridmido[1,2-*a*]pyrimidine) that promoted oxygenase-type reactivity in the α-hydroxylation of carbonyls with O_2 (Scheme

1.6).[31] NMR spectroscopy studies with labelled $^{18}O_2$ confirmed oxygen insertion and further mechanistic studies proposed a Pd(III)-Pd(III) intermediate was involved in the reaction. Notably, Pd dimers found in a bent structure have greater metal-metal interactions than edge-faced linear dimers and would more likely involve a binuclear pathway and could lead to interesting and effective O_2 activation.[33,34]

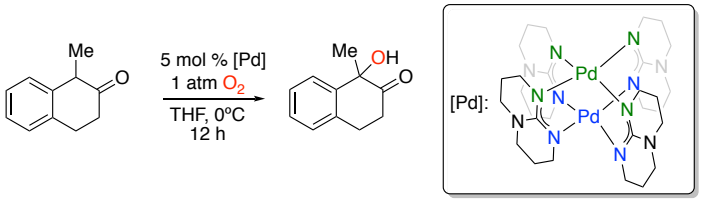

Scheme 1.6: Bimetallic Pd(II) catalyzed α-hydroxylation of carbonyls with O_2.[31]

1.2.2 Dihydrogen Activation by Organometallic Pd Species

Molecular hydrogen (H_2) has applications in energy storage, hydrogenation, hydrosulfurization, and hydrodenitrogenation reactions.[35,36] Harnessing H_2 can be difficult due to the strong σ-interaction between the two hydrogen atoms ($\Delta H°_{298K}$ = 104 kcal/mol).[35-37] Organometallic catalysts can activate this bond via d to σ^* back donation in two main ways: 1) homolytic cleavage, where H_2 is subject to oxidative addition onto the metal or 2) heterolytic cleavage, where the metal accepts the hydride and a Brønsted basic ligand(s) abstracts the proton. Experimental examples of Pd(II) performing homolytic cleavages of H_2 were not found in the literature, but one DFT study included an example of a unique Lewis-acid bearing Pd(0) model complex undergoing oxidative addition of H_2.[38] The DFT calculations showed that H_2 was activated by Pd and boron stabilised the now Pd(II) metal center (Scheme 1.7A). This was followed by a one proton transfer to boron and the other to the trans position on Pd to form a stabilized Pd(II) complex. In comparison, examples of H_2 heterolytic cleavage by Pd(II) for hydrogenation reactions (e.g., hydrogenation of alkenes and alkynes) are prevalent in the literature.[39-43] The specific example included demonstrates the heterolytic cleavage of H_2, where after activation, a pendent basic oxygen abstracted a proton and the Pd accepted a hydride through a four membered transition state (Scheme 1.7B).[44]

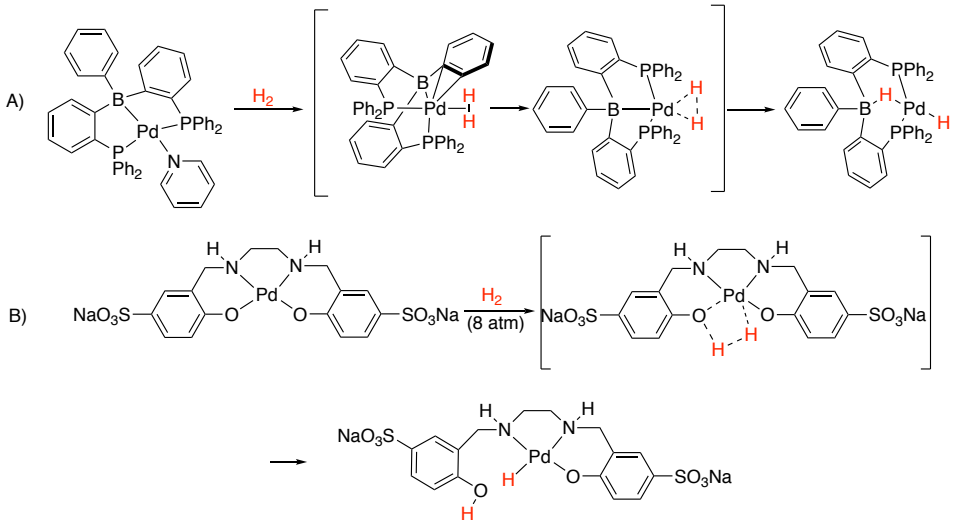

Scheme 1.7: A) A DFT study of Pd(0) complex that undergoes homolytic cleavage of H_2.[38] B) An example of the heterolytic cleavage of H_2 via a Pd(II) homogenous catalyst for the hydrogenation and redox isomerization of allylic alcohols.[44]

1.3 Metal Ligand Cooperativity

Metal-ligand cooperative (MLC) complexes contain a ligand with a cooperative group that directly promotes a chemical transformation.[45-49] The cooperative group on a ligand can assist the metal centre in performing a chemical transformation in different ways depending on the moiety. The assistance provided by the ligand of MLC complexes can often result in improved activity or selectivity over traditional metal complexes.

1.3.1 Proton-Transfer MLC

A common subset of MLC complexes are proton-shuttling complexes,[46,49-52] where a basic or acidic site on the ligand facilitates rapid protonation or deprotonation.[49,53,54] A notable example of a proton-shuttling MLC complex is the Fe complex, **A** in Scheme 1.8.[55] This complex was inspired by the active site of the hydrogenase enzyme and was designed with a basic pendent amine for activation of H_2. Complex **A** contained three notable functional components: 1) a diiron core; 2) an amine base on the bridging dithiolate ligand; and 3) a ferrocene group to act as a one-electron redox module. Reactivity of **A** with H_2 occurred over 1 h at room temperature and resulted in an Fe-H species, which was confirmed with D_2 studies. The synthesis of the Fe-H complex was promoted by MLC in

two ways: (1) a basic pendent amine that accepted a proton from H_2 and (2) a ferrocene ligand that acted as a redox acceptor.

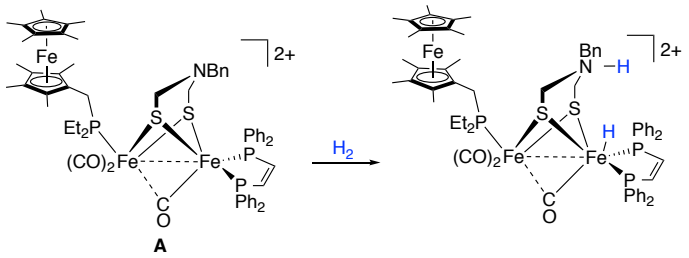

Scheme 1.8: Reactivity of a Fe complex (**A**) with H_2.[55] Where: Bn = CH_2Ph

1.3.2 Structurally Responsive Ligands

Structurally responsive ligands (SRLs) are a specific subset of MLC's. SRLs can be defined as ligands that reversibly alter their coordination mode on a metal center, through changes in denticity (number of donor groups bonded to a metal on a given ligand; κ) or hapticity (number of donor groups from a delocalized π system bonded to a metal; η).[56] A decrease in coordination number of a metal complex from changes in denticity or hapticity can open a coordination site on a metal to generate a low-coordinate reactive intermediate (Scheme 1.9A).[2,57,58] The reactive low-coordinate intermediate can be stabilized through an increase in coordination number by changing the binding mode of the SRL (i.e., changes denticity or hapticity) or binding of a Lewis base (or substrate). SRLs can aid in faster initiation rates (e.g., the indenyl effect) and could increase catalyst lifetime by preventing decomposition of the active low-coordinate catalyst. Furthermore, certain SRLs can promote reaction steps on the catalytic cycle in addition to substitution reactions. A notable example is the carboxylate ligand in Pd-catalyzed concerted metalation deprotonation (CMD) C-H activation (Scheme 1.9B).[59] The Brønsted basic pendent oxygen accepted a proton from an Ar ring, causing a change in carboxylate ligand coordination mode from κ^2-OO to κ^1-O, facilitating the C-H activation step observed.

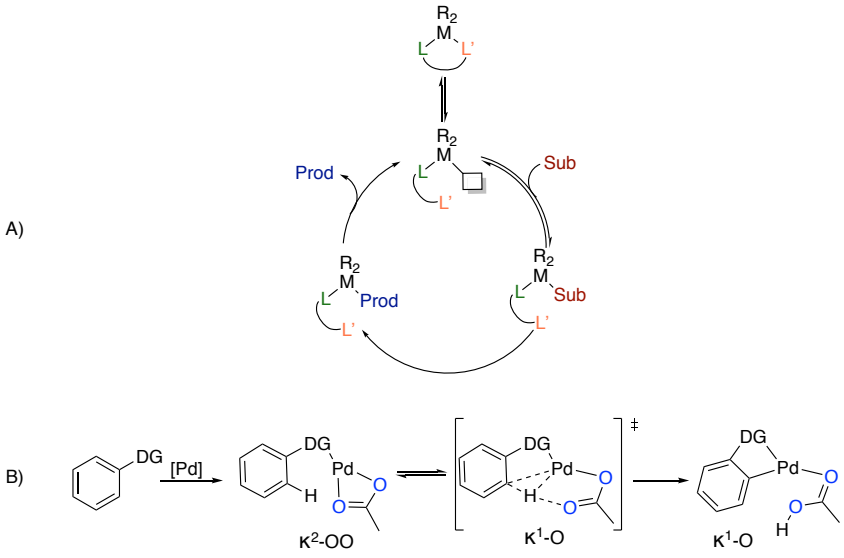

Scheme 1.9: A) Generic catalytic cycle involving an SRL.[2,57,58] B) General Pd-catalyzed C-H activation promoted by κ^2-OO to κ^1-O coordination change (DG = Directing Group).[59]

1.4.1 Structurally Responsive Ligands in Fundamental Reactions

Metal-ligand interactions have captivated the interest of synthetic inorganic and organometallic chemists as a means to develop new avenues of small molecule activation.[60] There are a number of ways that metals and ligands can cooperate to activate a host of small molecules and this section will highlight a few examples.

A non-SRL complex, Pd(OH)($^{t\text{Bu}}$PCP) ($^{t\text{Bu}}$PCP = 2,6-$(CH_2P^tBu_2)_2$), afforded Pd(O_2COH)($^{t\text{Bu}}$PCP) and Pd(H)($^{t\text{Bu}}$PCP) complexes following exposure to CO_2 and H_2, respectively.[61] Goldberg *et al* were interested in adding a structurally responsive attribute to the Pd complex to assess the implications on CO_2 and H_2 activation. The neutral ligand $^{t\text{Bu}}$PCO ($^{t\text{Bu}}$PCO = 2-$(CH_2P^tBu_2)$-6-$(CH_2OCH_3)C_6H_3$) was synthesised to contain a weakly donating ether arm. Coordination to Pd resulted in complex **B** where the $^{t\text{Bu}}$PCO ligand demonstrated a tridentate coordination mode (Scheme 1.10A/B). Upon exposure of **B** to CO_2, two new Pd compounds **C** and **D** were observed (Scheme 1.10A).[61] Goldberg *et al* proposed that first insertion of CO_2 into the Pd-OH bond occurred to give **C** where the $^{t\text{Bu}}$PCO ligand was in a tridentate coordination mode, identical to what was observed with non-SRL Pd complex (Pd(OH)($^{t\text{Bu}}$PCP)). In the Pd-$^{t\text{Bu}}$PCO system the Pd(II) dimer (**D**) was also observed as a result of the dissociation of the ether-linked donor group resulting in changes in $^{t\text{Bu}}$PCO ligand coordination mode from tridentate to bidentate. This suggested

that dimerization was possible due to the structural responsive nature of the $^{t\text{Bu}}$PCO ligand. Exposure of **B** to H_2 resulted in heterolytic cleavage of H_2 to yield a Pd(0) product (**E**; Scheme 1.10B). This likely occurred through dissociation of the ether-linked donor and coordination of H_2 followed by heterolytic cleavage of H_2 via an internal electrophilic substitution mechanism. After heterolytic cleavage of H_2 by **B**, water was released and reductive elimination of the Pd-hydride species yielded the observed product Pd(0) product, **E**. Changing one donor group in the $^{t\text{Bu}}$PCP ligand to a weakly bound oxygen (Pd-$^{t\text{Bu}}$PCO complex) provided interesting reactivity that was not previously observed by the non-SRL Pd complex (Pd-$^{t\text{Bu}}$PCP), displaying how an SRL ($^{t\text{Bu}}$PCO) can induce new and unexpected reactivity.

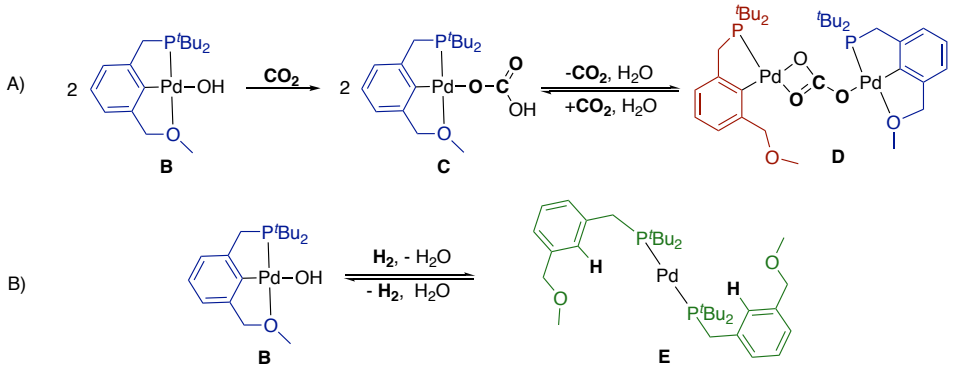

Scheme 1.10: The observed reactivity of ($^{t\text{Bu}}$PCO)PdOH ($^{t\text{Bu}}$PCO = 2-($CH_2P^tBu_2$)-6-(CH_2OCH_3)C_6H_3) with CO_2 (A) and H_2 (B).[61]

A non-SRL Pd(Xantphos)$_2$ (Xantphos = 4,5-bis(diphenylphosphino)-9,9-dimethylxanthene) was able to activate O_2 to synthesise a Pd(II)-O_2 complex, **F** (Scheme 1.11A).[62] Complex **F** was able to convert PPh_3 to O=PPh_3 in poor yields (31%) and was unable to demonstrate C-C coupling or C-H activation of added reagents. In order to improve reactivity, an SRL was explored, where one of the P donor groups in XantPhos was replaced with weakly donating Bi. Upon aerobic oxidation of the Pd[Xant(PPh_2)($BiPh_2$)]$_2$ complex, partial dissociation of the ligand via changes in coordination mode from κ^2-P,Bi to κ^1-P and generation of a Pd peroxo species, **G**, was observed (Scheme 1.11B). Upon re-dissolution of the isolated **G** in any solvent, in the absence of excess O_2, the pre-catalyst (Pd[Xant(PPh_2)($BiPh_2$)]$_2$) was regenerated. This was suggestive that an equilibrium existed between the pre-catalyst and **G**. Further reactivity of the **G** was assessed with PPh_3 and 2,4-di-*tert*-butylphenol. Upon addition of PPh_3 to **G**, the

catalytic conversion to $O{=}PPh_3$ (80% relative to PPh_3) was observed with a TON = 4.0. Addition of five equivalents of 2,4-di-*tert*-butylphenol to **G** afforded the C-C coupling product 3,3′,5,5′-tetra-*tert*-butyl-2,4-bisphenol, albeit in a poor yield (37%). Notably, reactivity of the non-SRL complex, **F**, was unable to perform C-C coupling reactions or catalytically convert PPh_3 to $O{=}PPh_3$. Demonstrating that an SRL (such as $Xant(PPh_2)(BiPh_2)$) can result in improved reactivity over non-SRL counterparts.

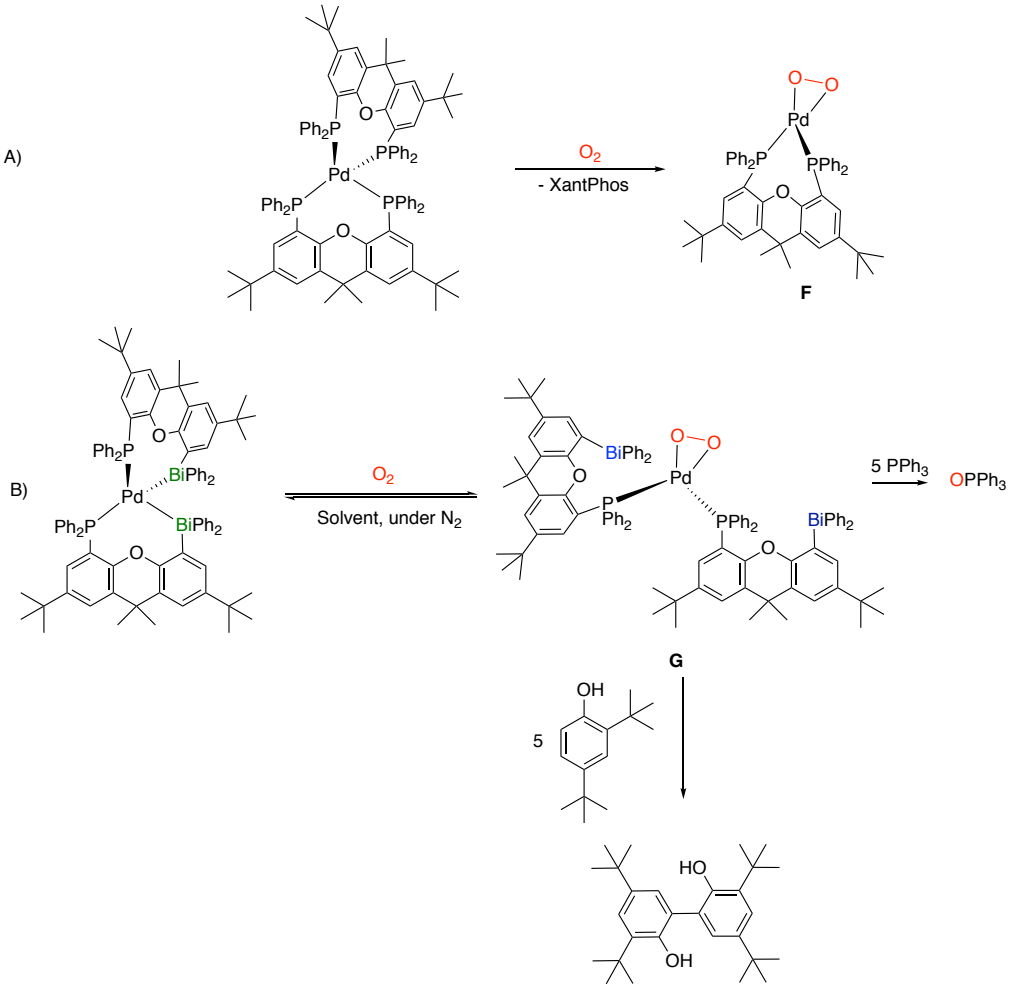

Scheme 1.11: Activation of O_2 by non-SRL $Pd(XantPhos)_2$ (A) and by SRL $Pd[Xant(PPh_2)(BiPh_2)]_2$ (B) and subsequent reactivity of its Pd(II)-O_2 complexes (**F** and **G**) with PPh_3 and 2,4-di-*tert*-butylphenol.[62]

1.4.2 Structurally Responsive Ligands in Homogenous Catalysis

A structurally responsive ligand ($P(1,4\text{-}OMePh)_2(CH)_2OMe$ = $\mathbf{L_a}$) was recently reported to promote the nucleophilic aromatic substitution (S_NAr) of aryl fluorides as the limiting reagent with the catalyst $[Ru(p\text{-cymene})Cl_2]_2/\mathbf{L_a}$ (2.5/10 mol%; Scheme 1.12A).[63]

The active cationic Ru(II) ligand complex presumably formed *in situ* from the $[Ru(cymene)Cl_2]_2$ dimer through Ag-promoted dichlorination followed by ligand coordination under catalytic conditions. Notably, without any ligand or Ru catalyst no reaction was observed. The $[Ru(cymene)Cl_2]_2$/**L$_a$** system was found to undergo S_NAr with a number of substituted arenes. Electron rich substituted arenes were well tolerated (i.e., OMe or NH_2), which was not previously observed for other catalysts. Furthermore, this procedure did not require excess aryl halide substrate, which made this procedure desirable over others that have been reported.

The structural responsiveness of the ligand **L$_a$** was explored through stoichiometric experiments. A simpler ligand ($PPh_2(CH)_2OMe$; **L$_b$**) was used to independently synthesize the proposed active catalyst (**H**) (Scheme 1.12B). In complex **H**, **L$_b$** was observed in two coordination modes κ^2-PO and κ^1-P demonstrating the structural responsiveness of **L$_b$** (and **L$_a$**). Upon addition of morpholine, rapid conversion to desired amination product was observed by NMR spectroscopy after 1 min (supposedly rapid release of HF occurred) and heating this solution for 12 h resulted in the release of the S_NAr product. Since product release was observed under these conditions it supported the proposal that **H** was likely the active catalyst under catalytic conditions. A pre-catalyst **I** was synthesised with the SRL ligand (**L$_b$; I$_a$**) and a non-SRL ($PPh_2(CH)_2Me$; **I$_b$**) to determine the importance of the structurally responsive OMe group (Scheme 1.12C). When **I$_a$** was subjected to catalytic conditions with one equivalent of **L$_b$**, a >95% yield of the S_NAr product was achieved. In comparison, when **I$_b$** was utilised only trace amounts of free product were observed. Therefore, the S_NAr of aryl fluorides by the proposed active catalyst (**H**) relied on the structural responsiveness of **L$_b$** (or **L$_a$**) to promote the reactivity observed. Therefore, the SRL **L$_a$** was proposed to promote the S_NAr of aryl fluorides with a Ru catalyst, where aryl fluorides were not required in excess for the first time for these systems.

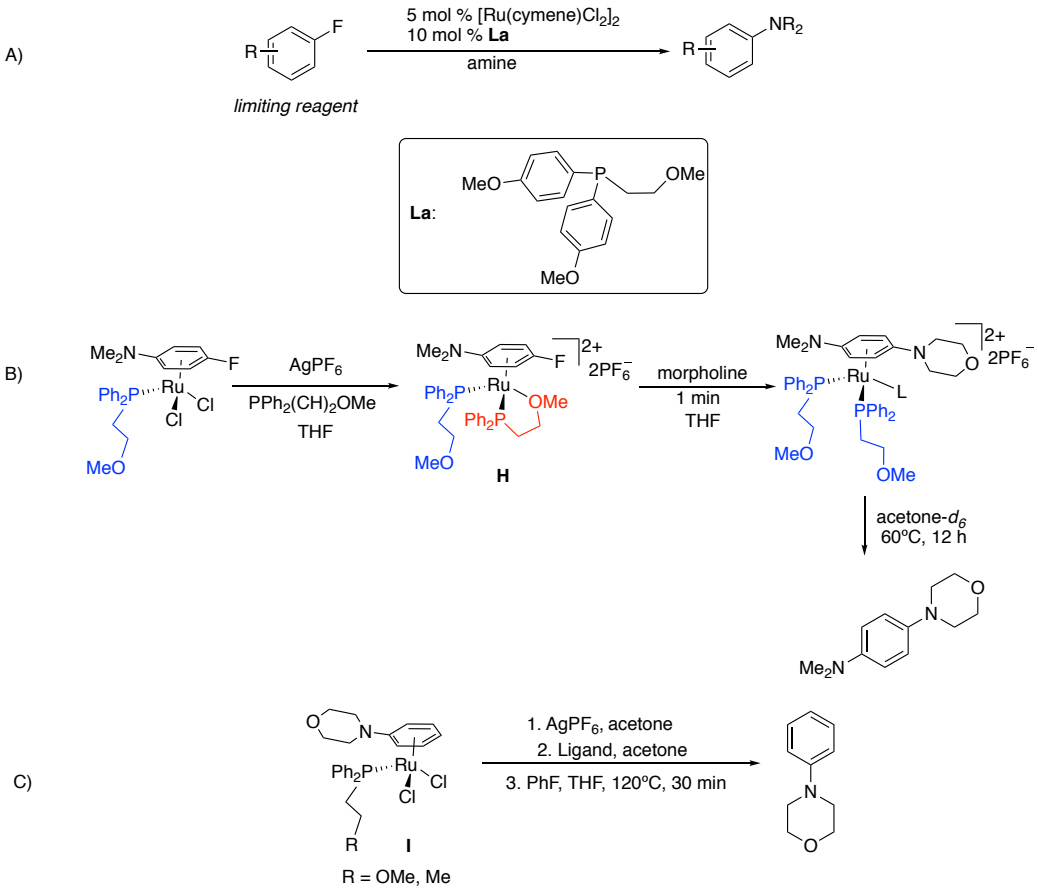

Scheme 1.12: A) General scheme of the Ru-**L** catalyzed S_NAr of aryl fluorides B) Independent synthesis of proposed active catalyst (**H**) and reactivity with morpholine. Where $\mathbf{L_a}$ is an unknown presumed donor ligand. C) Arene dissociation test with hemilabile ligand $PPh_2(CH)_2OMe$ or linear ligand $PPh_2(CH)_2Me$.[63]

Another notable example is the coordinatively unsaturated Ru catalyst (**J**). Complex **J** included a structurally responsive imidazole moiety on the diisopropyl(2-methyl-4-*tert*-butylimidazolyl)phosphine ligand (Scheme 1.13A).[64] Catalyst **J** performed well for the isomerisation of 1-hexene with a fast reaction rate (3 h; TOF: 5.4 min^{-1}) and a low catalyst loading (0.1 mol %).[64] Furthermore, **J** demonstrated excellent *E*/*Z* selectivity (>400:1 *E*/*Z* ratio) and was chemoselective for (*E*)-2-hexene over (*E*)-3-hexene (97% *E*-2-hexene). The imidazole moiety was deemed structurally responsive as it was shown to change from a four-electron donor in **J** to a two-electron donor in a alkene complex (**K**) or was not coordinated in allyl complexes that are formed following alkene deprotonation by the imidazole (**L**; Scheme 1.13A).

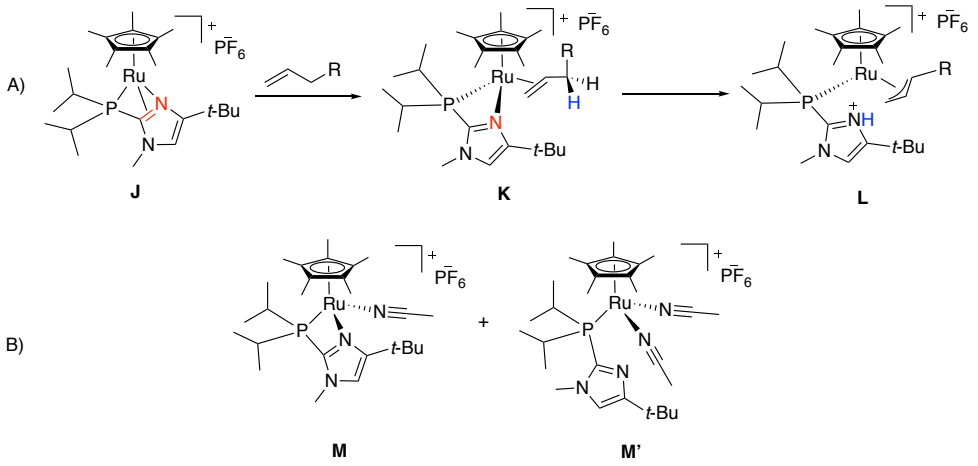

Scheme 1.13: A) Proposed structure and reactivity of Ru catalyst (**J**) for the (*E*)-selective monoisomerisation of propylene. There is some uncertainty with the best chemical depiction of H where there is meant to be a 4-electron bonding of the imidazole moiety. B) Previously reported Ru catalyst (**M**/**M′**) that demonstrated (*E*)-selective monoisomerisation of alkenes.[64]

Computed molecular orbitals for **J** found that the HOMO-7 orbital represented a π-bonding interaction between the N, the two neighbouring C of the imidazole, and the metal center, appearing as a ligand-to-metal π-donation (this 4-electron donation was represented by a bond from the N and the π C-C interaction to Ru). The π-donation from the imidazole provided the metal with two electrons extra to stabilise the formally 16-electron complex, **J**. The LUMO of **J** resided majorly on Ru (56%), which suggested that upon ligand coordination (i.e., alkene binding) to Ru, its electrons would populate the LUMO breaking the π bonding interaction between the imidazole and Ru creating a coordinatively saturated 18-electron complex. These calculations suggested that the imidazole ligand was structurally responsive. Addition of ethylene to **J** yielded an 18-electron Ru complex **K** where a change of ligand coordination to κ^2-PN was proposed. The ^{1}H NMR data suggested a single bound ethylene in **K**, this reactivity was also observed with propylene and 1-hexene. When propylene was introduced to **L** a second intermediate was observed by low temperature NMR spectroscopy (1D and 2D ^{1}H, ^{13}C, and ^{15}N NMR data), deemed to be complex **L**. Coordination mode of the ligand in **L** was proposed to be in a κ^1-P and the

imidazole moiety was found to be protonated. These proposed experimentally observed intermediates further support that the imidazole moiety was structurally responsive.

Similar catalysts have been reported for the isomerisation of terminal alkenes that are selective for the *E* over the *Z* isomer. However, they lacked one of the following desirable traits: positional selectivity (2-*E*-alkenes vs 3-*E*-alkenes), fast rates, functional group tolerance, catalyst stability at temperatures above −60 ºC, or tolerance for unpurified alkene substrates (e.g., distillation from $LiAlH_4$ was not required). When compared to another highly selective Ru catalyst (**M**/**M′**) for the isomerisation of 1-hexene, **J** was >400 x faster (48 h; TOF: 0.0034 min^{-1} for **M**/**M′**; Scheme 1.5B). The structure of **M**/**M′** was similar to **J** but contained nitrile ligand(s) for added stabilisation of the Ru complex. Catalyst **M**/**M′** required a 10 x higher catalyst loading (1 mol%) for the isomerisation of 1-hexene and had a 1/4 x lower *E*/*Z* ratio (>99:1) for all terminal alkene substrates. Notably, comparable *E*-2-hexene selectivity (>96% *E*-2-hexene) was achieved between **M**/**M′** and **J**. The increased activity **J** compared to **M**/**M′** arose due to the more easily accessible open coordination site (i.e., structurally responsive nature of the imidazole moiety) and lack of competitive nitrile ligand in the reaction mixture. For **M**/**M′**, the nitrile ligand stabilised the catalyst, but when excess nitrile (one equivalent) was added catalyst activity decreased by a factor of two.[64,65] Presumably, addition of excess nitrile favoured **M′** over **M** where nitrile binding may compete with alkene binding, which decreases the catalytic activity. Catalyst **J** was stabilised by the structural responsiveness of the imidazole moiety of the ligand that avoided any potential nitrile inhibition. Thus, the structural responsiveness of the imidazole moiety stabilised the Ru center without any nitrile additives which resulted in faster reaction rates for the isomerisation of 1-hexene.

1.5 Coordination Chemistry of 1-Azaallyl

A 1-azaallyl functionality has a π-delocalized N-C-C moiety with a negative charge, this can result in a variety of coordination modes with transition metals (Scheme 1.14).[66] Five coordination modes have been commonly observed: κ^2-NC, (i); η^3-NCC, (ii); κ^1-N, (iii); μ-(κ^1-N;κ^1-C), (iv); or μ-(κ^1-C; η^3-NCC), (v). For mononuclear metal complexes, the 1-azaallyl ligand could occupy one (κ^1-N) or two (κ^2-NC; η^3-NCC) coordination sites. The

substituent groups on the ligand (R, R′) and metal dictate the diverse coordination chemistry of the 1-azaallyl unit. Sterically large 1-azaallyl ligands typically favour κ^2-NC for mononuclear metal (II) complexes (e.g., Co, Ni, Sm, or Yb) in a low-coordination environment. Whereas asymmetric bonding (κ^1-N) have been observed with bulky 1-azaallyl ligands or with added strong neutral donors (e.g., THF). Dinuclear metal complexes have two potential binding modes with 1-azaallyl moieties, (1) μ-(κ^1-N;κ^1-C) observed for metal(I) complexes (Li, Cu, Ag, or Au), and (2) μ-(κ^1-C;η^3-NCC) specifically with lithium complexes such as [Li{μ-N(R)C(^{t}Bu)C(H)R}]$_2$.

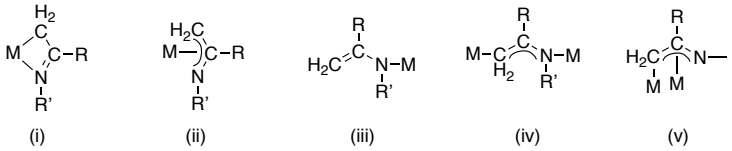

Scheme 1.14: The five common coordination modes observed upon complexation of 1-azaallyl ligands to transition metals (M = d-,f-block metals).[66] Coordination mode assignments: (i) κ^2-NC; (ii) η^3-NCC; (iii) κ^1-N; (iv) μ-(κ^1-N,κ^1-C) (v) μ-(κ^1-C,η^3-NCC)

A dynamic process of a Ni coordinated 1-azaallyl ligand was observed by variable-temperature (VT) NMR spectroscopy by Lappert *et al.*[67] The NMR data and crystal structure suggested the dynamic process to be the isomerisation between η^3-NCC and κ^1-N coordination modes via partial dissociation of the ligand (Scheme 1.15). The switch to κ^1-N may allow for an easily accessible coordination site on Ni, which could permit a substrate (or any Lewis base) to bind to Ni.[68,69]

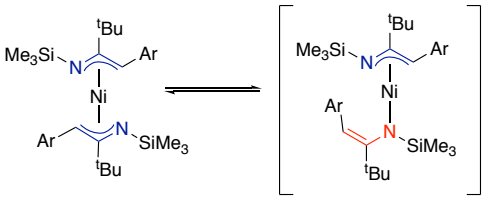

Scheme 1.15: The proposed isomerisation of the 1-azaallyl unit proposed by Lappert et al. between η^3-NCC (left) and κ^1-N (right) coordination modes.[67]

1.5.1 Phosphine 1-Azaallyl Ligand: Synthesis and Coordination Chemistry

The first entry of the phosphine-1-azaallyl (P^AzA) ligand was developed by the Blacquiere group and consisted of an aryl ring with a 1-azaallyl moiety and a PPh_2 group

ortho-subsituted to one another.[70-72] The P^AzA ligand (K[**L1**]) was synthesised via deprotonation of a phosphine-imine (P^I) precursor (H[**L1**]; Scheme 1.16) and it was chosen to study the binding modes with Ru and Pd.

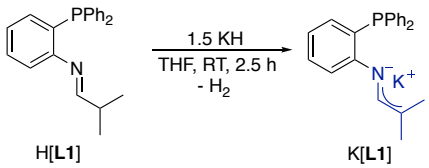

Scheme 1.16: Synthesis of P^AzA ligand, K[**L1**].[72]

The first study with **L1** involved the coordination of H[**L1**] to $RuCl_2(PPh_3)_3$ resulting in the P^I complex, **N**, and subsequent deprotonation by Li[HMDS] gave the P^AzA complex **O** (Scheme 1.17).[72] The presence of an L-type donor (pyridine) was required for the clean synthesis of, otherwise numerous unknown species were observed. Presumably many isomers of **O** or by-products were formed without pyridine present. In complex **N**, **L1** was observed in a κ^2-PN binding mode, which was likely due to the small bite angle of **L1** and the presence of excess L-donor.

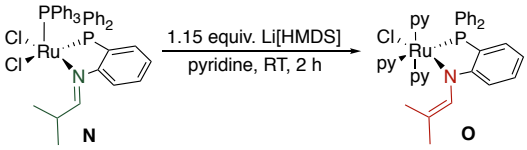

Scheme 1.17: Synthesis of **B** where only a κ^2-PN coordination mode for **L1** was observed.[72]

The second study with **L1** involved the coordination of K[**L1**] to PdClMe(COD), which resulted in the formation of a Pd(II) P^AzA dimer (**1**; Scheme 1.18A), Where **L1** was found in a bridging μ-(κ^1-P;κ^2-N) coordination mode.[71] Coordination of pyridine to **1** resulted in a change in **L1** binding mode to κ^2-PN, where pyridine occupied the vacated coordination site due to Pd(II) dimer cleavage (Scheme 1.18B). If a dissociative mechanism was at play, an open coordination site would be easily accessible from **1** for coordination of L-type donors. Additionally, **1** was observed to undergo the thermally induced Csp^3-Csp^3 reductive elimination of ethane (Scheme 1.18C). After ethane release, **L1** was observed in two distinct coordination modes, a μ-(κ^2-PN;η^2-CC) (**3**) and κ^2-P,N (**4**) demonstrating the structural responsiveness of the P^AzA ligand. Due to these changes in

coordination mode under thermal conditions, it is likely that **L1** was playing a role in the reactivity of **1** resulting in the synthesis of **3** and/or **4**.

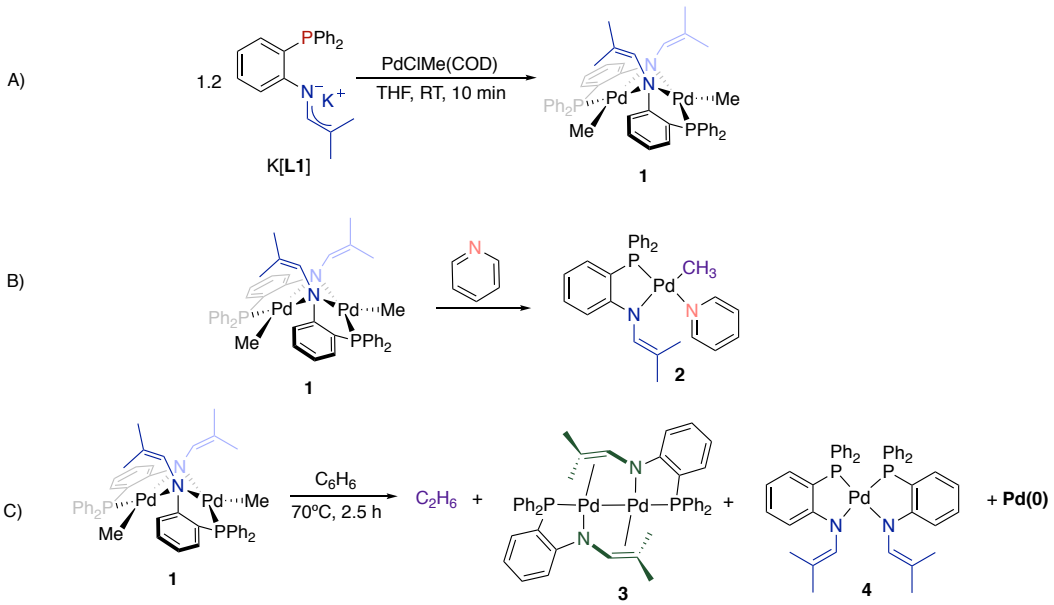

Scheme 1.18: A) The synthesis of **1** via the addition of K[**L1**] and PdClMe(COD).[71] B) Lewis acidic abstraction from **1** by pyridine to generate **2**. C) The Csp^3-Csp^3 reductive elimination of ethane and formation of Pd(I) dimer (**3**) and bis-ligated Pd complex (**4**) by heating of **1**.

In an effort to coordinate **L1** in a κ^1-P;η^3-NCC coordination mode, a new Ru precursor, $[Ru(Cp^*)(MeCN)_3]PF_6$, was explored (Scheme 1.19).[73] The Cp* ligand enforced a piano-stool geometry, restricting the available coordination sites for **L1** to three that are facially disposed, to limit variability in ligand coordination to Ru. Upon the addition of K[**L1**] to $[RuCp^*(MeCN)_3]PF_6$ the proposed κ^1-P;η^3-NCC complex was observed as a broad signal in the $^{31}P\{^1H\}$ NMR spectrum. The broad signal was expected as the equilibrium between **5a** and **5b** would likely occur on the NMR timescale. In an attempt slow the equilibrium between **5a** and **5b** to observe both coordination modes via NMR spectroscopy the temperature was lowered to –30 ºC, but decoalesence was not achieved. Upon addition of MeCN a sharp singlet was observed in the $^{31}P\{^1H\}$ NMR spectrum. This was indicative of the formation of **P**, where the coordination mode of **L1** was proposed to be in a κ^2-PN and MeCN occupied the easily accessible coordination site. Upon removal of solvent, the signal for the proposed complex **5** was regenerated demonstrating a reversible process. However, isolation of **5** or **N** was not achieved from traditional

separation techniques due the similar solubilities of observed impurities. Therefore, confirmation and characterisation of the proposed κ^1-P;η^3-NCC binding mode of **L1** has thus far not been achieved.

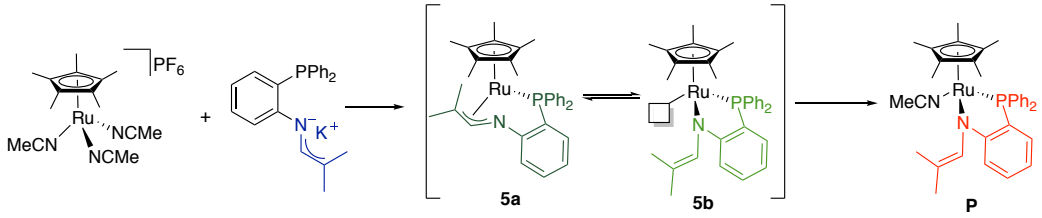

Scheme 1.19: A: Previously observed synthesis of proposed Ru P^AzA equilibrium between κ^1-P;η^3-NCC bound complex (**5a**) and κ^2-PN (**5b**) and generation of proposed upon addition of excess MeCN (**P**).[73]

1.6 Scope of Thesis

Herein, I report the further exploration into the reactivity and coordination of a P^AzA ligand. The second chapter will cover the synthesis of a Pd(II) P^AzA dimer (**1**) and the reactivity with small molecules (Scheme 1.20A; O_2, H_2O, E-H, where E-H = MeOH, BnOH, [HDMF]OTf, HOPh, $C_7H_8O_2$, and phenolphthalein; and H_2) in hopes of harnessing the structurally responsive nature of the 1-azaallyl unit in new and interesting ways. The third chapter will cover the synthesis of a Ru-P^I (**7**) and Ru-P^AzA (**8** and **5**) complexes (Scheme 1.20B). To limit the synthesis of impurities or by-products previously observed in the synthesis of **5**, a new protocol was employed with RuCl(Cp*)(PPh_3)$_2$ (**6**) as the precursor. Complex **6** has only two labile ligands in comparison to **[**RuCp*(MeCN)$_3$]PF_6, which further limits the coordination possibilities of **L1**. The reaction of **6** and H[**L1**] would enforce a κ^2-PN binding mode initially forming a Ru-P^I precursor (**7**). Then deprotonation and halide abstraction of **7** may limit the synthesis of observed impurities via the previous synthetic route to generate cleanly the desired 'low-coordinate' Ru-P^AzA complex, **5**. Complex **5** was proposed to exist as mixture of complexes in an equilibrium, where notably the binding mode of **L1** in **5b** was proposed to be κ^1-P;η^3-NCC binding mode.

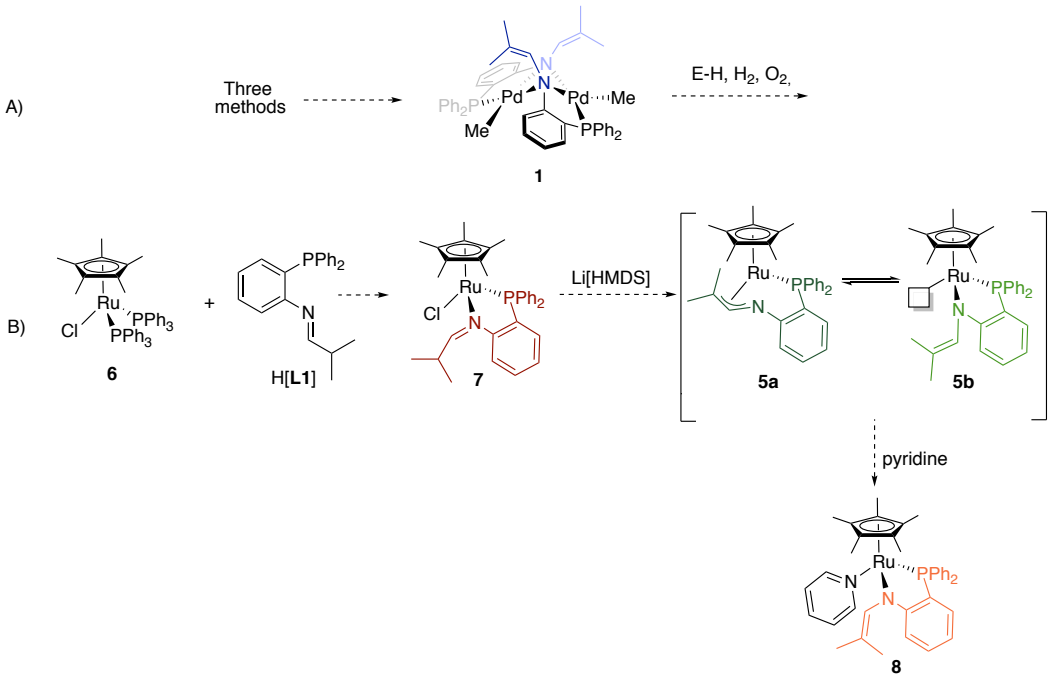

Scheme 1.20: A) Generic scheme of the synthesis and reactivity of **1** B) Proposed synthetic route to enforce a κ^2-PN coordination mode to gain clean Ru P^AzA (**5a-5b**) upon deprotonation by a base such as Li[HMDS] and potential isolation of pyridine bound Ru-P^AzA (**8**)

2 Reactivity of a Pd(II) Phosphine-1-Azaallyl Complex

2.1 Attempted Optimisation of the Synthetic Route to **1**

A Pd(II)-P^AzA dimer (**1**) was previously accessible by two synthetic routes that involved either deprotonation of a Pd-P^I complex (**9**; Scheme 2.1; Path A) or coordination of K[**L1**] to PdClMe(COD) (Scheme 2.1; Path B).[71] In each case, complete conversion to **1** was observed in a matter of minutes however; isolation of **1** remained an issue. Synthetic route A proved insufficient at producing >50 mg of **1** and the production of Pd black was observed, indicating decomposition during workup likely due to the instability of **1** toward excess H[$N(SiMe_3)_2$] or Li[$N(SiMe_3)_2$] in solution. Synthetic route B allowed for yields of up to 80%, but consistent yields were not achieved on scales >100 mg. This was likely caused by the unavoidable slow removal of COD (boiling point: 110 ºC) during the workup that may have allowed for the thermal decomposition of **1** or COD may play a role in the decomposition of **1**. The proposed routes to optimise the synthesis of **1** (Scheme 2.1) involved: changing the Pd precursor to one with a lower boiling point labile ligand(s) (Path C); Lewis acid abstraction from Pd-P^AzA monomer **2** (Path D); and deprotonation of **5** with a weaker base (K[OPh]) to yield **1** in a route similar to synthetic route A (Path E).

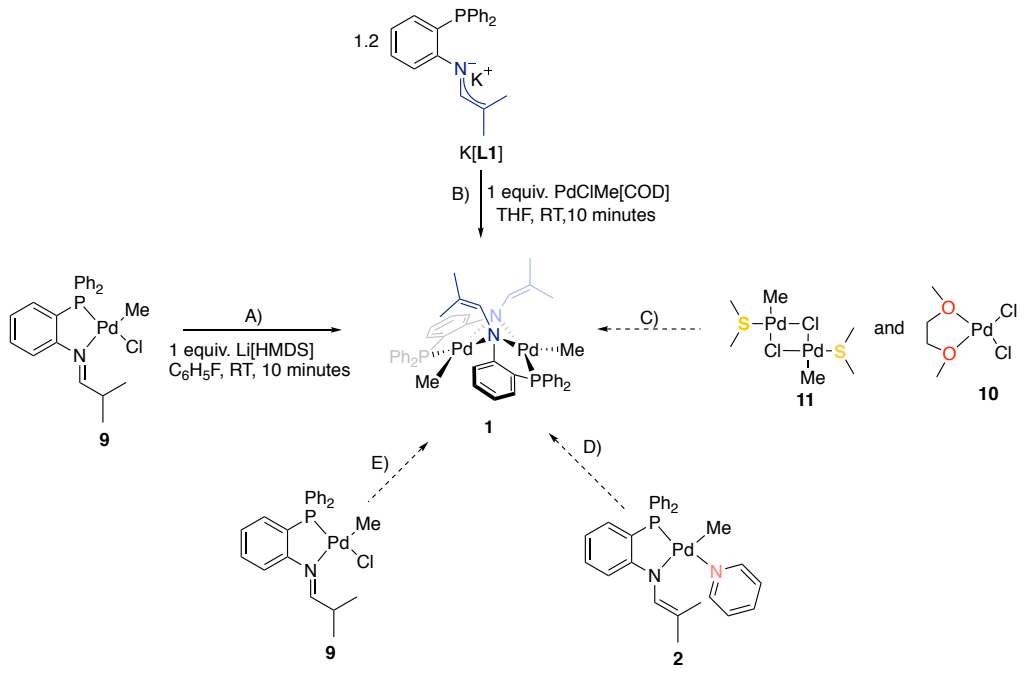

Scheme 2.1: Conditions A and B were previously developed procedures to **1**,[71] and C, D, and E were proposed routes to optimise the synthesis of **1**.

2.1.1 Strategy C: Alternative Pd(II) Precursor

Two new Pd(II) precursors, $PdCl_2$(DME) (**10**; DME = 1,2-dimethoxyethane) and [Pd(μ-Cl)]Me(SMe_2)]$_2$ (**11**; SMe_2 = dimethyl sulfide) were explored. These new Pd(II) precursors contain lower boiling point place holder ligands compared to COD and are attractive potential alternatives for the scaled-up synthesis of **1** to avoid decomposition during work up. With no literature precedent for the synthesis of **10**, procedures for similar complexes $NiCl_2$(DME) and $PdCl_2$(COD) where the metal (Pd vs Ni) or place holder ligand (DME vs COD) were altered.[74,75] When refluxing $PdCl_2$ in DME in the presence of ethyl orthoformate, no reaction was observed (Scheme 2.2A), likely due to poor solubility of $PdCl_2$ in DME. When dissolving $PdCl_2$ first in HCl and diluting with EtOH, as per the $PdCl_2$(COD) synthesis procedure, and subsequent DME addition and reflux for 24 h, two new broad signals were observed in the ^{1}H NMR spectrum of a crude reaction mixture (Scheme 2.2B). These new signals integrated to the correct relative to integrations for DME (i.e., $(CH_3)_2$: $(CH_2)_2$; 6H:4H) and were downfield from free DME indicative of the

formation of **10** (Figure 2.1A). These broad signals suggested that DME was weakly bound to Pd and may be undergoing a dynamic process between **10** and $PdCl_2$. Upon attempted isolation of **10**, these broad signals disappeared indicating that DME was indeed very labile and that **10** was not stable to solvent removal.

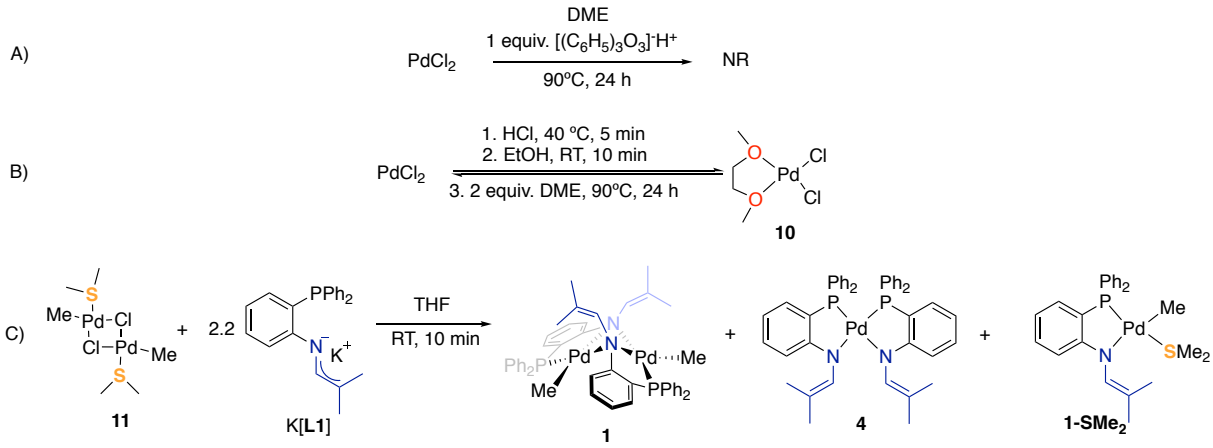

Scheme 2.2: The attempted synthesis of **10** (A & B) and Initial attempt to coordinate of K[**L1**] to **11** (C).

Due to the unsuccessful synthesises of **10**, the placeholder ligand SMe_2 was explored due to its soft S donor and very low boiling point (37 ºC). The precursor [Pd(μ-Cl)]Me(SMe_2)]$_2$ (**11**) was synthesised in good yields (75 %) via a procedure analogous to that for PdClMeCOD.[76,77] To synthesise **1**, K[**L1**] was added to **11** in a cold THF for 10 min, during which time the production of Pd black was observed. A 70% conversion to desired complex **1** was observed according to the $^{31}P\{^{1}H\}$ NMR spectrum. The reaction aliquot also revealed minor amounts of the Pd bisligated species (**4**), a SMe_2-**1** adduct, and other minor unidentified impurities. The identity of the SMe_2-**1** adduct was confirmed by spiking the sample with degassed SMe_2 and the assigned $^{31}P\{^{1}H\}$ signal (45.2 ppm) grew in comparison to the signal for **1**. Upon attempted isolation of **1**, most impurities were readily removed by filtration to give **1** (70% conv.) with a minor amount of the SMe_2 adduct (Figure 2.1B). Leaving the mixture under vacuum longer could remove the Pd-bound placeholder ligand SMe_2 and produce more of **1**. Suggesting that future attempts will result in high conversion and high yields of **1**.

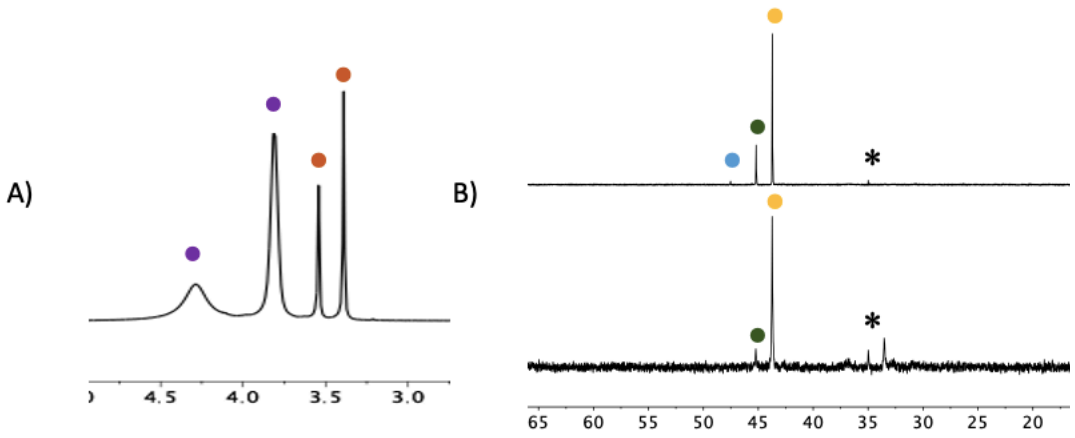

Figure 2.1: A) A section of the ^{1}H NMR spectrum (400 MHz, $CDCl_3$) from the attempted synthesis of **10** B) The $^{31}P\{^{1}H\}$ NMR spectrum (243 MHz, C_6D_6) of the filtrate (top) and solid (bottom) after attempted isolation of **1** from the addition of K[**L1**] to **11**. Signals indicated in ^{1}H NMR spectra: • free DME,[78] • proposed **10**; Signals indicated in $^{31}P\{^{1}H\}$ NMR spectra: • **1**, • **4**, • **1**-SMe_2 adduct, * unknown impurities; all other signals are unknown impurities; All integration values were found relative intensities without increased relaxation delay

2.1.2 Strategy D: Lewis Acid Abstraction from Pd-P^AzA Monomer **2**

It was anticipated that reacting **2** with a Lewis acidic borane would result in the generation of **1** and precipitation of a borane-pyridine Lewis acid-base adduct (Scheme 2.3). This would be an ideal synthetic route since **2** was easily synthesised in consistently high yields and is a thermally stable precursor.[71] Upon addition of one equivalent of BF_3•(Et_2O) to **2** (83 % conversion) to four new signals were observed by $^{31}P\{^{1}H\}$ NMR spectroscopy (Figure 2.2A). These signals were **1** (6 %) and other unidentified impurities (78 %). The conversion of the Pd(II) precursor **2** was high (83 %) but selectivity for **1** using BF_3•(Et_2O) was poor. Notably, the major unidentified signal (68 %; 41.1 ppm) in the $^{31}P\{^{1}H\}$ NMR spectrum was observed as an apparent quartet with a 1:3:3:1 ratio, this coupling pattern suggested ^{31}P-^{19}F coupling. If a BF_3-**L1** adduct was formed upon reaction of **2** and BF_3•(Et_2O), then coupling for both ^{31}P-^{11}B (that yields a signal with four lines in

a 1:1:1:1 intensity) and ^{31}P-^{19}F (that yields quartet in a 1:3:3:1 ratio) would be expected. The major identified signal could be comprised of these two coupling (^{31}P-^{19}F/^{31}P-^{11}B) patterns. The ^{11}B NMR spectrum indicated leftover BF_3•(Et_2O) and what appeared to be two overlapped signals with complex splitting (1.00-1.92 ppm; Figure 2.2B). Notably, ^{11}B-^{19}F coupling was not observed for authentic BF_3•(Et_2O) where only a singlet was observed in the ^{11}B NMR spectrum (Figure A1). Notably, a computational study suggested that the BF_3-pyridine adduct presented a ^{11}B signal as a singlet at ~0.15 ppm, which was not observed experimetnally.[79] Further suggesting that upon addition of BF_3•(Et_2O) to **2** undesired reactivity occurred that inhibited the synthesis of **1** in high yields as desired. The small amount of **1** detected (6%) was suggestive that another borane may gain **1** in higher amounts.

Next, a bulkier Lewis acidic borane, BEt_3, was explored. The added sterics of the Et substituent groups may limit the formation of previously observed K[**L1**]-borane adduct in favour of the desired pyridine borane adduct. One hour after the addition of BEt_3 to **1**, the solution was black in colour indicative of the formation of Pd black and decomposition. Additionally, no ^{11}B NMR signal was observed indicative of precipitation of a borane-pyridine Lewis acid base adduct. The $^{31}P\{^1H\}$ NMR spectrum further confirmed the proposed reactivity as **1** was detected; however, selectivity for **1** (39%) was poor with almost full consumption of **2** (95% conv.) being observed (Figure 2.2C). After 24 h complete decomposition occurred, as no signals other than internal standard ($O{=}PPh_3$) was detected. The addition of BEt_3 to **2** provided the desired complex **1** in poor selectivity (39 %) and so this borane was not further explored.

A third Lewis acidic borane, BPh_3 with bulkier Ph substituents was attempted, due to the partial success of BEt_3. Upon addition of a BPh_3 solution to **2** a colour change from orange to black was observed within seconds, indicative of the formation of Pd black and decomposition. After 15 min no $^{31}P\{^1H\}$ or ^{11}B NMR signal could be detected confirming that decomposition occurred upon addition of BPh_3 to **2**. Therefore, no further boranes were attempted, and strategy D was deemed ineffective at yielding **1** easily and in high yields.

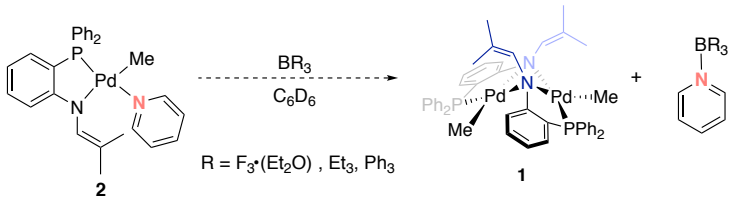

Scheme 2.3: Proposed synthesis of **1** via Lewis acid abstraction from **2**

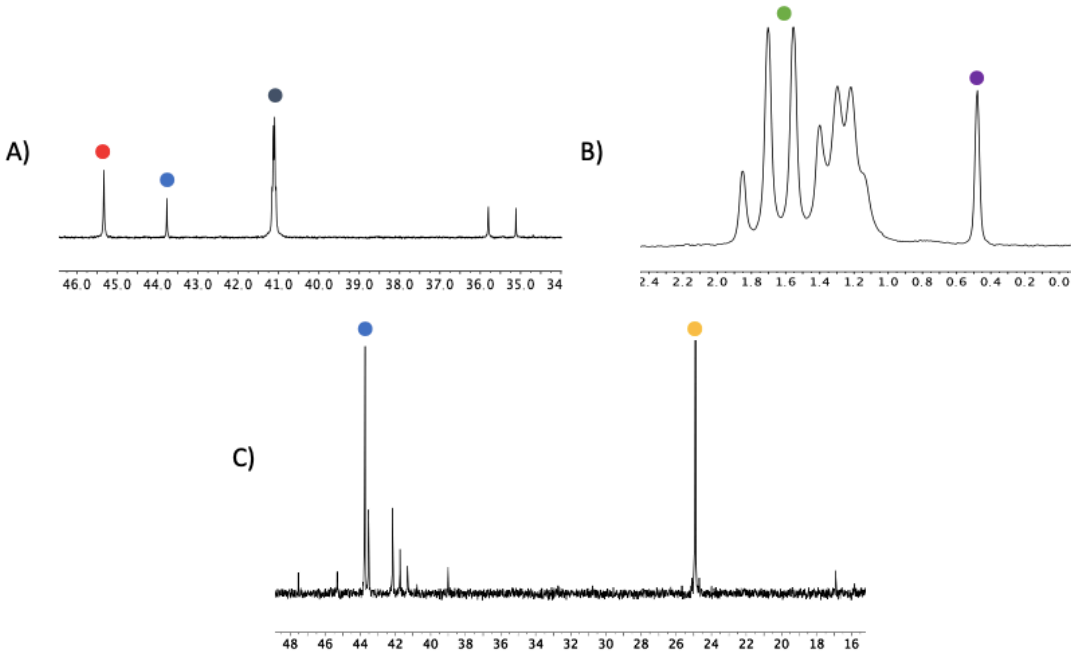

Figure 2.2: The $^{31}P\{^{1}H\}$ NMR spectrum (162 MHz; C_6D_6; 5 s relaxation delay; A) and the ^{11}B NMR spectrum (128 MHz; C_6D_6; B) after the addition of one equivalent of BF_3•(Et_2O) to **2**. The $^{31}P\{^{1}H\}$ NMR spectrum (243 MHz, C_6D_6; 5 s relaxation delay) 1 h after the addition of one equivalent of BEt_3 to **2** (C). Signals indicated in $^{31}P\{^{1}H\}$ NMR spectra: • **2**, • **1**, • Major impurity, • O=*P*Ph_3; Signals indicated in ^{11}B NMR spectrum: • Major impurity, • *B*F_3•(Et_2O); Yields determined from the $^{31}P\{^{1}H\}$ NMR spectrum BF_3•(Et_2O) trial were found through relative integrations; Yields were determined from the $^{31}P\{^{1}H\}$ NMR spectrum BEt_3 trial were found relative to an internal standard.

2.1.3 Strategy E: Attempted Synthesis of **1** via Deprotonation of **5** by Phenoxide Bases

Complex **1** can be synthesised via deprotonation of a P^I Pd complex, **9**, by Li[HMDS] (Scheme 2.1A).[71] This approach has been unsuccessful on large scales due to excess H[$N(SiMe_3)_2$]/Li[$N(SiMe_3)_2$] that lead to decomposition of **1** upon isolation. However, a weaker base (e.g., K[OPh]) could circumvent the isolation issues previously observed. Upon addition of K[OPh] to **9** in equimolar amounts (Scheme 2.4), **1** was formed

in a minor amount (ca. 9% **1**; 17% **12a**) with a major product being a Pd-phenol adduct (**12a**) (Figure 2.3A). Excess base K[OPh] was hypothesised to promote the production of **1** over **12a**, thus, five equivalents of K[OPh] were added to **9**. Unfortunately, at five equivalents of K[OPh], **1** was not observed. Additionally, the number and intensity of unidentified signals in the $^{31}P\{^{1}H\}$ NMR spectrum increased at higher equivalents of K[OPh] (Figure 2.3B). These unknown signals indicate that **12a** or **9** was unstable to excess phenoxide and that pathway E was not an efficient method for synthesis of **1**.

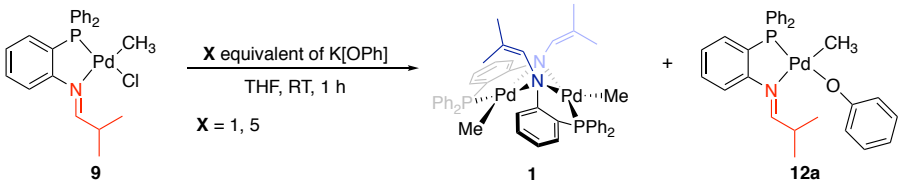

9 **1** **12a**

Scheme 2.4: The observed reactivity between **9** and varying equivalents of K[OPh] yielding **1** (only at one equivalent of K[OPh]) and **12a**.

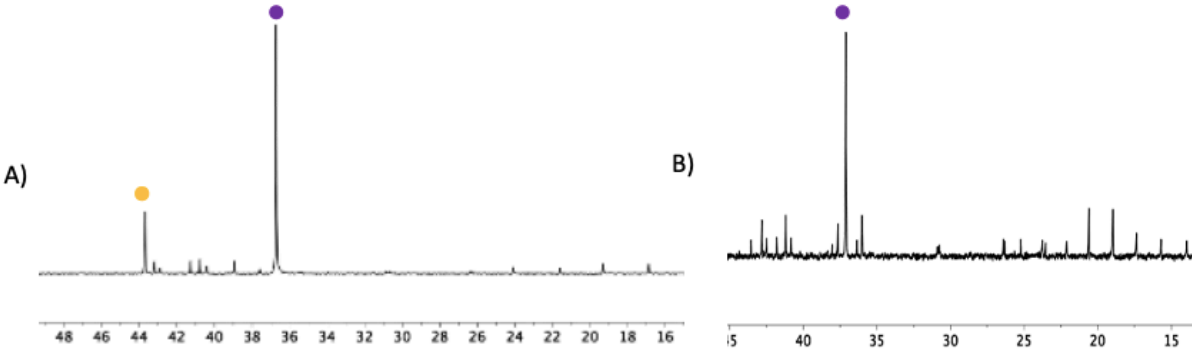

Figure 2.3: The $^{31}P\{^{1}H\}$ NMR Spectrum (243 MHz, C_6D_6) 1 h after the addition of one (A) or five (B) equivalent(s) of K[OPh] to **2**. $^{31}P\{^{1}H\}$ NMR signals identified: • **1**, • **12a** (all other signals are unidentified); %P are relative integrations

2.2 Reactivity of **1** with E-H (E-H = MeOH, BnOH, [HDMF]OTf, and various Ar-OH)

The activation of the E-H bond is an attractive area of research as the activation of E-H bonds (e.g. E = H, C, O) for catalytic reactions and/or as a method to functionalize an organic compound. The activation of C-H bonds of aryl compounds that are readily attainable for some Pd catalysts.[59] The reactivity with E-H bonds can be informative to determine the reactivity of complexes with small molecules like H_2O and H_2.

2.2.1 Reactivity of **1** with Alcohols (E-H = MeOH and BnOH)

Equimolar amounts of MeOH and **1** reacted over a 24 h period slowly resulted in a black solution with solids, indicative of the formation of Pd black and decomposition (Scheme 2.5). Full consumption of **1** occurred over 24 h according to the $^{31}P\{^1H\}$ NMR spectrum, but several products were observed (ten unidentified signals; Figure A3). The ^1H NMR spectrum contained several unidentified signals (Figure 2.4); therefore, it is proposed that MeOH deprotonation occurred upon addition to **1**, but the exact identities of these products remain unknown. Similarly, the addition of **1** with BnOH was explored; however, the ^1H and $^{31}P\{^1H\}$ NMR data (Figure A3) also suggested undesirable reactivity. The reactivity of two types of alcohols with **1** resulted in numerous products as determined by $^{31}P\{^1H\}$ NMR spectroscopy, this indicated that **1** was not stable toward alcohols and, therefore, no further alcohols were tested.

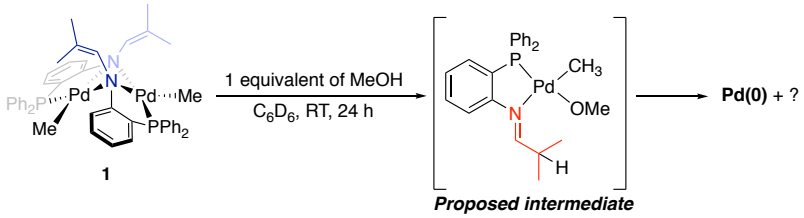

Scheme 2.5: Reactivity of **1** with MeOH.

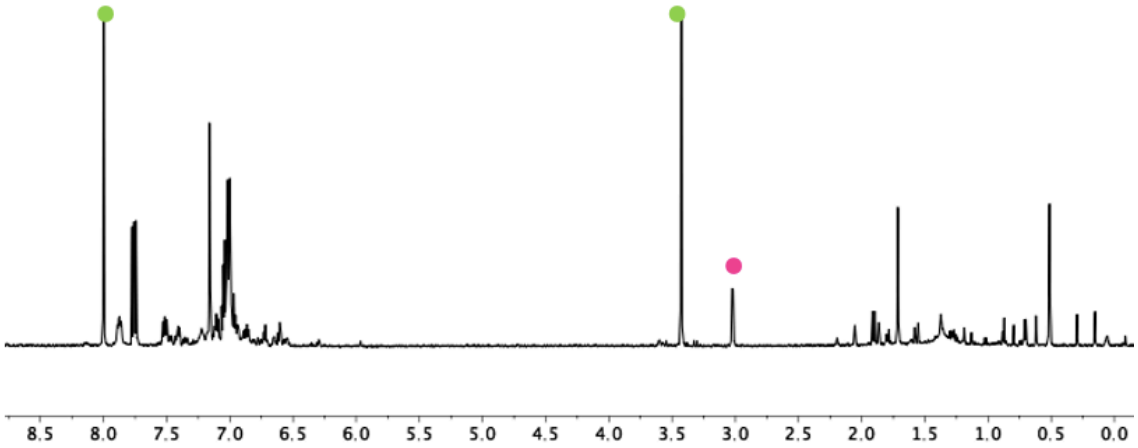

Figure 2.4: The ^{1}H NMR spectrum (600 MHz, C_6D_6) 24 h after MeOH addition to **1**. Signals indicated: • MeOH; • DMT-C*H*$_3$, • DMT-Ar *H*

2.2.2 Reactivity of **1** with Acids (E-H = [HDMF]OTf, Phenol, 4-Methoxyphenol, 4-*t*-Butylphenol, and Phenolphthalein)

Four different acids ([HDMF]OTf, phenol, 4-methoxyphenol, and phenolphthalein with pK_a(MeCN) values between 6.1-29.2[80,81] were added to **1** in C_6D_6 (phenol, 4-methoxyphenol, and phenolphthalein) or THF (for [HDMF]OTf) at room temperature (Scheme 2.6). Upon addition of two equivalents of phenol to **1**, the immediate formation of a Pd-phenol adduct (**12a**) was observed via NMR spectroscopy, and the synthesis confirmed via an independent synthesis route (*vide infra*; Figure 2.5A/B). The shift of the ^{31}P{^{1}H} NMR signal from 43.7 to 36.7 ppm indicated a new product had been formed (Figure 2.5A). The ^{1}H NMR spectrum demonstrated the formation of an isopropyl unit suggesting **1** had deprotonated phenol, which resulted in the formation of an imine functionality and a palladium phenol bond (Figure 2.5B). The acids [HDMF]OTf and 4-methoxyphenol reacted similarly with **1**, resulting in a bright yellow solution. Evidence of an isopropyl group was observed by ^{1}H NMR spectroscopy for **12c** and similar shift in the ^{31}P{^{1}H} NMR spectra were observed for **12b** (δ_p= 35.4, br; THF) and **12c** (δ_p=37.5, C_6D_6; Figure A4). Notably, **12b** required the presence of L-donor THF for stabilisation otherwise, only broad signals were observed by NMR spectroscopy. Therefore, **1** was found to readily

deprotonated E-H bonds with pK_a(MeCN) values between 6.1 ([HDMF]OTf) - 27.1 (HOPh) and pK_a(DMSO): 18.0 (HOPh)-19.1 (4-methoxyphenol). These experiments show the Bronsted basicity of the 1-azaallyl moiety of **L1**, and thus of the Pd(II) dimer, **1**. This MLC observed may be used in future catalysis attempts.

Interestingly, phenolphthalein and **1** resulted in an insoluble purple solid (**12d**; solvents tested: C_6D_6, toluene, 1,4-dioxane, acetonitrile, pyridine, $CDCl_3$, DCM, diethyl-ether, THF, and DMSO), and so the exact reactivity remains unknown. However, phenolphthalein is a widely used indicator in laboratory titration experiments and has been shown to exhibit a magenta colour upon deprotonation (i.e., pH = 8.2; pKa 9.4).[82] The colour of the insoluble solid from the addition of phenolphthalein to **1** was indicative of similar reactivity to the other acids tested; however, this was unable to be confirmed by typical spectroscopic techniques due to solubility issues.

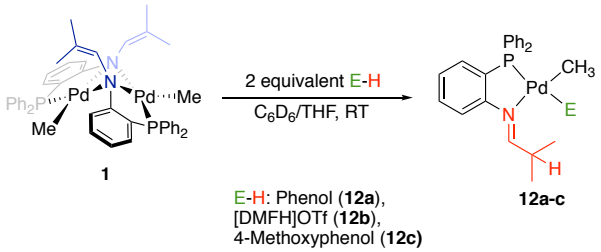

Scheme 2.6: Reactivity of **1** with [HDMF]OTf, phenol, and 4-methoxyphenol in C_6D_6 and THF.

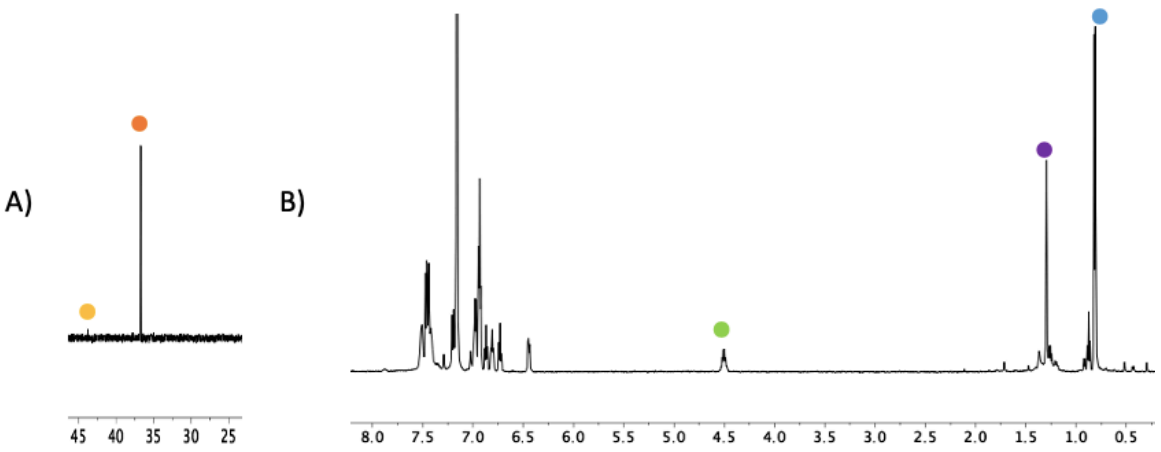

Figure 2.5: A) The $^{31}P\{^{1}H\}$ NMR Spectrum (243 MHz; C_6D_6; A) and ^{1}H NMR spectrum (600 MHz; C_6D_6; B) immediately after the addition of two equivalents of H[OPh] to **1**. Signals indicated in $^{31}P\{^{1}H\}$ NMR Spectrum: • **1**, • **12a**; Signals indicated in ^{1}H NMR spectrum: • Methine *H* of **12a**, • Pd-C*H*$_3$ of **12a**, • Isopropyl-C*H*$_3$'s of **12a**

Due to low yields of **1**, scale up of **12a** and complete characterisation via the addition of **1** to phenol was not explored. Therefore, to confirm the identity of **12a**, an independent synthesis route was utilised (Scheme 2.7). The addition of one equivalent of phenoxide to **9** gave two signals; the proposed compound **12a** (δ_p = 36.7) as the major product and trace amounts of **1** (δ_p = 43.7) were observed by $^{31}P\{^{1}H\}$ NMR spectroscopy (previously discussed in Section 2.1). Isolation of **12a** from these reaction mixtures proved unsuccessful via typical techniques (e.g., recrystallisation) since **1** had a similar solubility as **12a** in all solvents attempted. Increasing to 1.5 equivalents of phenoxide avoided the formation of **1** giving **12a** (80%) as the major product with only two minor impurities according to the $^{31}P\{^{1}H\}$ NMR spectrum (Figure 2.6A). Isolation of **12a** (70%) was successful, but the presence of minor amounts of **1** (10%) was unavoidable. Notably, a new sharp signal (*) observed by ^{1}H NMR spectroscopy may be indicative of free phenol was generated after attempted isolation of **12a** (Figure 2.6B). This could be confirmed by spiking a solution of authentic phenol to an NMR tube of **12a**. Two possible explanations for these observations are (1) the small excess phenoxide in solution may result in the production of **1** and free phenol via deprotonation of **12a**; and/or (2) the phenoxide was labile and may deprotonate some **12a** to yield **1** and phenol.

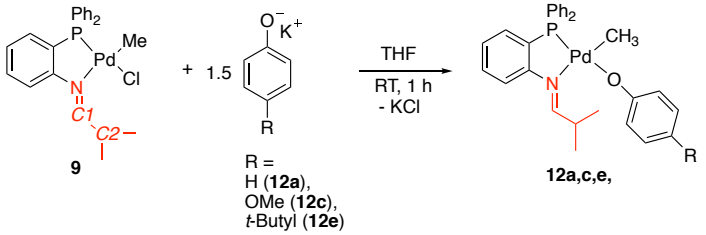

Scheme 2.7: The observed reactivity between **5** and varying phenoxides

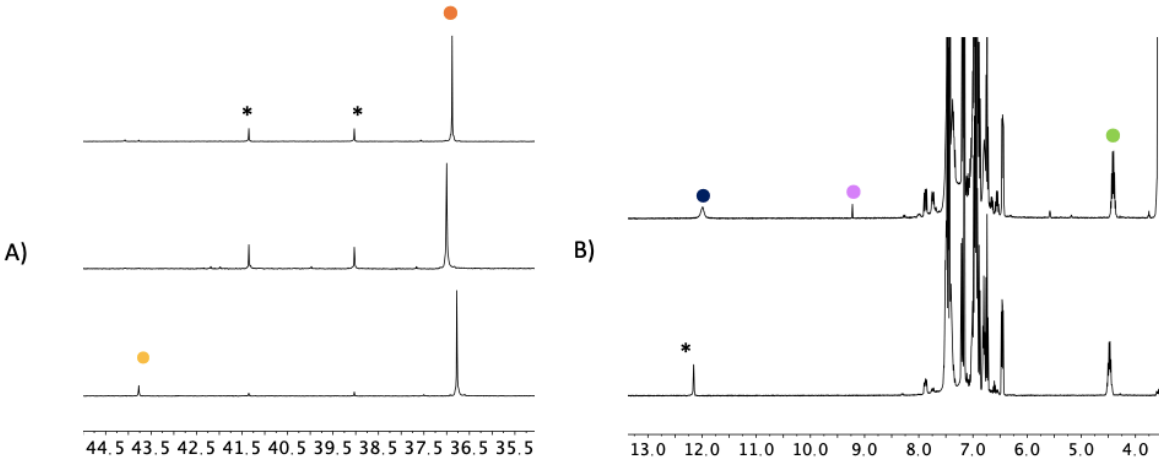

Figure 2.6: A) The $^{31}P\{^{1}H\}$ NMR Spectrum (162 MHz, C_6D_6) 1 h after the addition of 1.5 equivalents of K[OPh] to **9** (top); Filtrate after attempted isolation of **12a** (middle); Solid collected after attempted isolation of **12a** (bottom). B) The ^{1}H NMR Spectrum (400 MHz, C_6D_6; top) 1 h after the addition of 1.5 equivalents of K[OPh] to **9** and of solid collected after attempted isolation of **12a** (bottom): Signal indicated in $^{31}P\{^{1}H\}$ NMR spectra: ● **1**, ● **12a**; Signal indicated in ^{1}H NMR spectra: ● Methine *H*, ● proposed broad phenol O*H*, ● impurity isobutylaldehyde-*H*, * proposed free phenol O*H*

The structure of **12a** was elucidated through typical spectroscopic techniques (NMR, IR spectroscopy, and MALDI-MS). The ^{1}H NMR spectrum and the ^{1}H-^{1}H COSY demonstrated the presence of an isopropyl unit (Figure A5). New broad signals in the aromatic region of the ^{1}H NMR spectrum suggested that OPh was bound to Pd. The $^{13}C\{^{1}H\}$ NMR spectrum and ^{1}H-$^{13}C\{^{1}H\}$ HSQC experiment indicated that chemical shift of *C2* and *C1* (32.6 ppm and 182.4 ppm, respectively) were consistent with previously observed H[**L1**] bound to Pd or Ru.[71,72] Lastly, MALDI-MS demonstrated [$C_{22}H_{21}NPPd^{-}$] (*m/z* = 436.03), suggesting that H[**L1**] was still bound to Pd; however, this does not confirm

OPh bound to Pd. The structure of **12a** was not able to be confirmed by single crystal X-ray diffraction, since **12a** decomposed in all solvent systems attempted for crystallisation.

In an effort to generate X-ray quality crystals and to confirm the observed reactivity, two comparable phenoxides were added to **9**. Similar reactivity was observed with 4-methoxyphenoxide and 4-*t*-butylphenoxide, where upon addition of phenoxide to **9** one new major signal (**12c**: δ_p = 36.8; **12e**: δ_p = 36.7), minor impurities, and small amounts of **1** were observed in the $^{31}P\{^1H\}$ NMR spectra, similar to what was observed for **12a** (Figure A6 & A7). Complexes **12c** and **12e** were collected in modest yields (35% and 57%, respectively) and similar purity levels (**12c**: 80 % purity; **12e**: 70 % purity by $^{31}P\{^1H\}$ NMR spectroscopy). Compounds **12c,e** exhibited similar ^1H NMR spectra to **12a**; confirming H[**L1**] coordination to **2** (Figure 2.7). The ^1H NMR signals for the methyls of proposed bound 4-methoxyphenol and 4-*t*-butylphenol are broad and located slightly downfield from authentic samples, further suggesting synthesis of **12c,e**. The relative integration of the proposed methoxy signal for **12c** did integrate to the expected 3H relative to the methine H of **L1**. Additionally, the proposed signal for the *t*-butyl moiety of the phenoxide of **12e** was broad and overlapped with the Pd-Me and residual THF signals but was found to integrate to the expected 9H relative to the methine H of **L1**. These observations confirm that one phenoxide was bound to Pd in both **12c,e** however; the broad signals were suggestive that the Pd-phenoxide bond was labile like in **12a**. Similar to **12a**, any crystallisation attempts with **12c,e** resulted only in decomposition products, and to-date, solid-state structure confirmation of the proposed complexes has not been achieved. This study of **1** with E-H indicated the acid/base reactivity of the P^AzA ligand and was instructive to understand the reactivity with small molecules H_2O and H_2.

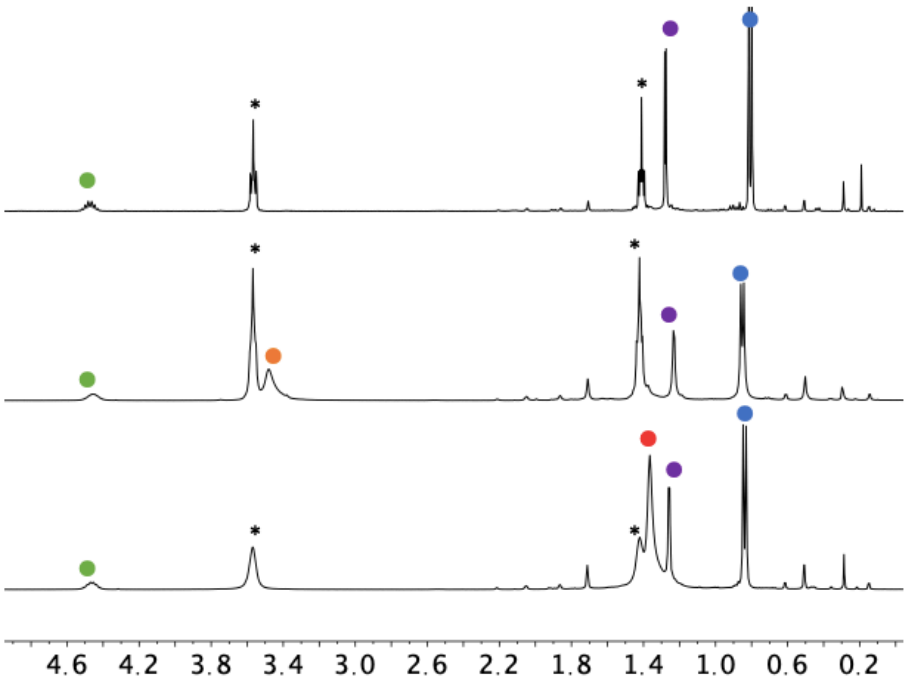

Figure 2.7: The ^{1}H NMR Spectrum (400 MHz, C_6D_6) 1 h after the addition of phenoxide to **9** to synthesize **12a** (top), **12c** (middle), and **12e** (bottom). Signals indicated in ^{1}H NMR spectra: • Methine *H*, • OMe *H*'s, • *t*-Butyl *H*'s, • Pd-C*H*$_3$, • isopropyl-C*H*$_3$, * THF

2.3 Reactivity of **1** with Water

The reactivity of **1** with water was explored to see if water resulted in decomposition of **1**. Upon the addition of one drop of degassed water (55 equiv.) to **1** in C_6D_6, **1** was fully consumed and four new signals were observed in the ^{31}P{^{1}H} NMR spectrum (Figure 2.8). Additionally, the production of solids of various colours (white, black, and yellow) were evident after a few hours; these solids accumulated over a 24 h period. The product distribution seen in the ^{31}P{^{1}H} NMR spectrum changes only slightly between 10 min and 24 h; from 43 % (•), 30 % (•), 19 % (•), 8 % (•) to 51 % (•) 41 % (•) 8 % (•). The identity of these signals and solids formed were not further investigated. From these studies, it is clear that **1** was not stable to excess water as it was fully consumed upon addition, forming various coloured solids and new signals in the ^{31}P{^{1}H} NMR spectrum.

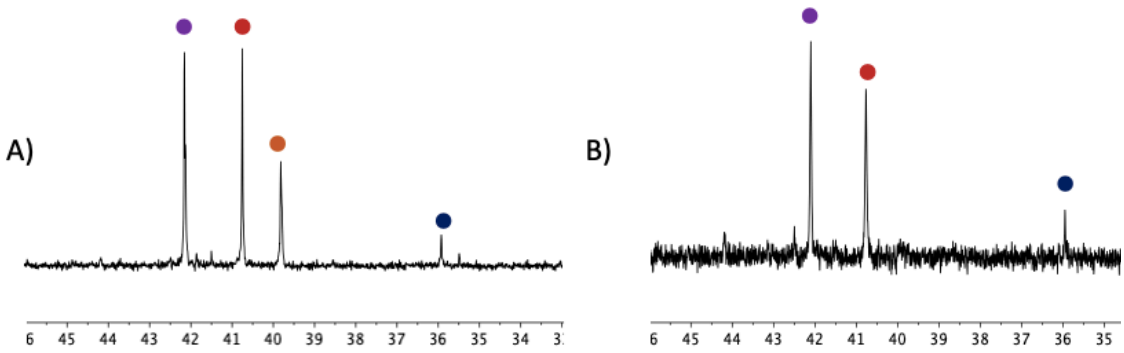

Figure 2.8: $^{31}P\{^{1}H\}$ NMR Spectrum (162 MHz, C_6D_6) 10 min (A) or 24 h (B) after H_2O was added to **1**. Signals Identified for $^{31}P\{^{1}H\}$ NMR δ = • 42.1, • 40.7, • 39.8, • 35.9; *In situ* consumption of **1** determined by relative integrations as no internal standard was utilised.

2.4 Activation of Dihydrogen

Complex **1** was treated with 1 atm of H_2 at room temperature and then heated to 38 ºC for 24 h in C_6D_6 which resulted in a black solution with solids, indicative of the formation of Pd black and decomposition (Scheme 2.8A). Complete consumption of **1** and production of numerous new signals were observed by $^{31}P\{^{1}H\}$ NMR spectroscopy (Figure A8). The ^{1}H NMR spectrum suggested the production of methane had occurred as a singlet at 0.15 ppm was observed (Figure 2.9A). Upon spiking the sample with methane (i.e., bubbling for 10 s) the signal increased, confirming methane production from H_2 and **1**. The ^{1}H-^{1}H COSY and the ^{1}H NMR spectrum showed the presence of an isopropyl unit, corresponding to the formation of H[**L1**] (Figure 2.9). The isopropyl signals were not consistent with free H[**L1**] ligand and so H[**L1**] was determined to still be bound to the Pd centre. Therefore, activation of H_2 by **1** likely occurred via metal-ligand cooperative heterolytic cleavage resulting in ligand protonation (H[**L1**]) and a Pd(II)-hydride species. The Pd(II)-hydride species then underwent reductive elimination to produce methane. This was expected as Pd(II)-hydride species are reactive and used for various transformations (e.g., hydrogenation).[83-89] No isolated Pd(II) compounds with cis or trans hydride and methyl groups have been found in the literature, but some have been computationally studied (e.g., Pd(II)-Me and R_3P-Pd(II)-Me hydrides),[89-91] indicating the proposed Pd(II)-Me hydride intermediate would be too unstable for isolation but may be useful in catalysis.

In comparison, examples of Pd(II) compounds with trans-disposed hydride and alkyl or aryl have been reported.[92,93]

In an effort to understand the reactivity of **1** with H_2 without competing reactivity of the Pd-Me functionality, a chloro analogue (**14**) was targeted. Upon exposure to H_2, **14** would presumably undergo similar ligand-metal cooperative activation of H_2 as proposed for **1**, without the possibility of reductive elimination of methane (Scheme 2.8B). The Pd(II) precursor, **13**, was chosen over $PdCl_2$(COD) due to concerns of generating the previously observed bisligated P^AzA Pd species (**4**). Upon attempted coordination of K[**L1**] to **13** in C_6D_6, **4** (47.7 ppm; 30%) and three minor new unidentified signals were observed by $^{31}P\{^1H\}$ NMR spectroscopy (Figure A9A). The reaction was repeated with both room temperature and cold THF in efforts to promote the formation of **14** over **4**. While **4** was not formed when using THF as a solvent, numerous unknown signals were observed in the $^{31}P\{^1H\}$ NMR spectrum, indicative of numerous products being formed (Figure A9B). Due to the presence of many species in solution it is possible that complex **14** was present but it was not confirmed. Thus, the synthesis of **14** via the addition of K[**L1**] to **13** was no longer explored.

The coordination of H[**L1**] to **13** to generate **15** was then explored, since deprotonation of **15** would afford **14** (Scheme 2.8C). Upon coordination of H[**L1**] to **13** in C_6D_6 or in THF numerous signals were observed by $^{31}P\{^1H\}$ NMR spectroscopy (Figure A10). Due to the presence of many species in solution it is possible that complex **15** was present but it was not confirmed. No further attempts to access **14** were performed as the coordination chemistry of H[**L1**] and K[**L1**] to **13** was complex and no single phosphorus signal could be isolated in high yield to permit isolation and characterisation.

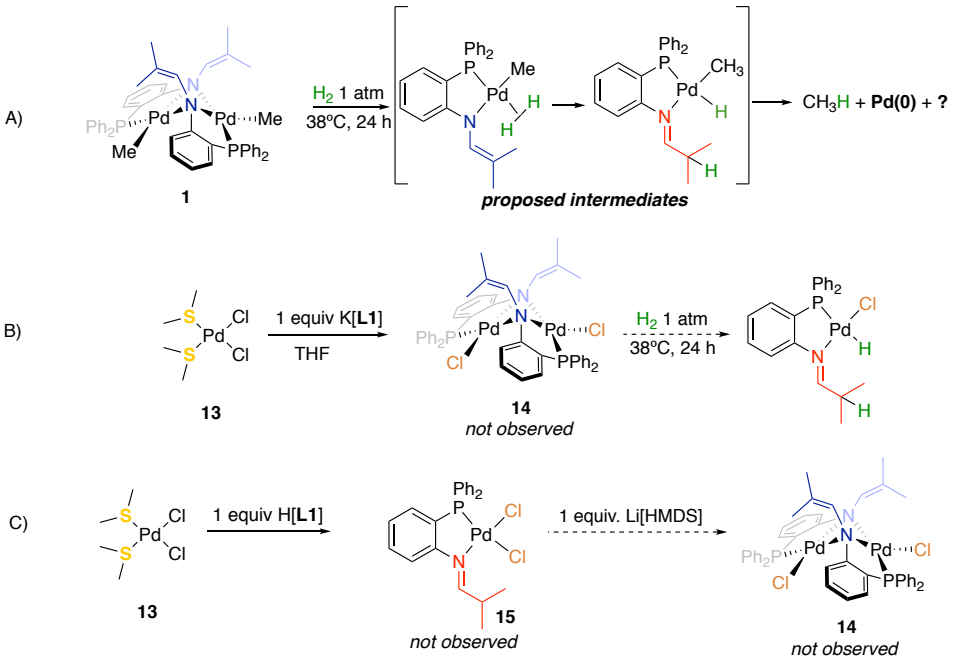

Scheme 2.8: A) The postulated mechanism of H_2 activation by **1** B) Proposed synthesis of **14** and strategy to confirm aforementioned possible H_2 activation by **1**. C) Additional approach to generate **14** by first synthesising a Pd-P^I precursor complex.

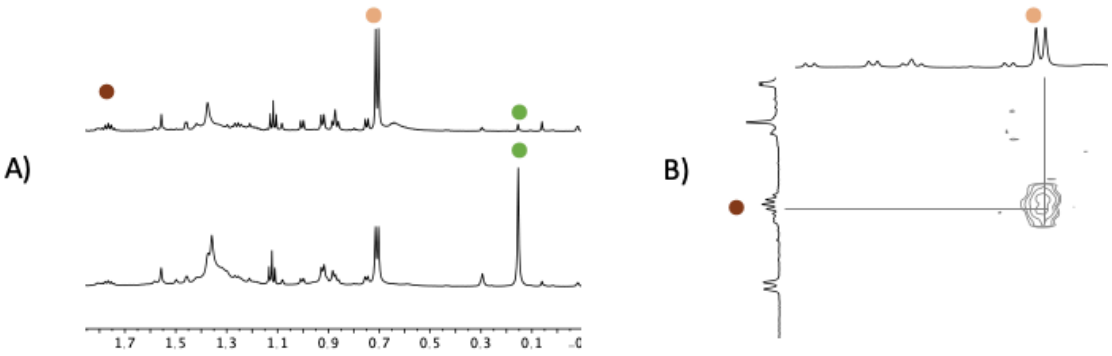

Figure 2.9: A) Section of the ^{1}H NMR spectrum (600 MHz, C_6D_6) 24 h after H_2 exposure to **1** (30 s) and heating at 38ºC (top) and after a spike of CH_4 (10 s) the solution (bottom). B) ^{1}H-^{1}H COSY 24 h after H_2 exposure to **1** (30 s) and heating at 38ºC. Signals indication in the ^{1}H NMR spectrum: • methine *H*, • isopropyl- C*H*$_3$, • C*H*$_4$

2.5 Activation of Dioxygen

2.5.1 Aerobic Oxidation of **1**

Complex **1** was treated with 1 atm of O_2 at room temperature, and after 24 h in C_6D_6 (Scheme 2.9), two new singlets in the $^{31}P\{^1H\}$ NMR spectrum evolved in a 2:1 ratio at 42.3 and 41.1 ppm that were assigned to **16a** and **16b**, respectively (Figure 2.10A). The aerobic oxidation of **1** could involve the Pd metal to yield a Pd-peroxo species or involve oxidation of the 1-azaallyl moiety. [9,18,26]Additionally, enamines (a N-C=C moiety) can undergo C-C or C-N bond cleavage to yield carbonyl, ketone, lactone, and ester compounds. [94-98]

The ^1H-^{31}P HMBC indicated the reaction mixture contained two distinct products, **16a** and **16b**; neither of the ^{31}P NMR signals for **16a** or **16b** correlated to the same ^1H NMR signal (Figure 2.10B). The ^1H NMR spectrum of **16a/b** has given insights into the possible products, however, the exact structures of **16a/b** are still unknown. Two doublets at 1.09 and –0.08 ppm were observed in the ^1H NMR spectrum that are consistent with Pd-Me signals for **16a**/**b** (Figure 2.10C). The small *J* coupling and chemical shift values were consistent with typical *cis* disposed R_3P-Pd-Me complexes.[99-101] In contrast, methyl peroxo (-PdOOCH_3) or methoxy (-PdOCH_3) Pd complexes in the literature have been observed Me protons between 3.50-4.10 ppm.[9,18,26] Which was suggestive that the aerobic oxidation of **1** did not occur through insertion into the Pd(II)-Me bond. To confirm that a Pd-peroxo species was not present, PPh_3 was added to a mixture **16a**/**b** (Scheme 2.9; path A). If $O{=}PPh_3$ was synthesised upon addition it would be indicative of a Pd peroxo (O_2^{-2}) species.[26] One equivalent (relative to **1**) of PPh_3 was added to a solution of **16a/b** in C_6D_6 and after 24 h at room temperature; there was no $O{=}PPh_3$ observed in the $^{31}P\{^1H\}$ NMR spectrum, suggesting that **16a/b** are not Pd peroxo species. A Pd(II)-O-O-Pd(II) dimer synthesised from a Pd(I)-Pd(I) dimer is known in the literature, but such a structure would not be an expected product from the aerobic oxidation of the Pd(II) dimer, **1**.[102]

A singlet at 1.55 ppm was in a 1.3:1 or 1.4:1 ratio with the Pd-Me signal for **16a** and **16b**, respectively. If the signal was the methyl groups of the 1-azaallyl moiety from **L1** for either **16a** or **16b** one would expect a ratio of 2:1. This singlet (1.55 ppm) did not correlate to anything in the ^1H-^1H COSY or the ^1H-^{31}P HMBC spectra (Figure 2.10B; A11). This was suggestive that the 1-azaallyl unit of **L1** was no longer intact in one of the products (**16a** or **16b**). In a reaction where **16a** was the major product (*vide infra*) the singlet (1.55

ppm) was a major signal in the ^{1}H NMR spectrum (Figure A12). Implying that this singlet was by-product of the synthesis of **16a**. The chemical shift of the singlet (1.55 ppm) was reminiscent of authentic acetone. Acetone could be a by-product of the synthesis of a Pd-formamide species (proposed **16a**) where C-C bond cleavage occurred after the insertion of O_2 into the 1-azaallyl unit of **L1** (**Int-1**; Scheme 2.9; pathway B).[94-98] There was some evidence that a Pd-formamide species was a product, as there was a singlet at 9.22 ppm in the ^{1}H NMR spectrum. A 1:3 ratio was expected for the aldehyde and Pd-Me groups, respectively; however, the singlet (9.22 ppm) integrated to 0.4 H relative to the Pd-Me signals (3 H) of **16a**. Additionally, 2:1 ratio of **16a** and acetone would be expected from the proposed reaction pathway; but a 1:1.3 ratio was experimentally observed. These two observations are not consistent the proposed structure of the Pd-formamide species from pathway B of Scheme 2.9.

The ^{1}H-^{1}H COSY revealed that a doublet at 0.71 ppm correlated to a small septet at 1.75 ppm that integrated 1:6 relative to one another (80% relative to **16a** or **b**), indicating the formation of an isopropyl unit. The isopropyl signals did not correlate to anything else in the ^{1}H-^{1}H COSY or the ^{1}H-^{31}P HMBC spectra (Figure 2.10B; A11). Notably, these signals match well with the ^{1}H NMR spectrum of authentic isobutylaldehyde in C_6D_6 where the methine H chemical shift is at 1.78 ppm and isopropyl methyl's at 0.71 ppm. This was suggestive that the aerobic oxidation of **1** resulted in a Pd complex with an isopropyl group and/or the formation of isobutylaldehyde. Since enamines are known to form ketones upon addition of O_2, perhaps a similar reaction occurred here.[94-98] A hydrogen transfer to *C2* and ketone formation at *C1* of the 1-azaallyl moiety to yield a Pd-amide complex would match the ^{1}H NMR data observed (Scheme 2.9; pathway C). This Pd-amide complex would be a possible structure for the second oxygenated product, **16b**. However, a possible mechanism to this product without a H^+ source is not well understood, as the literature suggested water as by-product of such a reaction.[98]

A final potential product of the activation of O_2 by **1** was a Pd superoxo (O_2^-) radical species.[25] However, complex **1** was almost fully converted to **16a**/**16b** (conv. 96 %) indicating that only diamagnetic compounds were formed upon activation of O_2 and that no radical species was present. The exact structures of **16a/b** are not clear from the experimental data collected. The ^{1}H NMR data suggested that insertion of O_2 into the 1-

azaallyl unit of **L1** had occurred and not the synthesis of a Pd-peroxo species. Thus far it is believed that the structures of **16a/b** are similar to the Pd-formamide and Pd-amide dimer complexes proposed in Scheme 2.9. Further work into the isolation of either **16a** or **16b** will aid in the structure elucidation without the added complications of a two-molecule system. And so, to understand the mechanism of O_2 activation by **1** and the role of the structural responsiveness of the P^AzA ligand, the isolation and complete structural characterisation of **16a** and/or **16b** is likely essential. However, first, the successful scale up of **1** is required.

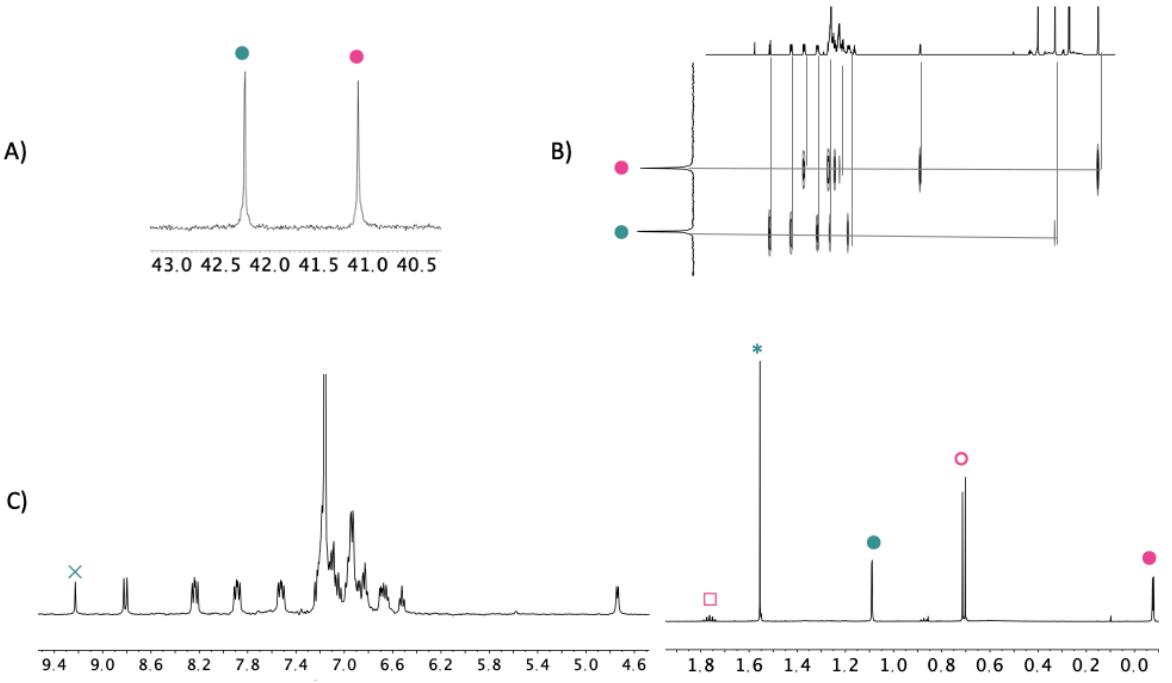

Figure 2.10: A) $^{31}P\{^{1}H\}$ NMR spectrum (162 MHz; C_6D_6; A), ^{1}H-^{31}P HMBC (^{1}H: 600 MHz, ^{31}P: 243 MHz, C_6D_6; B), and the ^{1}H NMR spectrum (400 MHz; C_6D_6; C) 24 h after **1** was exposed to 1 atm of O_2. $^{31}P\{^{1}H\}$ NMR signals identified δ = 42.3 (**16a**, •), 41.1 (**16b**, •); ^{1}H NMR signals identified δ = 9.22 (**16a**, aldehyde *H*?, ×, 0.5H), 1.75 (**16b**, methine *H*, □), 1.55 (s, acetone, ∗), 1.09 (**16a**, Pd-CH_3, •, $^{3}J_{P\text{-}H}$ = 1.3 Hz), 0.71 (**16b**, isopropyl-CH_3, d, •, *J* = 7.1 Hz), -0.08 (**16b**, Pd-CH_3, •, $^{3}J_{P\text{-}H}$ = 2.6 Hz)

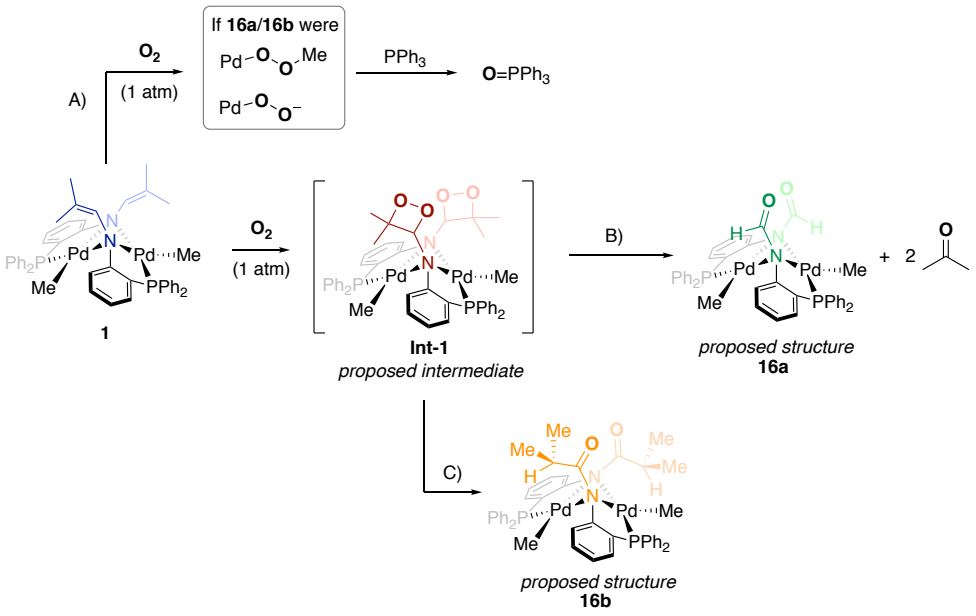

Scheme 2.9: Aerobic oxidation of **1** resulted in two distinct products **16a** and **16b** determined by $^{31}P\{^{1}H\}$ NMR spectroscopy. Possible products of included monomeric Pd-peroxo species (pathway A), a Pd-formamide complex and acetone (pathway B), and a Pd-amide complex (pathway C). Notably, if **16a**/**16b** were Pd peroxo species, then O=PPh_3 would be synthesised from PPh_3 (pathway A) but this was not observed.

2.5.2 Conditions Optimisation for the Reaction of **1** with Dioxygen

The aerobic oxidation of **1** was carried out under several conditions (e.g., solvent, additives, concentration, and temperature) to try to alter the ratio of **16a**/**16b**. First, the effect of the solvent (pyridine, THF, fluorobenzene, 1,4-dioxane, and toluene) on the aerobic oxidation of **1** was explored and the reactions were monitored by $^{31}P\{^{1}H\}$ NMR spectroscopy. When the Pd-P^AzA monomer, **2**, was exposed to O_2 in C_6D_6, **16a** and **16b** were produced in a 1.1:1 ratio, but a third major product was observed (Table 2.1, entry 2). In comparison, THF presented a similar ratio to C_6D_6 (2:1, **16a**:**16b**; Table 2.1, entry 3). The aerobic oxidation of **1** in fluorobenzene and 1,4-dioxane resulted in the synthesis **16a**/**16b** in a 0:6:1 or 1.1:1 ratio respectively, but a number of new products were also observed (Table 2.1, entries 4,5). Toluene, a slightly bulkier solvent than C_6D_6, favoured **16a** 9:1 (Table 2.1, entry 6). In general, the solvent chosen influenced oxidation products observed and for the synthesis of **16a**, toluene produced the best result. Complex **1** was exposed to O_2 in the presence of the radical trap, TEMPO$^{\bullet}$ (TEMPO$^{\bullet}$ = (2,2,6,6-tetramethylpiperidin-1-yl)oxyl), since O_2 activation by Pd can occur via a radical

mechanism.[18, 24, 103] A change in the **16a**:**16b** ratio from 2:1 to 15:1 was observed (Table 2.1 entry 7), suggesting that product **16b** was formed via a radical mechanism. At one equivalent of TEMPO• the formation of **16b** was suppressed; thus, higher equivalents of TEMPO• may allow for complete selectivity of **16a**. The reaction of **1** with O_2 was also done in the dark, where the ratio between species in solution remained the same as standard conditions (2:1, **16a**:**16b**; Table 2.1 Entry 8). Indicating that the radical mechanism of **16b** was not initiated by light, which has been seen previously in the literature for aerobic oxidation of Pd(II)-Me species by O_2.[9,61] The effect of concentration on the ratio of **16a**/**16b** in toluene was also tested. Under concentrated (47 mM) and dilute conditions (3.9 mM) **16a** was favoured 3:1 or 7:1, respectively (Table 2.1, entries 9,10). However, changes in concentration resulted in lower selectivity for **16a** (3:1 or 7:1 respectively) as compared to the standard concentration of 18 mM where a ratio of 9:1 for **16a**:**16b** was observed (Table 2.1, entry 6). Suggesting that concentration played a small role in selectivity for **16a** compared to solvent changes. Lastly, the addition of O_2 to **1** was done at –10 ºC, this yielded a 6:1 ratio of **16a**/**16b**, indicating that at colder temperatures the formation of **16a** was favoured (Table 2.1, entry 11). In fact, in most conditions, except for in fluorobenzene, **16a** formation was favoured over **16b**. Many attempts of crystallisation have been undertaken to isolate **16a** or **16b**, under inert and air atmosphere, but the decomposition of **16a** and **16b** occurred slowly over time likely due to trace amounts of H_2O. Upon independent addition of two drops of H_2O (109 equiv. relative to **1**) to **16a** and **16b** decomposition was observed (Figure A13). The aerobic oxidation of **1** in toluene or C_6D_6 in the presence of TEMPO• resulted in high selectivity for **16a**. The isolation of **16a** under these conditions is likely feasible, but, has not yet been explored as the scale up of **1** is still in progress.

Table 2.1 Attempted Isolation of **16a** or **16b** under Various Conditions.[a]

Entry	Solvent	Additive	Conc. (mM)	Conv. (%)	Yield of **16a**+**16b** (%)	**16a** (%)	**16b** (%)	**16a**:**16b**
1[b]	C_6D_6	n/a	18	>99	96	60	36	2 : 1
2	Pyridine	n/a	18	>99	>99	20	20	1.1 1
3	THF	n/a	18	>99	>99	78	22	4 :1
4	C_6H_5F	n/a	18	>99	>99	16	25	0.6 : 1
5	1,4-Dioxane	n/a	18	>99	>99	10	10	1.1 : 1
6[b]	Toluene	n/a	18	>99	73	66	7	9 : 1
7[b,c]	C_6D_6	TEMPO	18	>99	81	75	5	15 : 1
8	C_6D_6	Dark	18	>99	>99	67	33	2 : 1
9	Toluene	n/a	47	>99	>99	71	29	3 : 1
10	Toluene	n/a	3.9	>99	>99	88	12	7 : 1
11	Toluene	-10ºC	18	>99	>99	86	14	6 : 1

[a] Standard conditions: **1** exposed to 1 atm of O_2 at room temperature and the reaction was analyzed by $^{31}P\{^1H\}$ NMR spectroscopy after 24 h. [b] *In situ* consumption of **1** determined by integration of **1** relative to an internal standard ($O=PPh_3$) other are determined by relative integrations. [c] Reaction was analyzed by $^{31}P\{^1H\}$ spectroscopy after 48 h.

In summary, the activation of small molecules or E-H bonds by a Pd(II)-P^AzA complex, **1** was explored through small scale reactivity studies. These reactivity studies demonstrated that the P^AzA ligand was non-innocent ligand in reaction chemistry. The aerobic oxidation of **1** indicated that the P^AzA ligand was sensitive to O_2. In the future, oxygen environments should be avoided with **1** and likely other metal complexes of the P^AzA ligand. Reactivity studies with H_2 and E-H (organic acids) gave the most promising results. An open coordination site was available on Pd(II) as a result of the change in coordination mode from μ^2-N to κ^1-N and the generation of a Pd-P^I complex. This reactivity was promoted by how basic the P^AzA ligand was when bound μ^2-N to Pd(II). This MLC behaviour observed by **1** may be harnessed for future catalytic applications.

3 Synthesis and Characterisation of a 'Low Coordinate' Phosphine-1-Azaallyl Ru Complex

Chapter three covers the alternative synthesis route to a sought after "low coordinate" Ru-P^AzA complex (**5**). This new synthesis route involved a new Ru(II) complex (**6**) that had only two available coordination sites for the ligand to bind, this was proposed to limit coordination variability that had been previously observed when synthesising Ru(II)-P^AzA complexes. Furthermore, a Ru(II)-phosphine-imine precursor (**7**) was synthesised first, to enforce a κ^2-PN initially. This enforced that κ^2-PN coordination mode may avoid the synthesis of previously observed impurities upon synthesis of desired **5**.

3.1 Synthesis and Characterisation of a Ruthenium-Phosphine-Imine Precursor Complex (7)

3.1.1 Optimisation of the Synthesis of 7

The synthesis of **7** was optimised by conducting small-scale reactions (Scheme 3.1) where solvent (THF, Pyridine, 1,4-Dioxane, MeCN, and C_6H_6), temperature (45-120 ºC), concentration (3.7-30 mM), and time (0.15-18 h) were altered (Table 3.1). The first attempt to generate **7** involved heating a solution of **6** (20 mM) and H[**L1**] (1.5 equivalents) in THF at 66 ºC for 1 h (Entry 1). Conversion to **7** was 60% according to the $^{31}P\{^1H\}$ NMR spectrum where two new major signals were observed at 55.2 and 53.3 ppm in a 5.2:1 ratio, assigned as two conformational isomers of **7** (*vide infra*). In hopes of gaining a higher conversion to **7**, various small-scale experiments were conducted. First, the solvents pyridine, dioxane, and MeCN were tested (Entries 2-5) and each solvent was tested 10 ºC below its boiling point at a 30 mM concentration of **6**. Prior work in the group suggested **7** was unstable in chlorinated solvents ($CHCl_3$ and DCM) and when using toluene as a solvent **7** was not observed; thus, these solvents were not attempted here. Using the coordinating solvent pyridine full consumption of **6** was observed; but the yield of **7** was poor (30%) resulting in mostly unknown impurities (60%) and so this solvent was not tested again. Full consumption of **7** was not observed in 1,4-dioxane (90% conversion); however, a higher yield of **7** was achieved (70%) than in THF. In comparison, consumption of **6** in MeCN was only 70% at 1 h, likely due to poor solubility of **6** in MeCN. To circumvent solubility

issues, a more dilute reaction (3.7 mM of Ru) and a longer reaction time (24 h) in MeCN was attempted. Complete consumption of **6** was observed after 24 h; however, the yield of **7** was only 50%, identical to that observed using more concentrated conditions. The yield of **7** was low (50%) in MeCN and so this solvent was not tested further. THF was utilised in subsequent reactions due to the high yield of **7** (60%) and full consumption of **6** at a short reaction time. In an effort to promote the synthesis of **7** over other minor impurities, temperature was altered from the conditions in Entry 1 (Entries 6-7). At 80 ºC, an increased yield of **7** to 80% was observed. In comparison, at 45 ºC the yield of **7** (30%) decreased. To access higher temperatures, C_6D_6 was utilised as a non-coordinating and non-chlorinated solvent (Entry 8). Reaction at 95 ºC yielded 70% **7** and increasing the temperature further to 120 ºC resulted in a decreased yield of **7** (60%). Therefore, at higher temperatures **7** was not favoured or was unstable at high temperatures under reaction conditions (Entry 9). Due to the high yield of **7** (80%) in THF at 80 ºC, these conditions were used in all following reactions. Next, concentration of Ru was altered for the preparation of **7**. When the concentration was increased to 30 mM and only one equivalent of H[**L1**] was used, a yield of 80% **7** was achieved (Entry 10). However, lowering the concentration (4.2 mM) resulted in a decreased yield of **7** (50%), but longer a reaction time (2 h) favoured the synthesis of **7** (80%; Entries 11-12). These experiments indicated that a more concentrated (20 or 30 mM) solution at short a reaction time (1 h) favoured the formation of **7** and that an excess of H[**L1**] was not required. Lastly, the effect of time on the yield of **7** in THF (30 mM) at 80 ºC was tested (0.15-18 h; Entries 14-16). A reaction time of 15 min gave a maximum yield for **7** of 90% and longer reaction times only resulted in decomposition, since after 18 h the yield of **7** lowered to 40%. Therefore, based on these small-scale reactions, the optimum conditions for the synthesis of **7** (90% yield) are THF (30 mM) at 80 ºC for 15 min.

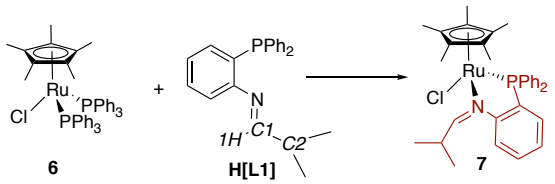

Scheme 3.1: General reaction scheme for the synthesis of **7**

Table 3.1: Optimisation of Reaction Conditions for the Synthesis of **7**.[a]

Entry	Solvent	Equiv. of H[**L1**]	**6** (mM)	Temp.(ºC)	Time (h)	% Conv.[b]	% **7**[c,d]
1	THF	1.5	20	66	1	>95	60
2	Pyridine	1	30	105	1	>95	30
3	Dioxane	1	30	90	1	90	70
4	MeCN	1	30	70	1	70	50
5	MeCN	1	3.7	70	24	>95	50
6	THF	1.5	20	80	1	>95	80
7	THF	1.5	20	45	1	40	30
8[e]	C_6H_6	1	30	95	1	>95	70
9	C_6H_6	1	20	120	1	>95	60
10	THF	1	30	80	1	>95	80
11	THF	1	4.2	80	1	>95	50
12	THF	1	4.2	80	2	>95	80
13	THF	1	30	80	0.25	>95	90
14	THF	1	30	80	0.50	>95	80
15	THF	1	30	80	5	>95	65
16	THF	1	30	80	18	>95	40

[a] H[**L1**] and **6** were reacted for the described time in either a pressure tube or NMR tube. Solvent was removed and all samples analyzed by $^{31}P\{^1H\}$ NMR spectroscopy in C_6D_6 (**7**: δ_p = 55.2 + 53.3). [b] % conversion = 100% – [integration of: **6**/ (integration of: (**6** + impurities + **7**)*100%] [c] % **7** = [(integration of: **7**)/(integration of: [**6**+ impurities + **7**]*100] [d] All $^{31}P\{^1H\}$ NMR spectra can be found in the appendix [e] Experiment was done in a J. Young tube

3.1.2 Synthesis and Characterisation of **7**

Scale-up of the synthesis of **7** was conducted under the optimal conditions, except a longer reaction time (1.5 h) was required for complete consumption of **6** and H[**L1**] to afford **7** (80 %). Notably, the two displaced PPh_3 ligands are completely converted to $O{=}PPh_3$ under reaction conditions. Initially, removal of $O{=}PPh_3$ was done by passing a solution of the crude product in diethyl ether through a silica plug. Recrystallisation of these crude products from a THF/pentane mixture afforded pure orange crystalline product (**7**; Figure 3.1A/B). However, upon scale-up the yield was consistently poor (~15%), due to the variable amounts of residual THF that influenced the solubility of **7** in diethyl ether and thus the effectiveness of the silica plug. Excess $MgCl_2$ has previously resulted in efficient

removal of $O{=}PPh_3$ by precipitation of a $MgCl_2$-$O{=}PPh_3$ complex.[104] Prior to the $MgCl_2$ treatment, minor impurities (Figure A14) observed as green solids were removed from crude **7** from a benzene/pentane precipitation. The crude reaction mixture was then dissolved in toluene with excess $MgCl_2$ with vigorous stirring at 30 ºC for 1.5 h proceeded by fine-filtration to achieve sufficient removal of $O{=}PPh_3$ and Mg-$O{=}PPh_3$. An additional benzene/pentane precipitation of green solids and then a recrystallisation afforded **7** in a suitable yield (52 %) at a 95% purity.

Performing a $MgCl_2$ treatment directly in THF (reaction mixture of **7**), resulted in production of major broad unidentified signal at 35 ppm in the $^{31}P\{^1H\}$ NMR spectrum and broaden signals for **7** (55.2 and 53.4 ppm). These results were suggestive that $MgCl_2$ or $O{=}PPh_3$-$MgCl_2$ were partially soluble in solution and were able to react with **7** and other impurities in THF; however, this undesired reactivity was limited in toluene.

An alternative procedure to remove $O{=}PPh_3$ using the iodo form of the Merifield Resin (MR-I) was attempted at room temperature in THF, but no $O{=}PPh_3$ was removed according to the $^{31}P\{^1H\}$ NMR spectrum. Further synthetic alterations (i.e., heating or increased equivalents of MR-I) have previously proven to aid in the removal of PCy_3 from reaction mixtures in THF.[105] Additionally, MR-I has been shown to be efficient with both $O{=}PPh_3$ and PPh_3 removal.[106] Due to time constraints, removal of $O{=}PPh_3$ was done using a $MgCl_2$/toluene treatment; however, this may be a fruitful path to gain high yield of pure **7**.

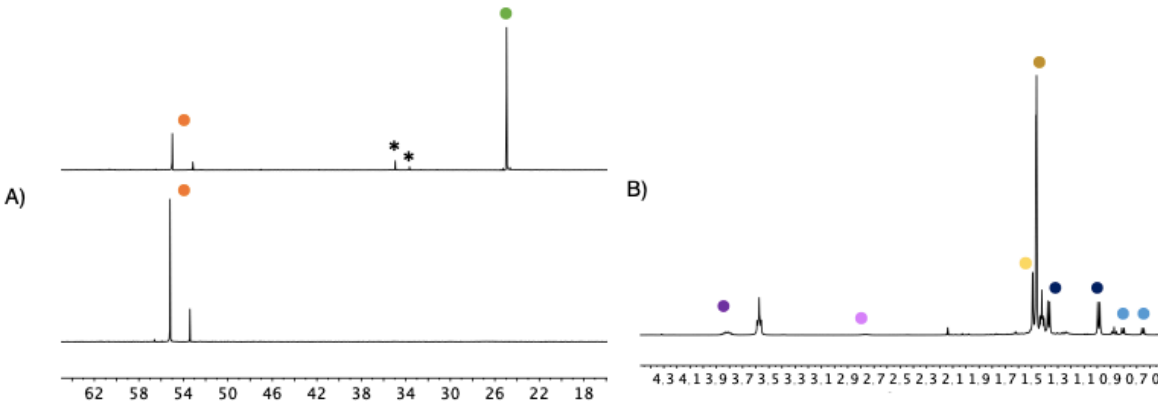

Figure 3.1: A) The $^{31}P\{^{1}H\}$ NMR (162 MHz, C_6D_6) after H[**L1**] and **6** stirred at 80 ºC in THF (top) and after isolation of **7** (bottom). B) Alkyl region of the ^{1}H NMR (400 MHz, C_6D_6) of isolated **7**. $^{31}P\{^{1}H\}$ NMR signals identified: **7** (●), $OPPh_3$ (●); ^{1}H NMR signals identified: Major Cp*C*H*$_3$ (●), Minor Cp*C*H*$_3$ (●), Major isopropyl-C*H*$_3$ (●), Minor isopropyl-C*H*$_3$ (●), Major methine-*H* (●), Minor methine-*H*(●)

Isolated **7** was observed as two configurational isomers (*vide infra*); however, the discussion here will focus on the spectroscopic data of the major species (55.2 ppm; Figure 3.1A/B). As previously mentioned, the chemical shift of the $^{31}P\{^{1}H\}$ NMR signals for **7** observed are consistent with H[**L1**] coordination (Figure 3.1B).[107,108] The ^{1}H NMR spectrum demonstrated a Cp* signal as a doublet due to ^{31}P-^{1}H coupling between the methyl's of Cp* and H[**L1**] (Figure 3.1B; ^{1}H-^{31}P HMBC Figure A15). The isopropyl methyl groups and the methine of H[**L1**] are shifted in the ^{1}H NMR spectrum indicative of retention and coordination of the imine functionality.[71,72] Correlation spectroscopy (^{1}H-^{1}H COSY Figure A16) aided in the assignment of *H1* at 7.61 ppm, which was consistent with literature values for a related Ru-P^I complex. Additionally, the $^{13}C\{^{1}H\}$ NMR signals of *C1* and *C2* (183.5 and 37.2 ppm, respectively) corresponded with previously observed H[**L1**] bound to Pd and Ru (Figure A17). MALDI-MS confirmed the expected chemical composition demonstrating an isotopic pattern consistent with [$C_{23}H_{37}ClNPRu$] with a *m/z* = 603.12 (calculated: *m/z* = 603.14).[107] Additionally, the IR spectrum matched that of other H[**L1**]-Pd or Ru compounds (Figure A18).[71,72] Lastly, the solid-state structure of **7** was confirmed via X-ray crystallography where N-C1 length was found to be 1.332 Å, consistent with an imine functionality (Figure 3.2; note image is labelled N1-C17).[71,72] The solid state structure of **7** demonstrated a weak hydrogen bond (Cl1···H = 3.400 Å, Cl-H-C18 = 115.5º) between the chloride (Cl1) and methine proton on *C2* (image has labelled C18).[71]

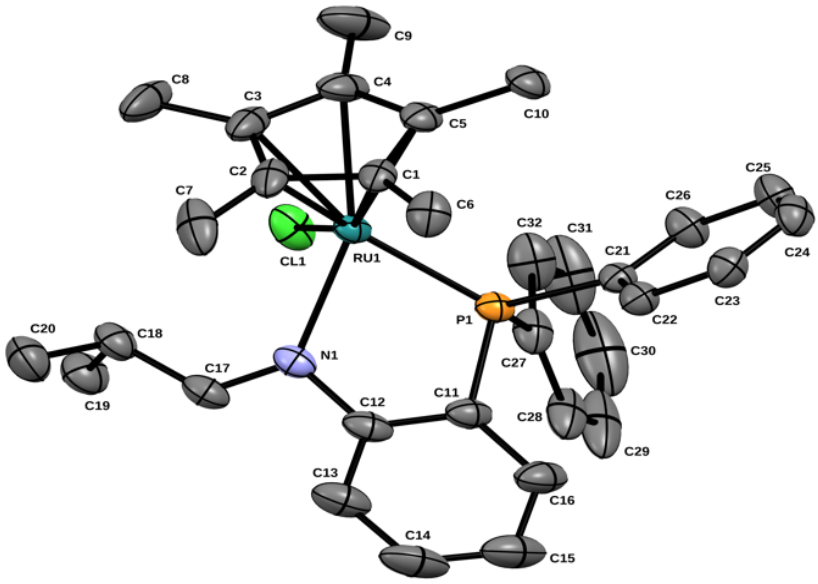

Figure 3.2: Displacement Ellipsoid (50% probability) plot of **7**. Where all hydrogen atoms have been omitted for clarity. Selected bond distance (Å) N1-C17 1.332, C18-Cl1 3.400; Selected bond angles (º): Cl1-H-C18 115.5

3.1.3 Configurational Isomers of **7**

The isolated orange crystalline solid, **7**, consistently presented two signals at 55.2 and 53.2 ppm in a 5.4:1 ratio in the $^{31}P\{^{1}H\}$ NMR spectrum. These two configurational isomers were also observed in the ^{1}H NMR spectrum of **7** demonstrated by two sets of Cp* and isopropyl methyl signals in a similar ratio, which indicated that the two species were structurally closely related. The observed ratio between major and minor species changed to 12.1:1 in CD_3CN, which was indicative of an equilibrium.[108] Variable temperature NMR spectroscopy was used to confirm an equilibrium between the major (55.2 ppm) and minor (53.4 ppm) species in solution. Upon increasing the temperature from 0 to 100 ºC the two $^{31}P\{^{1}H\}$ NMR signals began to converge in chemical shift and the ratio between minor and major species got closer to 1:1, which was characteristic of a temperature-dependent equilibrium (Figure 3.3A).[108] Similar behaviour was also observed by ^{1}H NMR spectroscopy and coalescence of Cp* signals were readily observed but coalescence of the methine-H and isopropyl methyl signals was less obvious (Figure 3.3B).

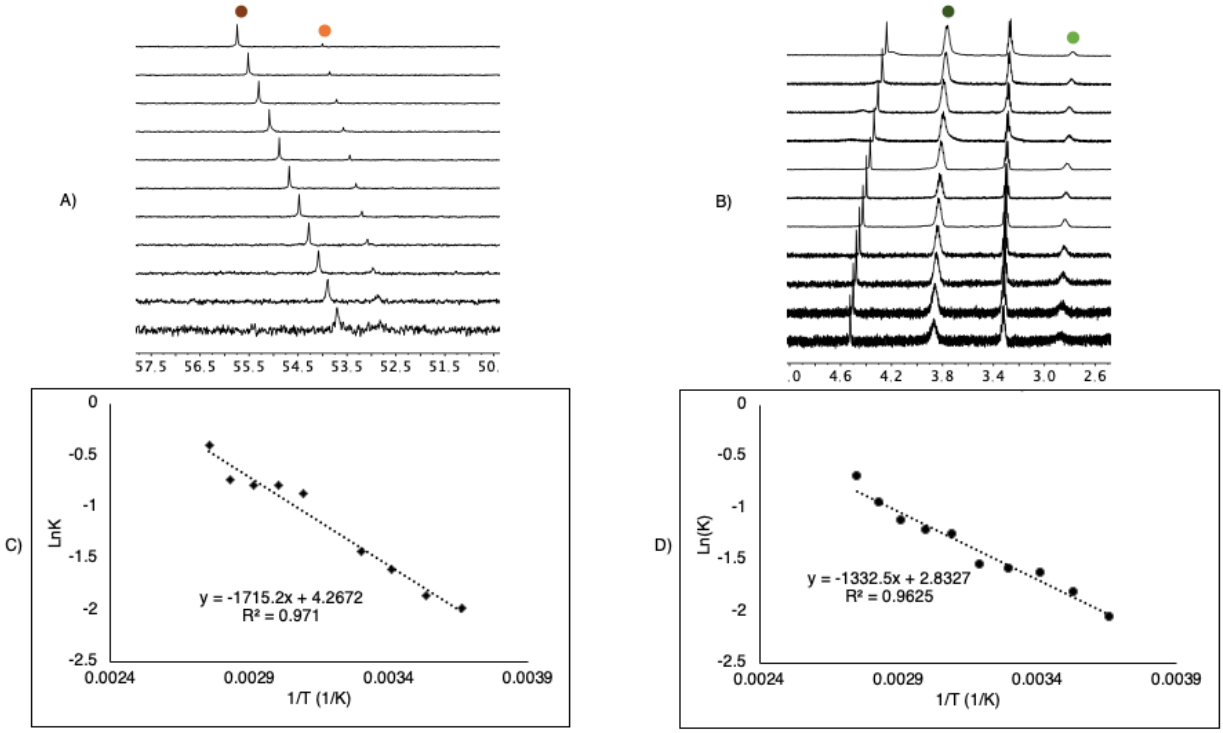

Figure 3.3: A) $^{31}P\{^{1}H\}$ NMR (243 MHz, Toluene-d_8) spectra of **7** from 0 (top) to 100 ºC (bottom) with spectra acquired at 10 ºC intervals. B) A section of the ^{1}H NMR spectra (600 MHz, Toluene-d_8) of **7** from 0 (top) to 100 ºC (bottom) with spectra acquired at 10 ºC intervals. C) Van't Hoff plot derived from $^{31}P\{^{1}H\}$ NMR integration values between major and minor signals. D) Van't Hoff plot derived from ^{1}H NMR integration values between major and minor methine H H[**L1**] signals. $^{31}P\{^{1}H\}$ NMR signals identified: ***Z*-7** (●); ***E*-7** (●); ^{1}H NMR signals identified: ***Z*-7** methine-*H* (●); ***E*-7** methine-*H* (●)

The ^{1}H NMR spectrum of **7** demonstrated a de-symmetrisation of the isopropyl methyl signals of Ru-bound H[**L1**] for both the major and minor species. This observation led to the hypothesis that the iso-propyl arm of H[**L1**] was constricted in either the *E* or *Z* configurational isomers as a result of ligand coordination (Scheme 3.2A). The major species of **7** (55.2 ppm) was found with a methine proton at 3.82 ppm while the minor was at 2.76 ppm. The crystal structure of **7** confirmed the major product was a *Z*-imine isomer or ***Z*-7** where methine H of H[**L1**] was in close proximity to the Ru bound Cl. The close proximity allowed for Cl···H interactions to occur resulting in the observed downfield shift of the methine H for the major species. The Cl···H interaction has also been previously observed in a Pd-H[**L1**] complex where the methine H of H[**L1**] was found at 4.19 ppm in $CDCl_3$ (Scheme 3.2B).[72] In comparison, the minor species would be the *E*-imine isomer or

E*-7** where the methine H was pointed away from the Cl and toward the backbone of H[**L1**]. In this case it would be unlikely that Cl-H interactions could occur, which is consistent with a more upfield location for the methine at 2.76 ppm. The ***E*-7** species would have more steric clash between the aromatic ring of H[**L1**] and isopropyl group and thus more unfavourable than ***Z*-7**, which was always observed as the major product experimentally (Scheme 3.2A). The thermodynamic parameters for the proposed unimolecular equilibrium of ***Z*-7**/E*-7** (ΔG, ΔH, and ΔS) were calculated from van't Hoff plots generated by integrations of ***Z*-7** and ***E*-7** (from both $^{31}P\{^{1}H\}$ and ^{1}H NMR spectra) at various temperatures (0 to 100 ºC).[109] The Gibbs free energy for the equilibrium of **7** was found to be ΔG_{avg} (25 ºC) = –21.5 ± 4.8 kJ mol^{-1} which agreed well with the experimentally observed $^{31}P\{^{1}H\}$ NMR spectra of **7** as ***Z*-7** and ***E*-7** were always both experimentally present. The change in enthalpy was calculated to be ΔH_{avg} = –12.7 ± 2.2 kJ mol^{-1}, this value is indicative that this equilibrium between ***Z*-7** and ***E*-7** is enthalpically driven. Lastly, the value calculated for ΔS was found to be ΔS_{avg} = 29.5 ± 8.4 J K^{-1} mol^{-1}. Typically, the entropy of reaction for a unimolecular equilibrium is ~ 0 J K^{-1} mol^{-1} as one reactant molecule is converted to one product molecule.[110] Due to the nature of the proposed equilibrium a value of 0 J K^{-1} mol^{-1} would not be expected for ***E*-7**/***Z*-7**, since the structure of ***Z*-7** was more ordered due to interaction between Cl and the methine H of H[**L1**] than ***E*-7** and so a small positive ΔS was expected. Notably, the value is much smaller than that generally expected from reactions in which one reactant is being converted into two products (A + B → C; ΔS^{o} = ~ 125.5 J K^{-1} mol^{-1}),[110] and so the calculated value of ΔS_{avg} (29.5 ± 8.4 J K^{-1} mol^{-1}) was supportive of the proposed ***E*-7**/***Z*-7** equilibrium.

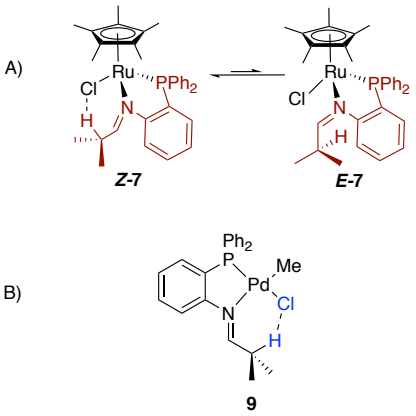

Scheme 3.2: A) Proposed equilibrium of **7** between ***Z*-7** (80%) and ***E*-7** (20%) B) Previously synthesized Pd-H[**L1**] (**9**) species with proposed methine H-Cl interactions.[71]

3.4 Synthesis, Characterisation, and Reactivity of Ru-P^AzA Complexes

3.4.1 Synthesis and Characterisation of **8**

Complex **8** was synthesised via the deprotonation of the phosphine-imine precursor **7** with excess Li[HMDS] and excess L-donor (pyridine; Scheme 3.3). The crude reaction mixture in the presence of excess pyridine showed two sharp singlets in the $^{31}P\{^{1}H\}$ NMR spectrum at 69.4 and 65.9 ppm observed in a 1:4 ratio (Figure A19). The more upfield signal corresponded to complex **8**, which could be easily isolated as a bright orange solid (Figure 3.4). Once **8** was dissolved in solvent without excess pyridine no $^{31}P\{^{1}H\}$ NMR signal could be detected. Thus, all NMR spectra collected of **8** had excess of pyridine (2 drops) added. The ^{1}H NMR spectrum of **8** showed deprotonation of the methine proton, *H2*, of **7**, which was indicative of the formation of a 1-azaallyl unit. The upfield chemical shift of *H1* (6.41 ppm) in isolated **8** from that of **7** (*H1*: 7.61 ppm) further confirmed synthesis of a Ru-P^AzA complex.[71,72] A 2D ^{1}H-^{13}C HMBC NMR experiment revealed *C2* to be located at 115.6 ppm, which was consistent with literature κ^{1}-N bound 1-azaallyl complexes (66.3-114.8 ppm).[111-115] X-ray quality crystals were not obtained because **8** was not stable in solution over time at room or cold temperatures.

Previously, MeCN was used as the L-donor to yield an MeCN complex, **N** (Scheme 1.19). Reaction mixtures of **N** were observed with broad signals in the NMR spectra unless CD_3CN was used as the NMR solvent. These results implied that a large excess of MeCN was required to form **N**. When dissolving proposed **N** in CD_3CN a colour change from

bright orange to dark brown and a number of $^{31}P\{^{1}H\}$ NMR signals were observed (Figure A20). These unidentified signals were never observed when using pyridine and only a small excess (five equivalents, *vide infra*) was required to observe good quality NMR spectra of **8**. Therefore, subsequent experiments always used pyridine as the L-donor for NMR analysis and synthesis of **5**.

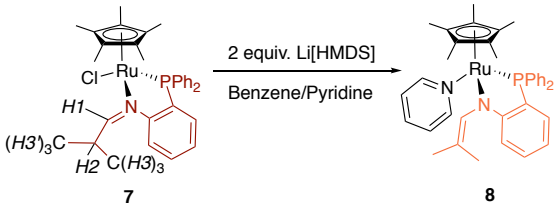

Scheme 3.3: Synthesis of **8** via the deprotonation of **7** and proposed L-donor (pyridine) equilibrium.

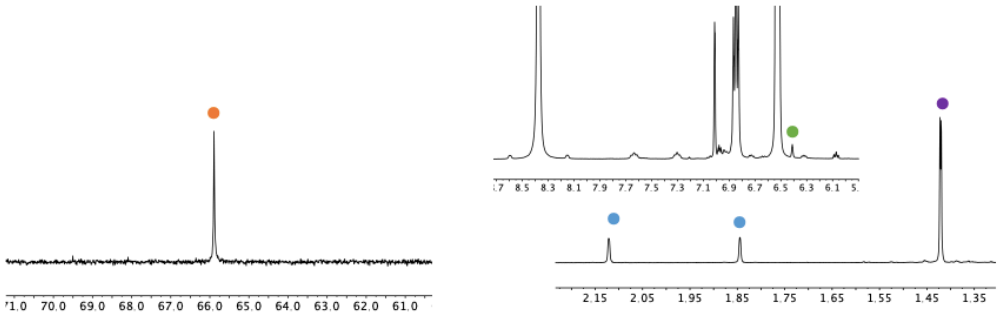

Figure 3.4: $^{31}P\{^{1}H\}$ NMR spectra (243 MHz; left) and ^{1}H NMR spectra (600 MHz; right) of **8** (C_6D_6) Signals indicated: • Cp*Me-*H*; • Azaallyl Me's-*H3*; • Azaallyl H-*H2;* • P of **8**

3.4.2 Synthesis and Characterisation of **5**

Once **8** was isolated as an orange solid, it was dissolved in a non-coordinating non-chlorinated solvent (i.e., benzene), and drastic colour change from orange to dark green was observed and removal of solvent afforded a dark brown solid (Scheme 3.4). The ^{1}H NMR spectrum in C_6D_6 without added pyridine revealed a number of things: 1) that pyridine was no longer present; 2) broad aromatic signals for **L1**; and a 3) relatively sharp signals for the 1-azaallyl unit (*H1, H3/H3'*) of **L1** and the Cp* ligand (Figure 3.5). No signal

was observed in $^{31}P\{^{1}H\}$ NMR spectrum at room temperature (Figure 3.5). The MALDI-MS spectrum indicated a *m/z* of 567.13, consistent with the expected *m/z* for the molecular cation of **5** (calc *m/z*: 567.16).[107] The IR spectrum of solid-state **5** showed disappearance of the proposed N=C stretch of **7** and the absorptions observed were consistent with a previously synthesised Ru-P^AzA complex (Figure A18;A21).[72] The broad signals detected in the aromatic region of the ^{1}H NMR spectrum and no signal in the $^{31}P\{^{1}H\}$ NMR spectrum was suggestive that **5** existed as multiple species in an equilibrium.[108] The 1-azaallyl unit of **L1** could bind in three fashions (Scheme 3.4). Complex **5a**/**5a′**, where the π-system of azaallyl unit of **L1** was bound in a η^3-NCC coordination mode, which can bind through the two different faces. In complex **5a**/**5a′**, the 1-azaallyl moiety of **L1** could then partially dissociate from the metal to give a κ^1-N coordination mode and provide an open coordination site in complex **5b**. A similar equilibrium was proposed by Lappert *et al* for a Ni-1-azaallyl complex (Scheme 1.15).[67] The $^{13}C\{^{1}H\}$ NMR resonance of *C2* was of interest to confirm the identity of **5a**/**5a′** and **5b** at room temperature.[72] The ^{1}H-$^{13}C\{^{1}H\}$ HMBC NMR spectra of **5** at room temperature demonstrated no correlations from *H1*; however, *H3*/*H3′* correlated with resonances at 139.8 and 118.1 ppm, *C1* and *C2,* respectively (Figure A22). Experimental resonances for averaged *C1* and *C2* suggested **5b** was present at room temperature as literature κ^1-N bound azaallyl complexes have *C1* and *C2* resonances can be found between 149.8-187.6 ppm or 66.3-114.8 ppm respectively.[111-115] Therefore, at room temperature the equilibrium of **5** was proposed to lie toward **5b** where the 1-azaallyl unit of **L1** was bound κ^1-N to Ru. VT NMR spectroscopy was utilised to attempt to trap the equilibrium complexes of **5** (Figure A23).[108] Complex **5** was cooled in toluene to −50 °C where sharp signals were observed in both the $^{31}P\{^{1}H\}$ and ^{1}H NMR spectra (Figure 3.5 & 3.6 & A23). At −50 °C only one singlet was seen in the $^{31}P\{^{1}H\}$ NMR spectrum indictive that only one Ru-species was trapped at low temperature. Cold temperature 2D NMR experiments revealed that *C2* was found at 115.2 ppm, consistent with literature compounds that have κ^1-N bound 1-azaallyl ligands (Figure A24).[111-115] The $^{31}P\{^{1}H\}$ and ^{1}H NMR data were suggestive that the proposed low-coordinate Ru complex (**5b**) was favoured over **5a**/**5a′** at cold temperatures. Re-warming proposed **5b** at high concentrations (> 20 mM)

from –50 to 25 °C re-introduced the broad signals in the ^{1}H and $^{31}P\{^{1}H\}$ NMR spectra, suggesting that the equilibrium was re-introduced at room temperature (Figure A25).

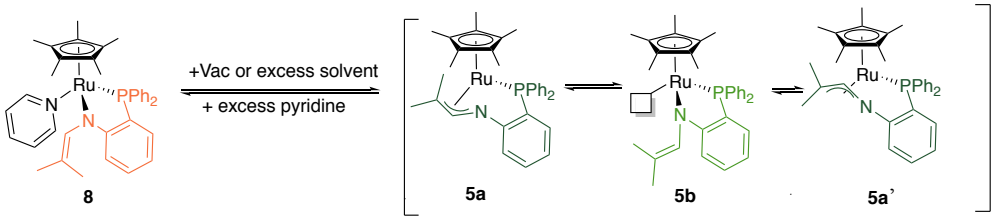

Scheme 3.4: Synthesis and proposed equilibrium of **5**

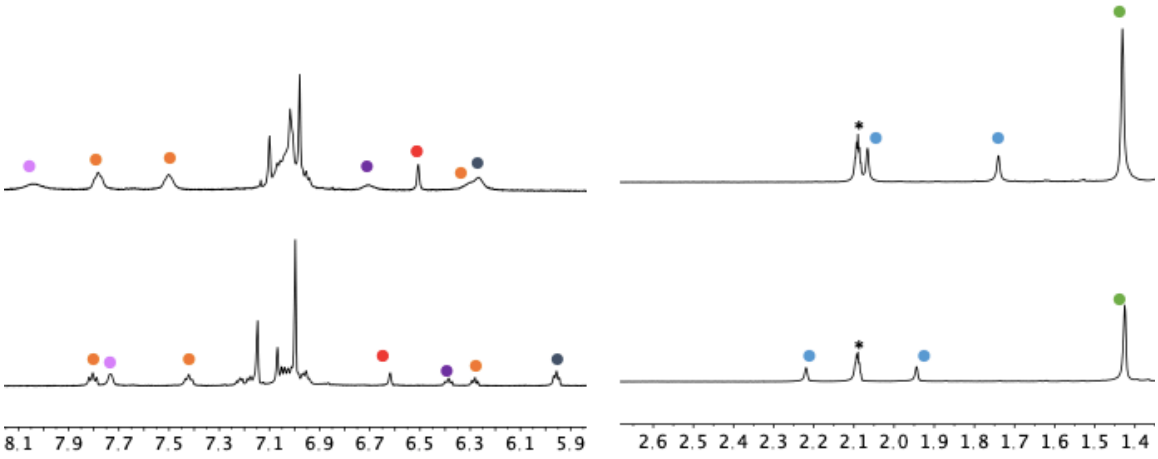

Figure 3.5: ^{1}H NMR spectra (600 MHz) of **5** at room temperature (top) and at –50 °C (bottom; toluene-d_8). Signals indicated: • Cp*Me-*H*; • Azaallyl Me's-*H3's*; • Azaallyl H-*H1*; • PPh-*H*; • L1-*ArH*; • L1-*ArH*; • L1-*ArH*; * toluene

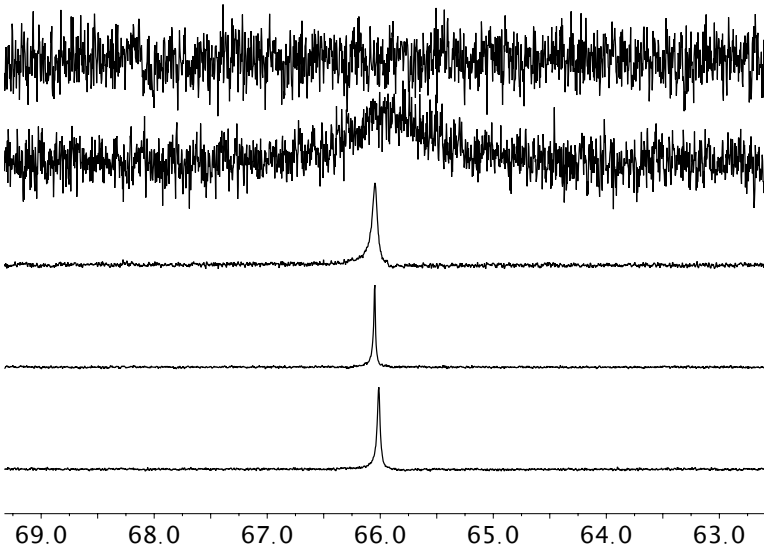

Figure 3.6: $^{31}P\{^{1}H\}$ NMR spectrum (243 MHz) of **5** from 25 (top) to −70 °C (bottom; toluene-d_8).

3.4.3 UV-vis Studies of **5**, **7**, and **8**

The UV-vis spectra were acquired for **5**, **7**, and **8** at various concentrations (Figure 3.7; Figure A26). The ε_{max} was calculated from these plots to gain insight into the coordination environment, and the d-d or charge transfer electronic transitions.[116] The Ru-P^I (**7**) complex was a weak orange colour with a λ_{max} at 723 nm, and a ε_{max} of 126 ± 10 L mol^{-1} cm^{-1} consistent with expected weak d-d transitions.[116] In comparison, **8** was a bright orange colour with a λ_{max} at 411 nm and a ε_{max} of 3530 ± 157 L mol^{-1} cm^{-1} consistent with a weak ligand-to-metal or metal-to-ligand charge transfer transition (LMCT/MLCT).[116] Without pyridine, **5** was observed as dark green solution with a λ_{max} at 630 nm and a ε_{max} of 551 ± 55 L mol^{-1} cm^{-1}, consistent d-d transitions where some p and d orbital mixing occurred to yield a more intense colour than observed by **7**.[116] Computational calculations will aid in assignment of the observed d-d transition.

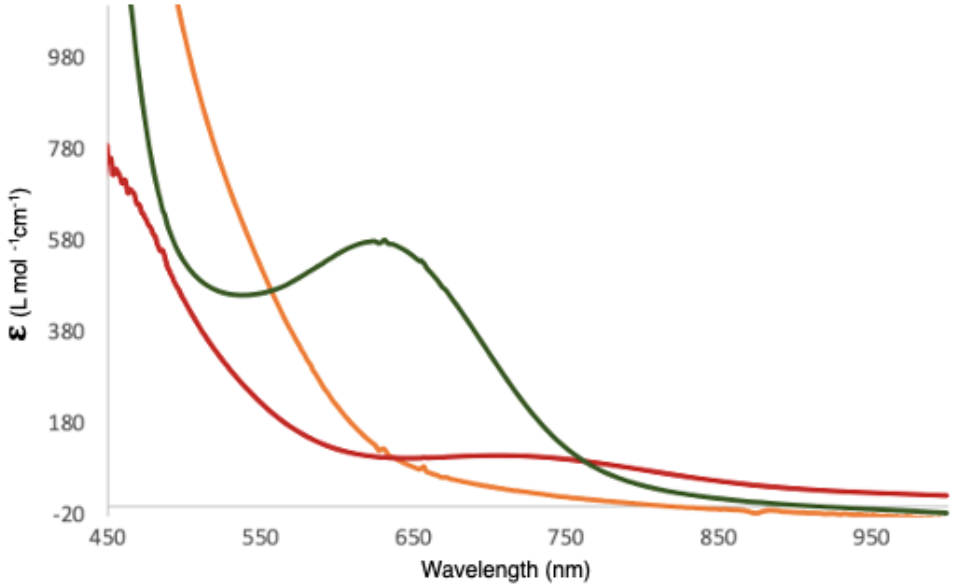

Figure 3.7: Plot of ε (L mol^{-1} cm^{-1}) vs the wavelength (nm) of **8** (0.3 mM; orange line), **7** (4.0 mM; red line), and **5** (1.5 mM; green line). Perturbations in the UV-vis spectrum are caused from data collection and represents experimental differences in absorbance readings at a specific wavelength (absorbance were collected at every wavelength 450 – 1000 at increments of one (e.g., 450,451…).

A titration of pyridine to a solution of **5** was conducted and observed by UV-Vis spectroscopy. Five equivalents of pyridine were required for full colour change from green to orange indicative of the change in coordination mode of the 1-azaallyl unit (η^3-NCC to κ^1-N) and subsequent coordination of pyridine (Figure 3.8). Over the course of the titration a reduction in absorption at 640 nm for **5** and an isosbestic point at 530 nm was observed, indicative of clean one-to-one reaction without any observed intermediates.[116] From the pyridine titration data, the K_{eq} between the reaction of **5** to **8** was calculated to be 0.11 at 25 ºC (Figure A27 and equation derivation in appendix).[117] The small K_{eq} indicated the reaction favoured the reactants (**5**) over the formation of the product (**8**) at equilibrium conditions.[118] This was consistent with experimental observations that required the addition of an excess of pyridine to **5** to yield **8**.

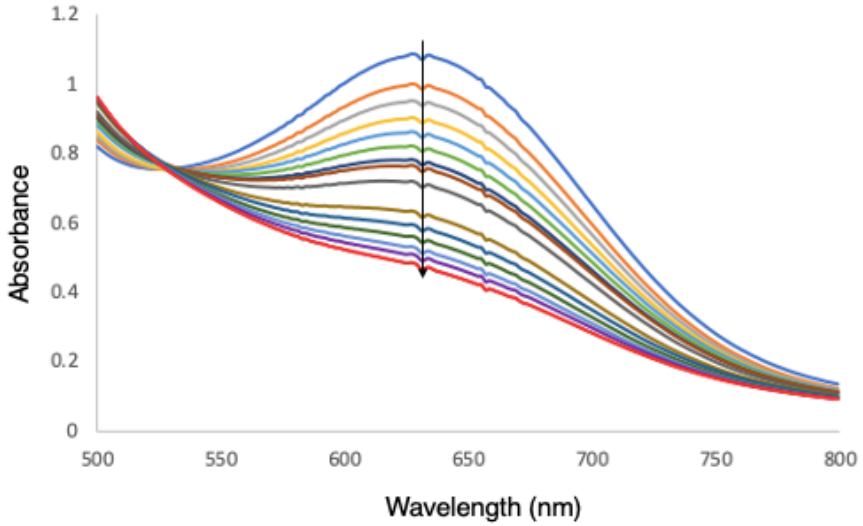

Figure 3.8: UV-vis spectra of the titration of five equivalents of pyridine to a 1.5 mM solution of **5**. Lines indicated: blue to grey one to two equivalents (0.25 equivalent intervals) and grey to red was two to five equivalents (0.5 equivalent intervals). Arrow was added to demonstrate the change in absorbance observed from **5** to **8** after adding various amounts of pyridine**.** Perturbations in the UV-vis spectrum are caused from data collection and represents experimental differences in absorbance readings at a specific wavelength (absorbance were collected at every wavelength 450 – 1000 at increments of one (e.g., 450,451…).

VT UV-vis of **5** (1.5 mM or 0.75 mM) from 25 to −50 ºC was conducted. At both concentrations a colour change from green to orange was observed, which corresponded to a decrease in absorption at 650 nm and an increase at 405 nm (Figure 3.9). The UV-vis spectra of cooling **5** to −50 ºC depicted similar absorption trends (from green to orange) to that of the pyridine titration to **5** at room temperature. This was not expected as there was no exogenous Lewis base present in which the azaallyl unit of **L1** was proposed to change coordination mode from η^3-NCC to κ^1-N to yield this orange colour. The VT NMR data indicated the synthesis of **5b** at cold temperatures, but the generation of orange complex was not consistent with the diagnostic blue colour of other 16-electron $RuCp^*$ complexes.[64] Furthermore, the decrease in absorption was concentration-dependent (Figure 3.7). Cooling a 1.5 mM solution of **5** from 25 to 0 ºC gave a change in absorption (Δ_{abs}) of 0.2447 at λ_{max} 650 nm, while a 0.75 mM solution of **5** had only a Δ_{abs} of 0.1043 over the same temperature range. Increasing the concentration by a factor of two almost doubled the absorption change observed. This suggested the concentration of Ru influenced the synthesis of this new

orange species that was favoured at cold temperatures. In other terms, cooling resulted in a Ru dimer, **17** (Scheme 3.5), where **L1** was in the a μ-(κ^1-P;κ^2-N) coordination mode, like the Pd-P^AzA dimer, **1**. This assignment would be consistent with the observed cold temperature NMR data that indicated only one Ru-**L1** species was present and that *C2* of the azaallyl unit was not involved in a metal-ligand bond. At cold temperature, the equilibrium between **5b** to **5a** and/or **5a′** would be slower, because heat would no longer be present to provide energy to convert between the three species at the same rapid rate. If **5b** was still not stable at cold temperature and another molecule of **5b** was in close proximity the nitrogen atoms of the 1-azaallyl unit could bind to the available coordination site of the Ru atoms to form **17**.

Warming 1.5- or 0.75-mM solution of **5** from –50 ºC to 25 ºC did not result in a colour change from orange to green, suggestive that an irreversible process had occurred. The $^{31}P\{^1H\}$ NMR spectrum of these UV-vis samples demonstrated proposed **17** at 68.0 ppm and a number of decomposition products (35-22 ppm) in a ratio of 1:8 (Figure 3.10). These decomposition products found in the $^{31}P\{^1H\}$ NMR spectrum have been observed from crystallisation attempts of **8** both at room and cold temperatures. Clearly the reaction chemistry between **5** and **17** was more complex at low concentrations (>1.5 mM; UV-vis conditions) than that at high concentrations (>29 mM; NMR conditions). It is possible that decomposition pathways are more prominent at low concentrations was due to the number of other signals observed by $^{31}P\{^1H\}$ NMR spectrum of UV-vis samples and only one signal observed at NMR concentrations (>29 mM).

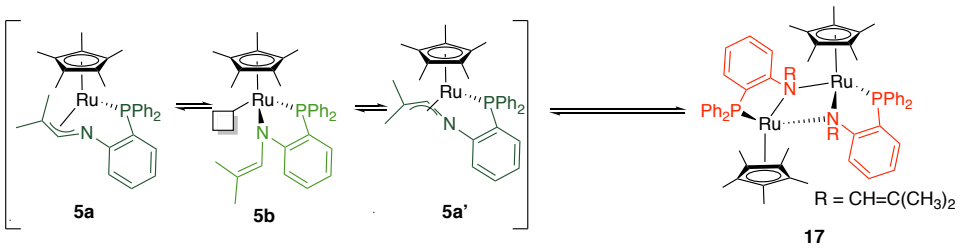

Scheme 3.5: Proposed equilibrium of **5** and **17** and possible decomposition pathways

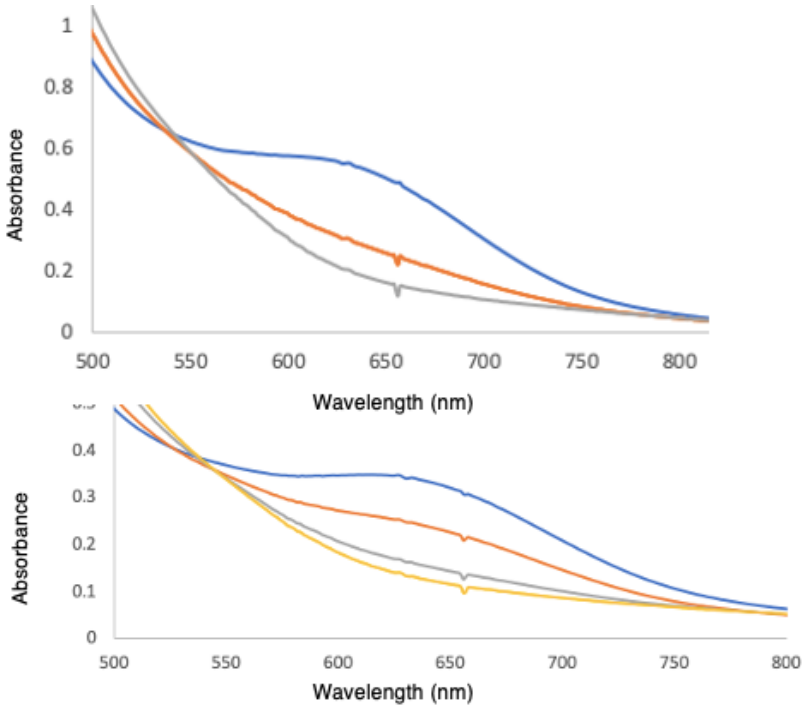

Figure 3.9: UV-Vis spectra of cooling **5** in toluene from 25 to – 50 ºC at 1.5 (top) and 0.75 mM (bottom). Lines: Blue; 25 ºC, orange; 0 ºC, grey; – 25 ºC, yellow; – 50 ºC; Perturbations in the UV-vis spectrum are caused from data collection and represents experimental differences in absorbance readings at a specific wavelength (absorbance were collected at every wavelength 450 – 1000 at increments of one (e.g., 450,451…).

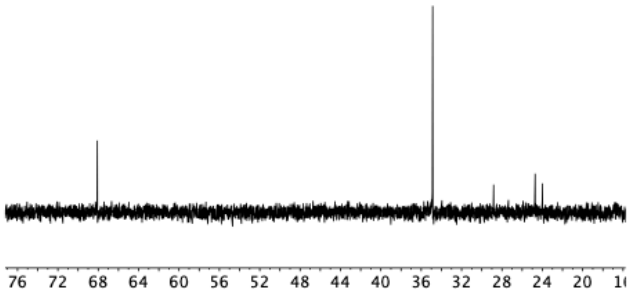

Figure 3.10: $^{31}P\{^{1}H\}$ NMR spectrum (162 MHz, C_6D_6) of warmed UV-vis samples, proposed to Ru-dimer (**17**) at room temperature.

The reactivity of **17** was explored with 2.5 equivalents of pyridine. The addition of five equivalents of pyridine to **5** at room temperature resulted in an immediate colour

change from green to orange. The addition of 2.5 equivalents of pyridine to **17** at –50 ºC was slow and occurred over 102 min (Figure 3.11). After the addition of pyridine an increase in absorption at 530 nm was notable, which increased for ~ 30 min (until the 42 min timepoint). At which time the absorption decreased at 630 nm until 102 min when no further changes were observed. The relatively flat UV-vis spectrum after 102 min was the same as room temperature pyridine-bound Ru-P^AzA (**8**; (Figure 3.7), suggesting that **17** reacted with excess pyridine to generate **8**, similar to formation of **8** from **5**. The two-step reactivity profile was indicative of the formation of an intermediate. This could be explained by a reaction in which one **L1** partially dissociated from κ^2-N to κ^1-N to provide an open coordination site on one Ru, where pyridine could bind to form a new Ru-dimer. This intermediate could quickly react with another equivalent of pyridine to form two equivalents of **8** (Scheme 3.6).

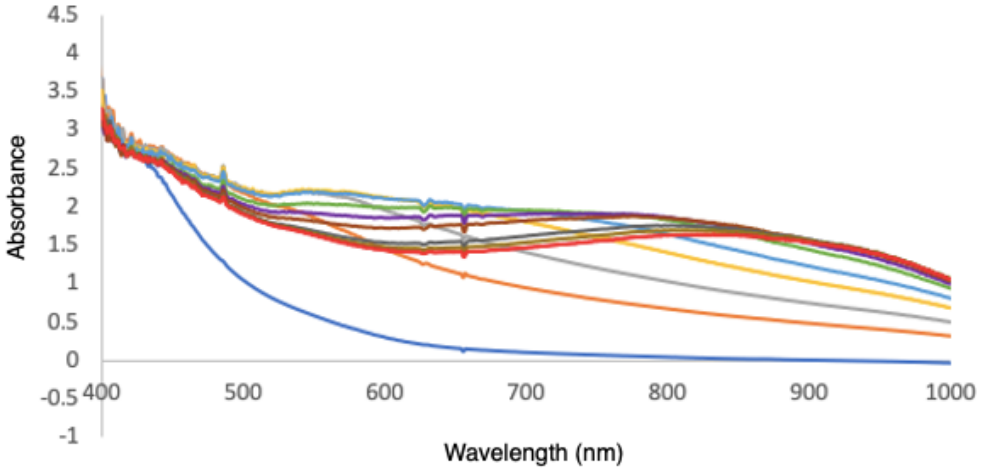

Figure 3.11: UV-Vis spectra of the addition of five equivalents of pyridine to **5** (1.5 mM) at – 50 ºC where spectra were acquired in 10 min intervals. Perturbations in the UV-vis spectrum are caused from data collection and represents experimental differences in absorbance readings at a specific wavelength (absorbance were collected at every wavelength 450 – 1000 at increments of one (e.g., 450,451…).

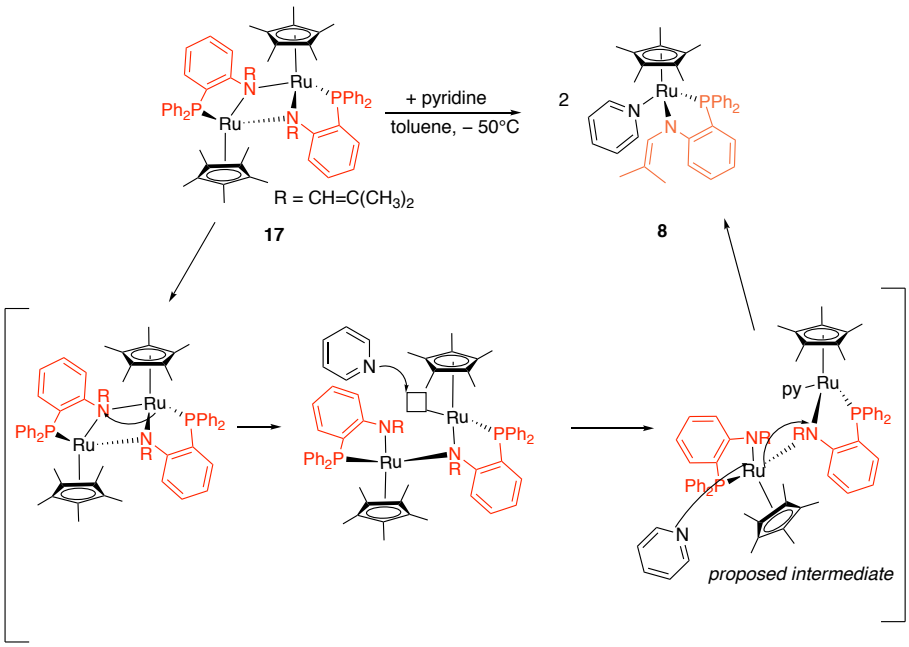

Scheme 3.6: Proposed mechanism of the synthesis of **8** upon addition of 2.5 equivalents of pyridine to **17** in toluene at –50 ºC.

3.4.4 Preliminary Reactivity Study of an Ru-P^AzA complex (**5**)

The addition of one equivalent of phenylacetylene to **5** at room temperature resulted in an immediate colour change from green to yellow indicative of the synthesis of a 18-electron Ru complex (Scheme 3.7).[64] Terminal alkynes can commonly bind with Ru to form either a π-bound alkyne or metal-vinylidene complex.[119-121] If a metal-vinylidene formed, an immediate rearrangement to form a metallacyclopentene Ru complex could be possible. Since the 1-azaallyl unit of **L1** was basic it may have attacked the electrophilic C_α of a Ru-vinylidene to form a Ru-metallacyclopentene complex.

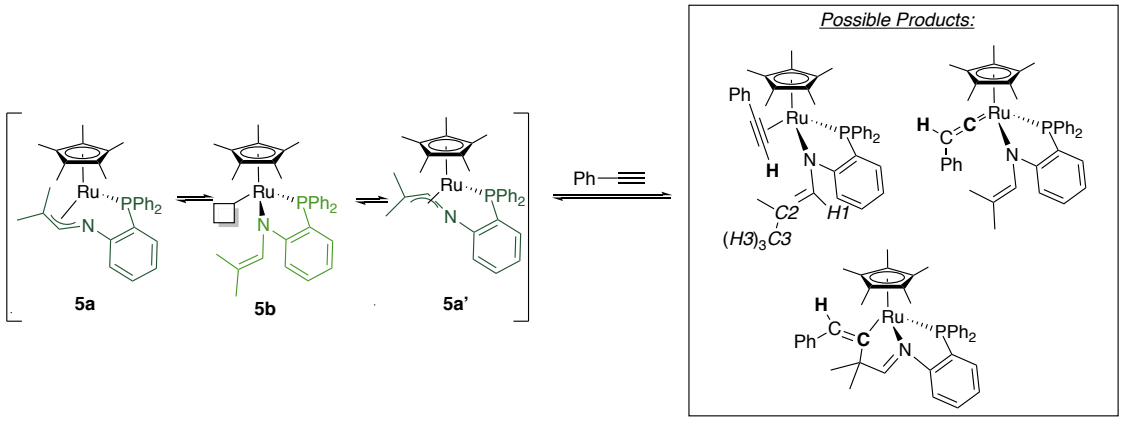

Scheme 3.7: Possible reactivity of **5** with phenylacetylene in C_6D_6

The $^{31}P\{^1H\}$ NMR spectrum presented as one sharp singlet implying the synthesis of only one new compound (Figure A28). In comparison, the ^1H NMR data demonstrate two sets of 1-azaallyl methyls (*H3/H3′*) in a 1:2.3 ratio (Figure 3.12). This was suggestive that two (major and a minor) species existed in solution. The chemical shifts of *H3/H3′* from one species were only slightly shifted from pure **5**, which was not visible by $^{31}P\{^1H\}$ NMR spectroscopy at room temperature. This was indicative that the reaction of **5** and phenylacetylene did not go to completion and that some of **5** remained (43% conversion to product was observed). Initially, the presence of **5** was not obvious as the conditions and equilibrium at play had shifted the observed signals in the ^1H NMR spectrum. An averaged Cp*H signal integrated to 18 H relative to the product instead of the expected 15 H, confirming that two species existed at room temperature. The *H1* product signal (5.99 ppm) integrated for one proton relative to six protons of the azaallyl Me's (*H3/H3′*), suggesting that **L1** was still intact in the product (^1H-^1H correlation experiment; Figure A29). The chemical shift of *H1* from the product (5.99 ppm) was upfield of that of **5** (6.50 ppm), indicative of an azaallyl moiety was still present.[71,72] A more downfield chemical shift of *H1* would be expected of an imine-moeity of the proposed metallocyclopentene product. Thus, the product was likely either an Ru η^2-alkyne or vinylidene complex of phenylacetylene. One broad signal was observed in the alkyl region that integrated for one proton relative to *H1* of the product. This signal could correspond to a H_{alkyne} or H_{alkene}, but the chemical shift was quite upfield (1.70 (•) ppm). Literature examples of Ru η^2-alkyne

or vinylidene complexes of phenylacetylene typically have more downfield alkyne or alkene protons in ^{1}H NMR spectrum than that observed here (e.g., 4.96-5.46 ppm for η^2-alkyne or 3.00-4.00 ppm for vinylidene).[119-121] The ^{1}H-^{13}C HMBC at room temperature of the reaction mixture did not demonstrate an characteristic electrophilic C_α signal (300-400 ppm; Figure A30).[121] Suggesting that at room temperature a Ru-η^2-alkyne complex formed; however, no reasonable H_{alkyne} proton signal was found. To confirm the structure, an excess of phenylacetylene (~ five equivalents) could be added to **5** to convert fully to the product and NMR analysis repeated without **5**.

Warming the reaction mixture resulted in a rapid colour change from yellow to dark green, reminiscent of **5**. Analysis of a sample heated to 60 ºC in the NMR spectrometer allowed for investigation of the green solution. Significant signal broadening was observed at warm temperature in both the ^{31}P{^{1}H} and ^{1}H NMR spectra (Figure 3.10). Signal broadening of **5** upon heating was expected; as, independently heating **5** in toluene-*d*$_8$ did result in signal shifting and broadening in NMR spectra (Figure A23). The broadened product signals observed at warm temperature of the product suggested a fluxional process (e.g., bond rotation) of the product occurred at 60 ºC since the **L1** proton signals of product did not shift significantly at higher temperatures. The fast and drastic colour change observed did suggest that **5** was favoured at high temperatures over the product. Notably, the ^{1}H-^{13}C HMBC spectrum of the reaction mixture at 60 ºC did presented a ^{13}C signal at 319.5 ppm indicative of a Ru-vinylidene or a Ru-vinylidene-like complex was present (Figure A31).[121] The C_α ^{13}C{^{1}H} signal only correlated to what appeared to be the averaged Cp*H signal suggesting that a four-bond coupling of C_α to Cp-CH_3 was occurring. No H_{alkene} signal was detected by the ^{1}H-^{13}C HMBC experiment (Figure A31). One new signal in the ^{1}H NMR spectrum did sharpen upon heating to 60 ºC, which was not present before the addition of phenylacetylene to **5**. This could be the emergence of the aromatic signals of a Ru-vinylidene that formed upon heating of the reaction mixture (^{1}H-^{1}H COSY Figure A32). The structure of the Ru-vinylidene complex was not confirmed due to signal broadness observed, but once the identity of the product room temperature complex is established this should be revisited.

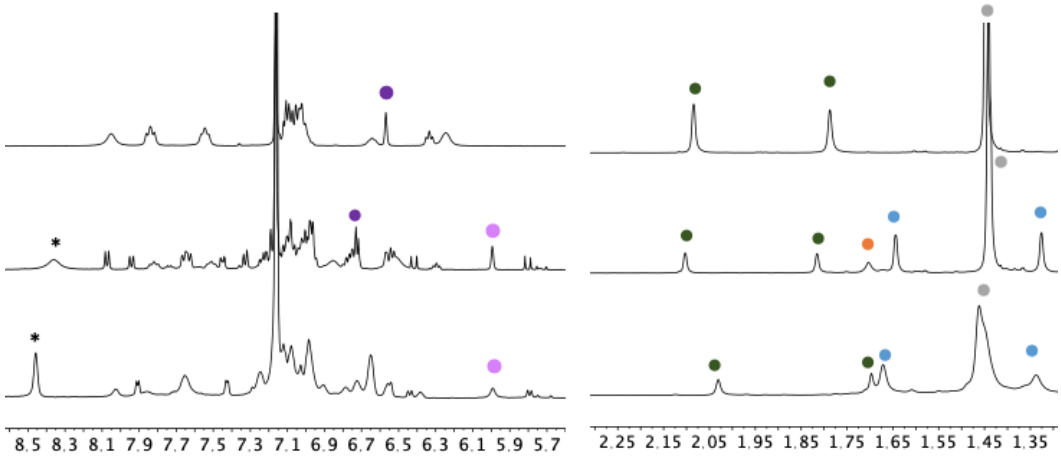

Figure 3.12: ^{1}H (400 and 600 MHz) of **5** (top), after the addition of one equivalent of phenylacetylene to **5** (middle), and while heating the reaction mixture to 60 ºC (bottom) in C_6D_6. Signals indicated: *aromatic H; • azaallyl *H1* of product; • azaallyl *H1* of **5**; • azaallyl *H3/H3′* of **5**; • azaallyl *H3/H3′* of product; • unknown signal that integrated for 1H; • Cp*Me-*H*

3.4.5 Attempted Kinetic Studies of an Ru-P^AzA complex (**5**)

Due to the pre-equilibrium experienced by **5** at room temperature (**5a**, **5b**, **5a′**) the change in coordination mode of **L1** resulted in a stable 18-electron Ru complex (η^3-NCC) and an active 16-electron Ru complex (κ^1-N). Furthermore, the NMR data suggested that the equilibrium of **5** lay towards **5b** at room temperature. This data suggested that in case of a substitution reaction with **5**, the active catalyst (**5b**) would be easily accessible. This would result in the rate of the given substitution reaction being dependent on the concentration of an incoming substrate (i.e., nucleophile or Lewis Base) and not the dissociation of a ligand (Scheme 3.8). In other terms, the reaction mechanism would represent formally an associative pathway instead of the typical dissociative pathway observed by an 18-electron non-SRL catalyst.

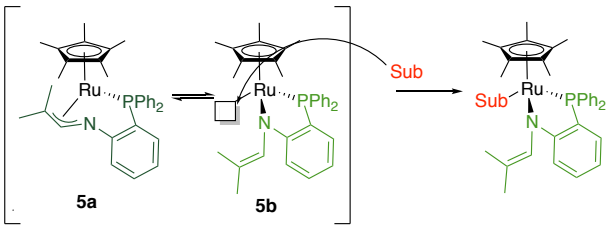

Scheme 3.8: Proposed associative mechanism upon addition of an incoming substrate (Sub) to **5**

Preliminary reactivity studies of **5** were performed with a few nucleophiles and Lewis bases in hopes of finding a slow clean reaction to perform UV-vis kinetic studies. Excess pyridine reacted cleanly with **5**, but the reaction was extremely fast and so no kinetic data could be recorded by UV-vis spectroscopy. The addition of one equivalent of phenylacetylene to **5** was also visually fast suggesting that kinetic data could not be recorded by UV-vis spectroscopy even if the reaction had gone to completion (i.e., addition of excess phenylacetylene). Due to the appearance of proposed **17** at cold temperatures, cooling the reaction to slow it down would not have been chemically relevant to assess the reactivity of pure **5**. And so, the addition of a bulky nucleophile and Lewis base to **5** was attempted in order to slow the reaction for UV-vis analysis. Specifically, one equivalent of 2-ethynyltoluene or 2,6-lutidene, either at room temperature or 60 ºC was added to **5** (Scheme 3.6). 2-Ethynyltoluene reacted with **5** at room temperature; but not cleanly, as a few signals were observed by $^{31}P\{^{1}H\}$ NMR spectroscopy. Upon addition of 2,6-lutidene to **5** only a broad signal emerged in the $^{31}P\{^{1}H\}$ NMR spectrum after heating for 3 h. The ^{1}H NMR spectrum was consistent with authentic **5** and 2,6 lutidine in solution. Since these bulky substrates did not provide clean $^{31}P\{^{1}H\}$ NMR data and no distinct colour changes were observed these reactions were not pursued further for UV-vis kinetic studies.

In summary, **5** likely existed as a mixture of three complexes due to the structurally responsive nature of the P^AzA ligand. The proposed change in coordination mode (η^3-NCC to κ^1-N) of the 1-azaallyl moiety allowed for fast association of pyridine and phenylacetylene. These reactivity studies highly suggested that **5** would be an active catalyst as an open coordination site was available within seconds.

4 Conclusion

The improved synthesis of a Pd(II) P^AzA dimer (**1**) was investigated via three experimental routes. The first method, and most successful, involved synthesis of a new Pd(II) precursor, [Pd(μ-Cl)]Me(SMe_2)]$_2$. The new Pd(II) precursor (**11**) contained a labile ligand SMe_2, that has a lower boiling point than COD, which was the labile ligand for the previous precursor [PdClMe(COD)] for the synthesis of **1**. This method resulted in high conversion to desired **1**, but a few impurities remained in product as observed by the $^{31}P\{^1H\}$ NMR spectrum. Due to time constraints this pathway was not further optimised; however, upon successful isolation of **1** this may prove to be a viable method to produce higher quantities of **1**, reproducibly. Other synthetic routes to **1** that were explored involved the Lewis acidic abstraction of pyridine from **2** and deprotonation of **9** by phenoxide bases. Neither proved sufficiently successful to pursue beyond small scale. Improved synthesis attempts of **1** indicated that the experimental route involving the addition of a ligand salt K[**L1**] to a Pd(II) precursor was best to produce clean Pd(II) dimer.

The reactivity of **1** with small molecules was explored and the molecules tested included were acids, alcohols, water, H_2, and O_2. The addition of water and alcohols to **1** was not explored further than initial reactivity studies. Reactivity of **1** with various acids and H_2 revealed that the ligand, **L1**, was basic resulting in protonation of the P^AzA ligand and generation of a proposed Pd-P^I complex. The proton-responsiveness of the P^AzA ligand may be able to be exploited for catalysis. The activation of O_2 resulted in conversion to two products (**16a/b**) according to the $^{31}P\{^1H\}$ NMR spectrum. The isolation of **16a** is likely feasible with excess radical trap, TEMPO$^{\bullet}$, that promoted the synthesis of **16a** over **16b**. Due to issues of synthesising **1**, only small-scale analysis was conducted thus far. The NMR studies of mixtures of **16a/b** suggested the presence of acetone, a Pd-formamide and a Pd-amide complexes. Of the reactions attempted, **1** successfully activated O_2, H_2, and various acids in organic solvents. Small-scale reactivity studies of **1** with acids and H_2 demonstrate the proton-responsive abilities of **L1** that may be exploited for catalysis. Reactivity of **1** with O_2 was less defined, but current spectroscopic data was suggestive that oxidation of **L1** occurred, implying that oxygenated environments should be avoided with complexes of **L1**. The reactivity studies performed demonstrate that **L1** was non-innocent

in reaction chemistry of **1**. The metal-ligand cooperativity observed between Pd and **L1** may be harnessed for future catalysis attempts.

Novel Ru-P^AzA and Ru-P^I complexes were synthesised and characterised by standard techniques. The isolation of **7** with yields above 50% was still challenging. To date a combination of precipitations and an $MgCl_2$ treatment provided the best yield of **7**. The iodo-form of the Merrifield peptide resin (I-MR) may also be fruitful for removal of the $O{=}PPh_3$ byproduct, but this method was not explored extensively. Complex **8** was synthesised by deprotonation of **7** by excess strong base and in the presence of excess L-donor. Dissolving **8** in benzene or toluene resulted in the synthesis of **5**. Compared to the previous synthetic route, which involved the addition of a ligand salt K[**L1**] to a Ru(II) precursor, this method provided consistent results and cleaner complexes (**5** & **8**). Unexpectedly, cooling **5** resulted in the synthesis of a Ru-dimer (**17**). Complex **17** was in equilibrium with **5** at high concentrations (> 29 mM) but demonstrated complex chemistry at low concentrations (< 1.5 mM).

The NMR data of **5** suggest that **5** existed as an equilibrium mixture of three complexes, **5a**, **5b**, and **5a′**. This was indicative that **L1** was structurally responsive by reversibly coordinating the 1-azaallyl unit of **L1**. Likely a change in coordination mode occurred between η^3-NCC (4 e^--donation; **5a**/**5a′**) and κ^1-N (2 e^--donation; **5b**) modes. This reversible coordination would result in an open site on Ru (**5b**) which would be available for an incoming substrate to bind. The equilibrium of **5** occurred at room temperature and NMR experiments revealed that the equilibrium lay towards **5b** (κ^1-N) suggesting that **5b** and an open coordination site was easily accessible for **5**. Which implied that substrate association would be fast, and the rate of association would be dependent on substrate concentration. Preliminary reactivity studies of **5** with one equivalent phenylacetylene appeared to partially convert **5** to a new product within seconds, proposed to be a Ru-η^2-alkyne complex. Heating the reaction mixture resulted in a ^{13}C signal consistent with a Ru-vinylidene complex, indicative of conversion from a Ru-η^2-alkyne to a vinylidene was possible. The addition of excess phenylacetylene (five equivalents) may be required to convert **5** to the product completely to confirm the proposed reactivity. This was suggestive that cyclisation catalysis of alkyne substrates may be fruitful with **5**. Synthesis and reactivity studies with **5** suggested that reversible binding of η^3-NCC to κ^1-N coordination

mode of the azaallyl unit of **L1** was occurring. This structural responsive attribute observed by the P^AzA ligand may positively influence the association of a substrate onto the proposed ‘low coordinate’ Ru-P^AzA catalyst (**5**).

5 Future Work

Since the Pd(II) precursor, **11**, permitted high conversion to the Pd(II)-P^AzA dimer, **1**, the isolation should be pursued (Scheme 5.1A). If **1** is accessible in a high yield and purity, then this procedure could be used in the future. With larger amounts of **1** on hand, the isolation of **16a** would be more feasible and various characterisation techniques would confirm the structure (Scheme 5.1B). Isolation of **16a** should be done in the presence of excess TEMPO•, as **16a** was favoured 15:1 over **16b** under such conditions. After O_2 insertion, a four-membered ring intermediate was proposed, followed by C-C bond cleavage, and generation of a Pd-formamide complex and acetone as a by-product. The Pd-formamide complex was deemed to be **16a** from the large amount of acetone found in the ^{1}H NMR spectrum when using the additive TEMPO•. The presence of acetone should be confirmed using a simple spiking experiment of dried and degassed acetone. The ^{1}H NMR data suggested **16b** was most likely a Pd-amide species where the 1-azaallyl unit of **L1** was replaced with an isobutyramide functionality. The ^{13}C{^{1}H} resonances of the 1-azaallyl unit C's would be more downfield as they would be close proximity to electron-withdrawing O atoms. A DOSY experiment could confirm if **16a/b** were dimer or monomer Pd complexes. Additionally, $^{18}O_2$ labelling experiments would be useful to confirm the role of O_2 to produce **16a**/**b**. The MALDI MS would be useful to determine if **16a/b** were dimer or monomer Pd complexes and to confirm the addition of O_2 to **1**. Furthermore, X-ray crystallography would confirm the proposed structures of **16a/b**. Additionally, other potential oxidants like oxone or *t*-butyl peroxide may also provide a distinct reactivity trend of **1** with oxidants.

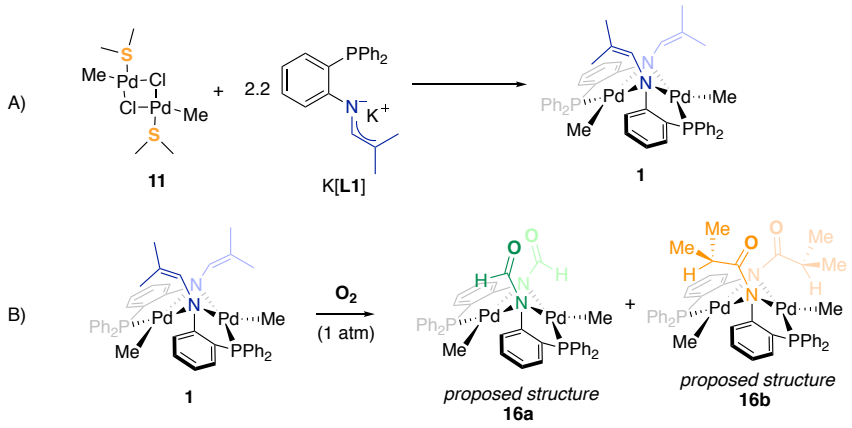

Scheme 5.1: Proposed future experiments involving the isolation of **1** via the addition of K[**L1**] to **11** (A) and the aerobic oxidation of **1** to proposed structures of **16a** and **16b**.

Complex **5** exists as an equilibrium mixture, but the exact structures have thus far only been suggested to be **5a/5b/5a′**. Calculations and X-ray diffraction could aid in the structural assignments of **5a/5b/5a′**. Specifically, simulated UV-vis data will aid in the assignment of observed d-d transitions and thus the likely structures of **5**. If the relative energies calculated for the isomers of **5** are close in proximity this would support the idea that the Ru-P^AzA complex existed as multiple complexes in an equilibrium at room temperature. The calculated relative stability of the complexes will also aid in the understanding of preliminary reactivity studies.

Complex **5** has shown promising reactivity with phenylacetylene suggesting the synthesis of an alkyne to form a metal vinylidene was possible with **5**. The structural responsiveness of **L1** was suggested to promote the synthesis of a Ru-vinylidene. Currently, the hypothesis was that the structurally responsiveness of **L1** in **5** would increase the TON and TOF as compared to a non-structurally responsive derivative. The Ru-catalyzed organic transformation of 3-en-5-ynyl and *o*-alkynylphenyl nitrones to 3(2*H*)-isoquinolones and α-pyridones is of particular interest to test the general catalytic abilities of **5** (e.g., in Scheme 5.2A).[122] This organic transformation was successful with similar Ru complexes, like $RuCl(Cp)(PPh_3)_2$, where high catalyst loadings (10 mol %), high temperature (90 ºC), and long reaction times (6 h) were required. This catalytic transformation should be attempted to assess the catalytic abilities of **5** and **8** and if they perform comparable to similar Ru catalysts. A control complex where the π-system of the

1-azaallyl unit was not present should be synthesised and catalytic ability tested (Scheme 5.2B). Direct comparison from this control complex, **5**, and **8** would confirm if the 1-azaallyl unit of **L1** promotes reactivity as hypothesised.

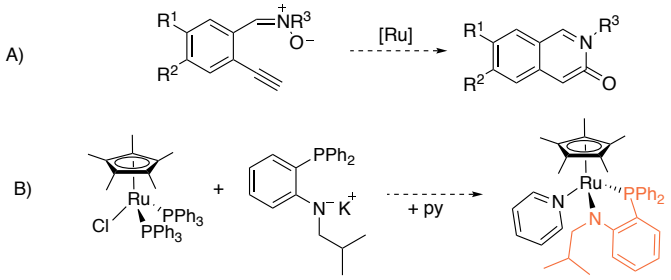

Scheme 5.2: The cycloisomerization of nitrones with [Ru] (A) and the proposed synthesis of a control complex (B).[122]

6 Experimental

6.1 General Experimental Conditions

All reactions were performed under an inert (Ar or N_2) atmosphere using standard Schlenk line techniques and/or an MBRAUN glovebox, unless otherwise stated. Vials, flasks, and NMR tubes were oven dried (156 °C) and cooled under inert atmosphere before use. Unless otherwise stated, all reaction solvents were dried and degassed, and obtained from an Innovative Technology 400-5 Solvent Purification system and stored over 4 Å molecular sieves prior to use. Pyridine was dried over CaH_2, distilled under reduced pressure and stored over 4 Å molecular sieves under an inert atmosphere. The following materials were prepared using literature procedures [$PdCl_2$(COD)],[75] [PdClMe(COD)],[77] **1**,[71] **2**, [71] **9**, [71] **6**,[123] and **13**[124] All other reagents were purchased from commercial sources and used without further purification. Deuterated solvents were obtained from commercial sources and were degassed and stored over 4 Å molecular sieves. Ampoules of acetone-d_6, methylene chloride-d_2, and toluene-d_8 were purchased from Sigma Aldrich and stored over 4 Å molecular sieves before use. Dioxygen and dihydrogen gas were purchased from Praxair and passed through a tube filled with Drierite prior to use.

All NMR spectra were obtained on a 400 or 600 MHz Varian or 400 MHz Bruker spectrometer at 25 °C unless otherwise stated. ^{1}H (TMS at $\delta = 0$) and ^{13}C{^{1}H} NMR spectra were referenced internally using residual solvent (for ^{1}H) or solvent signals (^{13}C) signals as follows: $CDCl_3$ ($\delta_H = 7.26$; $\delta_c = 77.4$), C_6D_6 ($\delta_H = 7.16$; $\delta_c = 128.1$), Toluene-d_8 ($\delta_H = 2.09$, $\delta_c = 20.4$). ^{31}P{^{1}H} NMR spectra obtained in proteo solvents were externally referenced to a sample of 85% H_3PO_4 at $\delta_P = 0$. Many *In situ* yields determined for Chapter 2 from ^{31}P{^{1}H} NMR spectra were determined relative to an internal standard solution of O=PPh_3 in C_6D_6 sealed in a capillary and ^{31}P{^{1}H} NMR spectra were acquired with delay times of 5 s unless otherwise stated. *In situ* yields determined in Chapter 3 from ^{31}P{^{1}H} NMR spectra were done without an internal standard however spectra were run with an increased delay time of 5 s unless otherwise stated. Multiplicities are described as s (singlet), d (doublet), t (triplet), sept (septet), br (broad), ov (overlapping), and m (multiplet). Charge-transfer Matrix Assisted Laser Desorption/Ionization Mass Spectrometry data were collected on an AB Sciex 5800 TOF/TOF mass spectrometer using

pyrene as the matrix in a 20:1 molar ratio to complex. Solutions were prepared in benzene and spotted on a sample plate under an inert atmosphere and transferred to the instrument in a closed resealable plastic bag. The instrument is equipped with a 349 nm OptiBeam On-Axis laser. The laser pulse rate was 400 Hz and data were collected in reflectron positive mode. Reflectron mode was externally calibrated at 50 ppm mass tolerance. Each mass spectrum was collected as a sum of 500 shots. Infrared spectra were collected on solid samples using a Bruker ALPHA II ATR FTIR spectrometer. UV-Visible spectra were collected using an Agilent Technologies Cary 8454 UV-Visible spectrometer, fitted with a Unisoko CoolspeK UV USP-203-A cryostat for low temperature analyses. Crystal samples were mounted on a Mitegen polyimide micromount with a small amount of Paratone N oil. All X-ray measurements were made on a Bruker Kappa Axis Apex2 diffractometer at a room temperature. The unit cell dimensions were determined from a symmetry-constrained fit and compared to crystal structures in the Cambridge Crystallographic Database Center (CCDC).

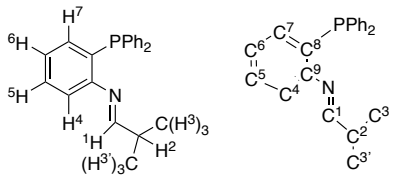

Scheme 6.1: General labelling scheme for the P^I ligand H[**L1**]

6.2 Alternative Synthesis to **1** and Attempted Synthesis of **10**

6.2.1 Attempted Synthesis of **10** by Reaction of palladium dichloride, DME, and ethyl orthoformate

Following the procedure for the analogous compound $NiCl_2$(DME):[125] $PdCl_2$ (50 mg, 0.28 mmol) was combined with ethyl orthoformate (68 uL, 0.62 mmol) in DME (5 mL) and left to stir at room temperature for 24 h under air conditions. The reaction was refluxed for an additional 24 h. Reaction progress was monitored by removal of an aliquot of the reaction solution, of which the solvent was removed using rotary evaporation. A ^{1}H NMR spectrum was obtained in $CDCl_3$ which demonstrated no new products were synthesised.

6.6.2 Attempted Synthesis of **10** by Reaction of Palladium Dichloride and DME

Following similar procedures for the related compound $PdCl_2(COD)$:[75] $PdCl_2$ (50 mg, mmol) was dissolved in concentrated HCl (250 uL) at 40 °C. After 5 min, ethanol (7.6 mL) was added to dilute the solution and the mixture was allowed to stir at room temperature for 10 min. The solution was degassed by bubbling with Ar for 30 min before an excess of DME (1.2 mL, 0.56 mmol) was added. The reaction was stirred at room temperature for 24 h, followed by heating to 90 °C for 24 h. Reaction progress was monitored by removal of an aliquot of reaction solution and the solvent was removed using rotary evaporation. A ^1H NMR spectrum was obtained in $CDCl_3$ which demonstrated proposed signals for **10** but proposed **10** was not stable to isolation.

6.2.3 Alternative Synthesis of **1** by Reaction of **11** and K[**L1**]

The procedure for the synthesis of **1** by reaction of PdClMeCOD and K[**L1**] (on 100 mg scale of K[**L1**])[77] was followed, except, **11** was used as the Pd precursor and THF as the solvent. The $^{31}P\{^1H\}$ and ^1H NMR spectra matched those of literature for **1** (70% purity) with minor impurities.

6.2.4 General Attempted Synthesis of **1** by Lewis Acid Abstraction of Pyridine from **2**

Complex **3** (10 mg, 0.019 mmol) was dissolved in C_6D_6 (~ 0.6 mL) and transferred to an NMR tube. A solution of BEt_3 (1M in hexanes, 19 uL, 0.019 mmol) was added to the solution of **3** in the NMR tube. The tube was then inverted three times and reaction progress was monitored via ^1H and $^{31}P\{^1H\}$ NMR spectroscopy. For reactions with BF_3•Et_2O, and BPh_3, a stock solution was prepared for each borane in C_6D_6 (70 or 41 mM, respectively), and one equivalent (267 uL or 456 uL, respectively) was added to the NMR tube containing **3**.

6.2.5 Attempted Synthesis of **1** by Reaction of K[OPh] and **9**

One or five equivalents of K[OPh] was dissolved in minimal amounts of THF. The base was added to a solution of **2** (0.11 mmol, 0.020 mmol, respectively) in THF (0.022, 0.014 M solutions, respectively). These reactions were allowed to stir at room temperature

for 1 h. The solvent was removed under vacuum and ^{1}H and $^{31}P\{^{1}H\}$ NMR spectra were acquired in C_6D_6.

6.3 Reactivity of **1** with E-H, Water, Alcohols, Dioxygen, and Dihydrogen

6.3.1 General procedure for liquid additions (E-H, Water, Phenylacetylene)

Complex **1** (10 mg, 0.011 mmol) was dissolved in C_6D_6 or THF (0.6 mL) and transferred into an NMR tube, a capillary containing $O{=}PPh_3$ in C_6D_6 was added and the tube was closed with a septum cap. A solution of E-H ($[DMFH]^+[OTf]^-$, phenol, 4-methoxyphenol, phenolphthalein, MeOH, BnOH) was prepared by dissolving E-H (10 mg) in C_6D_6 or THF (1 mL) in a 4 mL vial sealed with a screw cap fitted with a septum. Using a microliter syringe one equivalent of E-H solution, or one drop of degassed H_2O was added to the NMR tube, which was then inverted three times. The reaction progress was analyzed by ^{1}H and $^{31}P\{^{1}H\}$ NMR spectroscopy either: 1) approximately 10 min after addition (E-H: $[DMFH]^+[OTf]^-$, phenol, 4-methoxyphenol) or 2) monitored over 24 h (H_2O).

6.3.2 General Procedure for Gas Additions (Dioxygen and Dihydrogen)

Complex **1** (10 mg, 0.011 mmol) was dissolved in C_6D_6 (0.6 mL) and transferred into an NMR tube containing a sealed capillary of $O{=}PPh_3$ in C_6D_6 that was then closed with a septum cap. The dried gas (O_2 or H_2) was passed through the headspace of the NMR tube for 30 s through a needle and the excess pressure was vented through a bleed needle. The NMR tube was inverted three times and left at room temperature (O_2) or submerged in an oil bath at 38 ºC (H_2), the reactions were monitored by ^{1}H and $^{31}P\{^{1}H\}$ NMR spectroscopy over 24 h.

6.4 Representative Synthesis of Phenol Adduct (**12a**) by reaction of Phenoxide and **9**

The base K[OPh] (20 mg, 0.15 mmol, 1.5 equiv) was dissolved in THF (4 mL) and added dropwise to a stirring suspension of **9** (50 mg, 0.10 mmol) in THF (1 mL). Upon addition, the solution became yellow and the reaction was left to stir for 1 h at room temperature. The solution was filtered through a microfiber plug to remove KCl and the volume was reduced to ca. 1 mL. Cold pentane (10 mL) was added while stirring, resulting in the precipitation of a white solid. The excess solvent was decanted off and the remaining

solid was washed with cold pentane (2 x 1 mL) affording **12a** as an off-white powder. Yield: 18% (95% purity by $^{31}P\{^{1}H\}$ NMR spectroscopy); ^{1}H NMR (400 MHz, C_6D_6): δ = 7.57-7.32 (m, 8H, O(Ph-*H*), P(Ph-*H*)), 7.20 (d, *J* = 8.4 Hz, 1H, *H1*), 7.04-6.90 (m, 7H, P(Ph-*H*)), 6.87 (dd, *J* = 8.0, 7.6 Hz, 1H, *H5*), 6.81 (dd, *J* = 7.6, 7.1 Hz, 1H, *H6*), 6.73 (dd, *J* = 7.1, $^{3}J_{H-P}$ = 1.3 Hz, 1H, *H7*), 6.45 (dd, *J* = 8.0 Hz, $^{3}J_{H-P}$ = 4.5 Hz, 1H, *H4*), 4.50 (d of sept, *J* = 8.4, 6.7 Hz, 1H, *H2*), 1.29 (d, $^{3}J_{H-P}$= 2.8 Hz, 3H, Pd-C*H*$_3$), 0.81 (d, *J* =6.7 Hz, 6H, *H3/H3'*); $^{31}P\{^{1}H\}$ NMR (162 MHz, C_6D_6): δ = 36.7; $^{13}C\{^{1}H\}$ NMR (100 MHz, C_6D_6): δ = 181.4 (s, *C1*), 156.5 (d, J_{C-P} = 17.3 Hz, *C9*), 134.1 (d, J_{C-P} = 12.7 Hz, P(Ph-*C*)), 132.8 (d, J_{C-P} = 15.0 Hz, *C8*), 131.2 (s, Ar-*C*), 130.6 (s, Ar-*C*), 130.0 (s, Ar-*C*), 129.7 (s, Ar-*C*), 129.3 (d, J_{C-P} = 11.1 Hz, P(Ph-*C*)), 121.5 (s, Ar-*C*), 119.3 (d, J_{C-P} = 8.1 Hz, *C4*), 113.8 (s, *C7*), 33.4 (s, *C2*), 20.0 (s, *C3/C3'*), 2.1 (d, $^{1}J_{C-P}$ = 4.6 Hz, Pd-*C*H$_3$); MALDI MS (pyrene): *m/z* found 436.03 [**12a**-OPh-Me-H$^+$] calc 436.05

6.5 Attempted Syntheses of **14** by Reaction of **13** and K[**L1**]:

Complex **13** (10 mg, 0.033 mmol) was dissolved in C_6D_6 (0.2 mL) and transferred to an NMR tube. A solution of K[**L1**] (83 mM, 0.033 mmol) was added dropwise to avoid the formation of complex **4**. The reaction was conducted in THF and followed a similar procedure however the solution was mixed in a 20 mL vial then allowed to stir for 2 min, during which the solution changed from orange to black. The solvent was removed under high vacuum and the residue was redissolved in C_6D_6 for analysis by NMR spectroscopy.

6.6 Attempted Synthesis of **15** by Reaction of **13** and H[**L1**]:

Representative Procedure: Complex **13** (10 mg, 0.033 mmol) was dissolved in C_6D_6 (0.2 mL) and a solution of H[**L1**] (91 mM, 0.037 mmol) was added dropwise. Reaction progress was monitored by ^{1}H and $^{31}P\{^{1}H\}$ NMR spectroscopy. Reactions conducted in THF followed a similar procedure; however, the solution was mixed and allowed to stir for 1 h. The solvent was removed under vacuum and the residue dissolved in C_6D_6 for analysis by NMR spectroscopy.

6.7 Synthesis of **7** by Reaction of **6** and H[**L1**]:

6.7.1 General Procedure for Small-Scale Optimisation of the Synthesis of **7**:

An aliquot of H[**L1**] (1.0 or 1.5 equivalents, 0.014 or 0.021 mmol) from a stock solution was added to **6** (10 mg, 0.014 mmol) in a pressure tube (15 mL) or in an NMR tube and the reaction was diluted to various concentrations (3.7-30 mM) in several solvents. Solvents tested included: THF, Me-THF, C_6D_6, Pyridine, 1,4-Dioxane, and MeCN. The reaction vessels were sealed upon dilution and the reaction mixtures were heated to various temperatures (45-120 ºC) for various times (0.15-18 h). Reactions conducted in a pressure tube were stirred while heated. The reaction solvents were removed under vacuum (except C_6D_6) and the residue was redissolved in C_6D_6 for analysis by ^{1}H and $^{31}P\{^{1}H\}$ NMR spectroscopy.

6.7.2 Optimised Synthesis of **7**:

A solution of H[**L1**] (183 mg, 0.553 mmol) in THF (6.0 mL) was added to a suspension of **6** (400 mg, 0.502 mmol) in THF (10.7 mL) in a 75 mL pressure tube with a stir bar. The pressure tube was sealed under inert atmosphere and the reaction mixture was stirred at 80 °C for 1.5 h. The pressure tube was brought back into the glovebox and the solvent was completely removed under vacuum in a 20 mL vial yielding a dark bubbly solid. The $^{31}P\{^{1}H\}$ NMR spectrum (acquired with 5 s relaxation delay) of the crude reaction mixture indicated ~ 80% conversion to **7**. The crude solution of **7** was dissolved in benzene (5 mL) and, while stirring pentane (10 mL) was added over 5 min to precipitate green fluffy solids. The green solid was removed by passing the suspension through a celite plug and washed with toluene (3 x 3 mL). The brown filtrate was collected, and the solvent was fully removed under vacuum. To remove the $O{=}PPh_3$ by-product, the crude oil was dissolved in toluene (11 mL) and excess $MgCl_2$ (ca. 3 scoops) was added. The suspension was allowed to stir at 30 ºC under argon atmosphere for 1.5 h. Excess $MgCl_2$, $MgCl_2$-$O{=}PPh_3$, and $O{=}PPh_3$ were removed by filtration through a celite plug. The resulting dark filtrate was collected, and the was solvent removed under vacuum. The brown oil was redissolved in benzene (2 mL) and, while stirring, pentane (10 mL) was added over 5 min. Green solids precipitated, which were removed by filtration through a celite plug. The filtrate was then placed in the freezer (– 20 ºC) overnight to precipitate **7** as a dark crystalline solid. Complex

7 was collected by decanting the green solution, followed by washing the solids with hexanes (5 mL) and drying under vacuum. Further precipitations of green solids and follow up recrystallisations afforded a higher yield of **7**. Yield: (126 mg, 0.209 mmol) 52 % (purity > 95 % by $^{31}P\{^{1}H\}$ NMR spectroscopy) ***Z*-7** ^{1}H NMR (400 MHz, C_6D_6) (note: the signals between 6.80-7.30 ppm are overlapped with ***E*-7** aromatic signals) δ = 8.03-7.97 (m, 2H, P(Ph-*H*)), 7.61 (d, *J* = 9.3 Hz, 1H, *H1*), 7.52 – 7.42 (m, 1H, *H5*), 7.29-7.38 (m, 2H P(Ph-*H*)), 7.24-7.18 (m, 3H, P(Ph-*H*)), 7.10-7.04 (m, 1H, P(Ph-*H*)), 7.02-6.96 (m, 4H, P(Ph-*H*)), 6.94-6.89 (m, 2H, *H6* & *H7*), 6.73 (dd, *J* = 7.1, 3.8 Hz, 1H, *H4*), 3.82 (d of sept, *J* = 9.3, 6.5 Hz, 1H, *H2*), 1.47 (d, $^{3}J_{H\text{-}P}$ = 1.7 Hz, 15H, Cp**H*), 1.37 (d, *J* = 6.5 Hz, 3H, *H3*), 0.98 (d, *J* = 6.5 Hz, 3H, *H3'*); ***Z*-7** $^{13}C\{^{1}H\}$ NMR (101 MHz, C_6D_6) δ = 183.5 (s, *C1*), 163.3 (s, *C9*), 134.6 (d, $J_{C\text{-}P}$ = 10.7 Hz, P(Ph-*C*)), 133.4 (d, $J_{C\text{-}P}$ = 2.0 Hz, *C5*), 133.1 (d, $J_{C\text{-}P}$ = 9.9 Hz, P(Ph-*C*)), 130.3 (d, $J_{C\text{-}P}$ = 2.1 Hz, *C6*/*C7*), 128.9 (d, *J* = 2.2 Hz, P(Ph-*C*)), 128.5 (d, *J* = 1.5 Hz, P(Ph-*C*)), 126.8 (d, *J* = 3.7 Hz, P(Ph-*C*)), 82.9 (d, $J_{C\text{-}P}$ = 3.7 Hz, *C8*), 37.2 (*C2*), 21.9 (*C3*), 20.7 (*C3'*), 10.0 (Cp**C*); ***Z*-7** $^{31}P\{^{1}H\}$ NMR (162 MHz, C_6D_6) δ = 55.2 (80 %). ***E*-7** ^{1}H NMR (400 MHz, C_6D_6) (Diagnostic signals) δ = 8.30 (d, *J* = 9.6 Hz, 1H, *H1*), 2.76 (sept, *J* = 9.6, 6.5 Hz, 1H, *H2*), 1.49 (d, $^{3}J_{H\text{-}P}$ = 1.6 Hz, 15H, Cp**H*), 0.80 (d, *J* = 6.5 Hz, 3H, *H3*), 0.65 (d, *J* = 6.5 Hz, 3H, *H3'*); ***E*-7** $^{31}P\{^{1}H\}$ NMR (162 MHz, C_6D_6) δ = 53.4 (20 %); ***E*-7** $^{13}C\{^{1}H\}$ NMR (101 MHz, C_6D_6, Diagnostic signals) δ = 182.4 (*C1*), 32.6 (*C2*), 20.5 (*C3*), 19.8 (*C3'*); MALDI-MS (pyrene): *m/z* found: 603.12 Calc: 603.15; X-ray quality crystals were grown from a THF/Pent mixture at – 20 ºC; ATR-FTIR (cm^{-1}): ν 1463.09 (N=C)

6.8 Synthesis of Ru-P^AzA complexes

6.8.1 Synthesis of **8** by deprotonation of **7** in the presence of Lewis Base:

Two equivalents of Li[HMDS] (36 mg, 0.22 mmol) were added to a solution of **7** (65 mg, 0.11 mmol) in a mixture of benzene (6.5 mL) and pyridine (3.2 mL). The reaction was left to stir at room temperature for 1 h. The crude $^{31}P\{^{1}H\}$ NMR spectrum indicated 80% conversion to the desired product **8**. The solvent was reduced under vacuum to ca 0.5 mL and hexanes (3 mL) was added. The mixture was stirred for 15 min at room temperature, during which an orange solid precipitated. The orange solid was collected by filtering the crude solution through a microfibre plug and washing the solid with cold

hexanes (2 x 1 mL). The hexane wash procedure was repeated twice with the leftover filtrate to collect the product until no traces of **8** were found in the filtrate $^{31}P\{^{1}H\}$ NMR spectrum. ^{1}H NMR (400 MHz, C_6D_6) (note: aromatic region was predominately pyridine): δ = 6.41 (s, 1H, *H2*) 2.12 (s, 3H, *H3*), 1.85 (s, 3H, *H3′*), 1.42 (d, *J* = 1.6 Hz, 15H, Cp*-*H*); $^{31}P\{^{1}H\}$ NMR (162 MHz, C_6D_6) δ = 65.9; $^{13}C\{^{1}H\}$ NMR signals found through 2D HMBC correlation experiment (101 MHz, C_6D_6) (note: direct detect not acquired because of stability of **8**): δ = 138.6 (*C1*), 115.6 (*C2),* 22.2 (*C3′*), 18.7 (*C3*).

6.8.2 Synthesis of **5** by dissolving **8** in non-coordinating, non-chlorinated solvents:

Synthesis of **5** was easily accomplished upon dissolving orange solid, **8**, in benzene or toluene at room temperature. When **8** was dissolved a drastic colour change from orange to an intense dark green occurred. Removal of solvent resulted in a dark brown solid; Yield: 41 mg; 84 % (0.072 mmol); ^{1}H NMR (400 MHz, C_6D_6, 298 K): δ = 7.90 (s, 1H, *H7*), 7.69 (t, *J* = 9.0 Hz, 2H, P(Ph-*H*)), 7.39 (t, *J* = 8.2 Hz, 2H, P(Ph-*H*)), 6.50 (br, 1H, *H5*), 6.42 (s, 1H, *H2*), 6.18 (t, *J* = 6.9 Hz, 1H, P(Ph-*H*)), 6.10 (br, 2H, *H4* & *H6*), 1.94 (s, 3H, *H3*), 1.65 (s, 3H, *H3′*), 1.30 (d, $J_{H\text{-}P}$ = 1.5 Hz, 15H, Cp**H*); $^{31}P\{^{1}H\}$ NMR (243 MHz, C_6D_6, 298 K): no signal; Diagnostic $^{13}C\{^{1}H\}$ NMR signals found through 2D correlation experiments (101 MHz, C_6D_6, 298 K) (note: due to the equilibrium no other $^{13}C\{^{1}H\}$ signals were observed at room temperature): δ = 139.8 (*C1*), 118.1 (*C2*), 22.6 (*C3′*), 18.8 (*C3*); MALDI-MS (pyrene): *m/z* found: 567.13 Calc: 567.16;

6.8.3 Low Temperature *in-situ* NMR analysis of **5**:

^{1}H NMR (599 MHz, Toluene-d_8, 223 K): δ = 7.85 – 7.75 (m, 2H, P(Ph-*H*)), 7.73 (d, *J* = 5.4 Hz, 1H, *H7*), 7.42 (t, *J* = 8.2 Hz, 2H, P(Ph-*H*)), 6.62 (s, 1H, *H2*), 6.43 – 6.32 (m, 1H, *H5*), 6.28 (t, *J* = 7.0 Hz, 1H, P(Ph-*H*), 5.97-5.94 (m, 2H, *H4* & *H6*) 2.22 (s, 3H, *H3*), 1.94 (s, 3H, *H3′*), 1.42 (s, 15H, Cp*-*H*); $^{31}P\{^{1}H\}$ NMR (243 MHz, Toluene-d_8, 223 K) δ = 66.1; $^{13}C\{^{1}H\}$ NMR signals found through 2D correlation experiments (151 MHz, Toluene-d_8, 223K) (note: due to cold temperature analysis no single detect $^{13}C\{^{1}H\}$ spectrum was acquired at cold temperature): 153.6 (*C7),* 138.7 (*C1*), 122.8 (*C4 & C6),* 115.2 (*C2*), 110.3 (*C5*), 22.5 (*C3′*), 20.1 (*C3*)

6.9 General Procedure for Small Scale Reactivity of **5** with Phenylacetylene

Complex **5** (10 mg, 0.018 mmol) was dissolved in C_6D_6 (0.6 mL) and transferred into an NMR tube. A solution of phenylacetylene was prepared by dissolving (10 mg) in C_6D_6 (1 mL) in a 4 mL vial. Using a microliter pipette one equivalent of phenylacetylene (0.018 mmol, 20 uL) was added to the NMR tube, which was then inverted three times. The reaction progress was analyzed by ^1H and $^{31}P\{^1H\}$ NMR spectroscopy either right after the addition of phenylacetylene or at 60 ºC at the NMR spectrometer.

6.10 UV-Vis Studies:

6.10.1: General Procedure for Preparing complexes for UV-Vis Experiments

A 3.5 mL glass cuvette (optical path length 1 cm) was charged with benzene or toluene (3.5 mL), capped with a fitted septum screw cap, and removed from the glovebox. The blank was obtained at room temperature on the UV-vis spectrometer. The cuvette was then brought back into the glovebox. The desired metal complex was dissolved in either toluene or benzene in a 4 mL vial creating a 1 mL stock solution. The cuvette was then emptied and filled with a solution a complex and diluted with benzene or toluene. The cuvette was capped, removed from the glovebox, and placed in the spectrometer to obtain spectra.

6.10.2 Representative Procedure for Determination of Molar Absorptivity (ε) of **7**, **8**, and **5**

A solution of **7** (4 mM, 3.0 mL) was prepared in benzene (in the case of **8,** a 50/50 benzene/pyridine mix was used) and placed into a 3.5 mL cuvette at room temperature. The sample was diluted to various concentrations (4-1 mM at 0.5 mM intervals) by adding C_6H_6 through the septa cap using a gas tight syringe or by returning the solution to the glovebox. Solutions were mixed well (~ 30-60 s) before acquiring a UV-Vis spectrum.

6.10.3: Pyridine Titration to **5**

A solution of **5** in benzene (1.5 mM; 3 mL) was added to cuvette at room temperature. A separate solution of pyridine (10 mg, 0.12 mmol) in benzene (4 mL) was prepared in 4 mL screw cap vial with a red septum top. A UV-vis spectrum of **5** was

recorded. Pyridine was added in varying equivalents using a 250 uL gas tight syringe, specifically 1-2 equivalents (0.25 equivalent intervals) and then 2-5 (0.5 equivalent intervals). The solution was mixed well (30 s) after each addition and before a spectrum was recorded.

6.10.4: Variable Temperature Observation of **5** by UV-Vis

A solution of **5** in toluene at 1.5 mM or 0.75 mM (3 mL) was added to a cuvette and a UV-vis spectrum recorded at room temperature. The solution was cooled in the UV-Vis spectrometer sample holder to 0, –25, and –50 ºC, and a spectrum was collected at each temperature. A colour change from green to orange was observed. A fresh solution (0.75 mM) was also heated from 25 to 30, 40, and 50 ºC. UV-Vis spectra were recorded at the desired temperatures.

6.10.5: Low Temperature Addition of Pyridine to **5**

A solution of **5** in toluene at 1.5 mM (3mL) was added to cuvette and a UV-vis spectrum was recorded at room temperature. The solution was cooled at the UV-Vis spectrometer to –50 ºC and five equivalents of pyridine were added from a stock solution (130 uL, 177 mM). The reaction was monitored over 1 h and a spectrum was recorded every 10 minutes.

7 Appendix

7.1 Crystallographic Data for **7**

Data Collection and Processing: The sample was mounted on a Mitegen polyimide micromount with a small amount of Paratone N oil. All X-ray measurements were made on a Bruker Kappa Axis Apex2 diffractometer at a temperature of 110 K. The unit cell dimensions were determined from a symmetry constrained fit of 9964 reflections with 4.84º < 2θ < 64.56º. The data collection strategy was a number of ω and φ scans which collected data up to 65.39º (2θ). The frame integration was performed using SAINT.[126] The resulting raw data was scaled, and absorption corrected using a multi-scan averaging of symmetry equivalent data using SADABS.[127]

Structure Solution and Refinement: The structure was solved by using a dual space methodology using the SHELXT program.[128] All non-hydrogen atoms were obtained from the initial solution. The hydrogen atoms were introduced at idealized positions and were allowed to ride on the parent atom. The structural model was fit to the data using full matrix least-squares based on F^2. The calculated structure factors included corrections for anomalous dispersion from the usual tabulation. The structure was refined using the SHELXL program from the SHELX suit of crystallographic software.[129] Graphic plots were produced using the mercury program suite.[130]

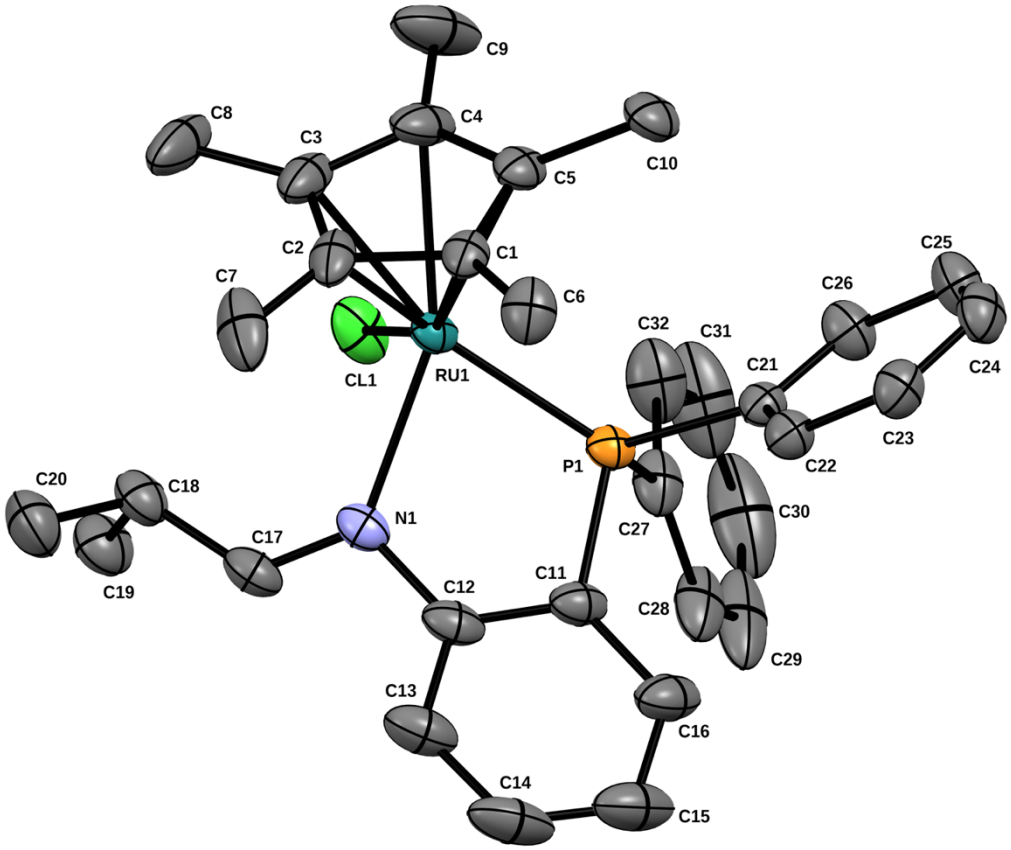

ORTEP drawing of **7** showing naming and numbering scheme. Ellipsoids are at the 50% probability level and hydrogen atoms were omitted for clarity.

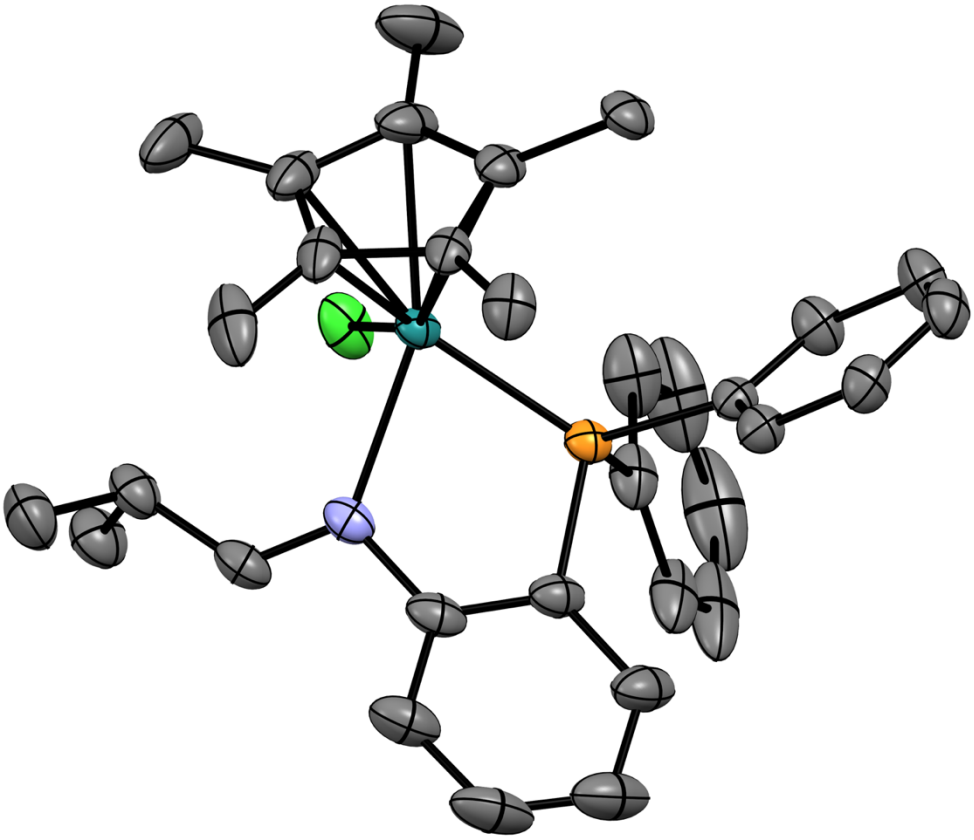

ORTEP drawing of **7**.
Ellipsoids are at the 50% probability level
and hydrogen atoms were omitted for clarity.

Table A1. **Summary of Crystal Data for *7***

Formula	$C_{32}H_{37}ClNPRu$
Formula Weight (*g/mol*)	603.11
Crystal Dimensions (*mm*)	0.148 × 0.086 × 0.081
Crystal Color and Habit	orange prism
Crystal System	monoclinic
Space Group	P 2_1/c
Temperature, K	110
a, Å	16.261(3)
b, Å	11.225(3)
c, Å	16.025(3)
α,°	90
β,°	103.873(10)
γ,°	90
V, $Å^3$	2839.8(11)
Number of reflections to determine final unit cell	9964
Min and Max 2θ for cell determination, °	4.84, 64.56
Z	4
F(000)	1248
ρ (*g/cm*)	1.411
λ, Å, (MoKα)	0.71073
μ, (cm^{-1})	0.724
Diffractometer Type	Bruker Kappa Axis Apex2
Scan Type(s)	phi and omega scans
Max 2θ for data collection, °	65.39
Measured fraction of data	0.998
Number of reflections measured	95988
Unique reflections measured	10400
R_{merge}	0.0800
Number of reflections	10400

included in refinement	
Cut off Threshold Expression	I > 2sigma(I)
Structure refined using	full matrix least-squares using F^2
Weighting Scheme	$w=1/[sigma^2(Fo^2)+(0.0382P)^2+0.9731P]$ where $P=(Fo^2+2Fc^2)/3$
Number of parameters in least-squares	332
R_1	0.0394
wR_2	0.0835
R_1 (all data)	0.0616
wR_2 (all data)	0.0918
GOF	1.036
Maximum shift/error	0.001
Min & Max peak heights on final ΔF Map (e^-/Å)	-0.869, 0.660

Where:

$R_1 = \Sigma(|F_o| - |F_c|) / \Sigma F_o$

$wR_2 = [\Sigma(w(F_o^2 - F_c^2)^2) / \Sigma(w F_o^4)]^{½}$

GOF = $[\Sigma(w(F_o^2 - F_c^2)^2) / (\text{No. of reflns.} - \text{No. of params.})]^{½}$

Table A2*. Atomic Coordinates for *7

Atom	x	y	z	$U_{iso/equiv}$
Ru1	0.23204(2)	0.44509(2)	0.35916(2)	0.02291(5)
Cl1	0.35834(3)	0.32390(5)	0.36579(3)	0.03915(14)
P1	0.26525(3)	0.57651(5)	0.26328(3)	0.02381(11)
N1	0.30969(9)	0.56939(16)	0.44661(11)	0.0271(4)
C1	0.09984(11)	0.47768(19)	0.35741(13)	0.0279(4)
C2	0.13936(12)	0.4204(2)	0.43735(14)	0.0362(5)
C3	0.16885(13)	0.3073(2)	0.41933(17)	0.0437(6)
C4	0.14931(14)	0.2929(2)	0.32649(17)	0.0442(6)
C5	0.10436(11)	0.3961(2)	0.28944(14)	0.0308(4)
C6	0.04962(13)	0.5909(2)	0.35000(15)	0.0367(5)
C7	0.14138(15)	0.4735(3)	0.52324(15)	0.0533(8)
C8	0.20936(17)	0.2123(3)	0.4819(2)	0.0723(11)
C9	0.16652(18)	0.1839(2)	0.2795(2)	0.0713(11)
C10	0.05886(13)	0.4085(2)	0.19646(14)	0.0360(5)
C11	0.29262(12)	0.70969(19)	0.32862(14)	0.0312(4)
C12	0.30676(11)	0.69079(19)	0.41686(14)	0.0317(4)
C13	0.31587(13)	0.7882(2)	0.47242(17)	0.0421(6)
C14	0.31630(15)	0.9018(2)	0.4400(2)	0.0533(7)
C15	0.30682(15)	0.9212(2)	0.3534(2)	0.0542(8)
C16	0.29396(14)	0.8257(2)	0.29764(18)	0.0444(6)
C17	0.36198(12)	0.5492(2)	0.51973(14)	0.0335(5)
C18	0.37811(13)	0.4348(2)	0.56707(14)	0.0356(5)
C19	0.47145(14)	0.3995(3)	0.57642(16)	0.0448(6)
C20	0.36106(17)	0.4518(3)	0.65681(15)	0.0490(7)
C21	0.18279(11)	0.63140(18)	0.17182(12)	0.0246(4)
C22	0.12413(11)	0.71625(19)	0.18419(13)	0.0272(4)
C23	0.05614(12)	0.7479(2)	0.11671(14)	0.0319(4)
C24	0.04593(12)	0.6949(2)	0.03726(14)	0.0363(5)
C25	0.10411(13)	0.6132(2)	0.02366(14)	0.0383(5)
C26	0.17255(13)	0.5816(2)	0.09084(14)	0.0332(5)
C27	0.35296(12)	0.5523(2)	0.21147(14)	0.0354(5)

C28	0.41000(13)	0.6416(3)	0.20293(16)	0.0507(7)
C29	0.47246(15)	0.6160(4)	0.15719(19)	0.0747(11)
C30	0.47574(19)	0.5057(5)	0.1210(2)	0.0887(14)
C31	0.4211(2)	0.4202(4)	0.1301(2)	0.0765(11)
C32	0.35977(16)	0.4404(3)	0.17594(16)	0.0487(7)
H6A	0.038888	0.620710	0.290892	0.055
H6B	0.081596	0.650559	0.389409	0.055
H6C	-0.004450	0.575368	0.364856	0.055
H7A	0.083529	0.479288	0.530972	0.080
H7B	0.166567	0.553216	0.526700	0.080
H7C	0.175365	0.422911	0.568417	0.080
H8A	0.218436	0.242964	0.540705	0.108
H8B	0.263902	0.189601	0.470713	0.108
H8C	0.172165	0.142521	0.475182	0.108
H9A	0.147768	0.197527	0.217380	0.107
H9B	0.135648	0.116089	0.295526	0.107
H9C	0.227401	0.166904	0.294709	0.107
H10A	0.003114	0.370460	0.186785	0.054
H10B	0.092021	0.369912	0.160444	0.054
H10C	0.051773	0.493116	0.181513	0.054
H13	0.321737	0.776253	0.532253	0.050
H14	0.323268	0.967852	0.478092	0.064
H15	0.309118	0.999826	0.332130	0.065
H16	0.285956	0.838942	0.237672	0.053
H17	0.393950	0.615618	0.546372	0.040
H18	0.340070	0.371434	0.534965	0.043
H19A	0.480189	0.377118	0.520065	0.067
H19B	0.485472	0.331796	0.615894	0.067
H19C	0.508061	0.467135	0.599257	0.067
H20A	0.399986	0.511796	0.688669	0.074
H20B	0.369851	0.376020	0.688095	0.074
H20C	0.302513	0.478299	0.650755	0.074
H22	0.130545	0.752682	0.238883	0.033
H23	0.016700	0.806136	0.125524	0.038

H24	-0.001377	0.715045	-0.008078	0.044
H25	0.097825	0.578166	-0.031476	0.046
H26	0.212651	0.525056	0.080916	0.040
H28	0.407052	0.718130	0.227327	0.061
H29	0.512303	0.675484	0.151506	0.090
H30	0.517029	0.489920	0.089372	0.106
H31	0.424268	0.344389	0.104745	0.092
H32	0.322571	0.378028	0.183016	0.058

Table A3*. Anisotropic Displacement Parameters for *7

Atom	u^{11}	u^{22}	u^{33}	u^{12}	u^{13}	u^{23}
Ru1	0.01459 (6)	0.02229 (8)	0.02886 (8)	0.00095 (5)	-0.00068 (5)	-0.00094 (6)
Cl1	0.0305 (2)	0.0417 (3)	0.0402 (3)	0.0177 (2)	-0.0015 (2)	-0.0048 (2)
P1	0.01469 (19)	0.0250 (3)	0.0301 (2)	0.00099 (16)	0.00226 (16)	-0.00085 (19)
N1	0.0174 (7)	0.0333 (10)	0.0298 (8)	-0.0002 (6)	0.0041 (6)	-0.0054 (7)
C1	0.0157 (7)	0.0338 (11)	0.0330 (9)	-0.0029 (7)	0.0036 (6)	0.0080 (8)
C2	0.0188 (8)	0.0508 (14)	0.0369 (11)	-0.0086 (8)	0.0024 (7)	0.0184 (10)
C3	0.0250 (9)	0.0379 (13)	0.0589 (14)	-0.0095 (9)	-0.0082 (9)	0.0225 (11)
C4	0.0277 (10)	0.0276 (11)	0.0643 (15)	-0.0065 (8)	-0.0144 (10)	0.0029 (10)
C5	0.0171 (8)	0.0303 (11)	0.0398 (11)	-0.0041 (7)	-0.0032 (7)	0.0030 (9)
C6	0.0247 (9)	0.0480 (14)	0.0398 (12)	0.0087 (9)	0.0126 (8)	0.0070 (10)
C7	0.0273 (11)	0.100 (2)	0.0343 (12)	-0.0006 (12)	0.0105 (9)	0.0180 (13)
C8	0.0448 (14)	0.0517 (17)	0.098 (2)	-0.0178 (13)	-0.0259 (15)	0.0471 (17)
C9	0.0535 (16)	0.0277 (13)	0.108 (3)	0.0041 (11)	-0.0294 (16)	-0.0154 (15)
C10	0.0240 (9)	0.0383 (12)	0.0389 (11)	-0.0050 (8)	-0.0061 (8)	-0.0021 (9)
C11	0.0202 (8)	0.0247 (10)	0.0441 (11)	-0.0001 (7)	-0.0016 (7)	-0.0025 (8)
C12	0.0162 (8)	0.0317 (11)	0.0433 (11)	0.0002 (7)	-0.0002 (7)	-0.0095 (9)
C13	0.0267	0.0396	0.0550	0.0012	0.0001	-0.0194

	(10)	(13)	(14)	(9)	(9)	(11)
C14	0.0313 (11)	0.0321 (12)	0.0858 (19)	0.0030 (10)	-0.0070 (12)	-0.0246 (13)
C15	0.0320 (12)	0.0272 (12)	0.090 (2)	0.0001 (9)	-0.0107 (12)	-0.0068 (12)
C16	0.0304 (10)	0.0293 (12)	0.0632 (15)	-0.0049 (9)	-0.0089 (10)	0.0023 (11)
C17	0.0225 (8)	0.0406 (12)	0.0341 (10)	-0.0023 (8)	0.0006 (7)	-0.0095 (9)
C18	0.0245 (9)	0.0454 (14)	0.0324 (10)	-0.0025 (9)	-0.0018 (7)	-0.0024 (9)
C19	0.0279 (10)	0.0516 (15)	0.0476 (13)	0.0009 (10)	-0.0052 (9)	0.0015 (12)
C20	0.0450 (13)	0.0634 (18)	0.0334 (11)	-0.0016 (12)	-0.0007 (10)	-0.0010 (11)
C21	0.0168 (7)	0.0257 (10)	0.0304 (9)	-0.0005 (6)	0.0040 (6)	0.0026 (7)
C22	0.0216 (8)	0.0279 (10)	0.0320 (9)	0.0019 (7)	0.0063 (7)	0.0015 (8)
C23	0.0240 (9)	0.0334 (11)	0.0384 (11)	0.0069 (8)	0.0078 (7)	0.0065 (9)
C24	0.0240 (9)	0.0477 (14)	0.0337 (10)	0.0028 (9)	0.0001 (7)	0.0086 (10)
C25	0.0318 (10)	0.0514 (15)	0.0293 (10)	0.0054 (10)	0.0027 (8)	-0.0024 (10)
C26	0.0242 (9)	0.0409 (13)	0.0337 (10)	0.0064 (8)	0.0055 (7)	-0.0024 (9)
C27	0.0173 (8)	0.0539 (14)	0.0347 (10)	0.0073 (8)	0.0058 (7)	0.0101 (10)
C28	0.0173 (9)	0.085 (2)	0.0448 (13)	-0.0034 (10)	-0.0024 (8)	0.0270 (13)
C29	0.0176 (10)	0.152 (3)	0.0502 (16)	-0.0046 (15)	0.0006 (10)	0.0471 (19)
C30	0.0306 (14)	0.186 (4)	0.0524 (18)	0.041 (2)	0.0160 (12)	0.024 (2)
C31	0.0498 (17)	0.133 (3)	0.0511 (16)	0.0529 (19)	0.0204 (13)	0.0063 (18)

C32	0.0382 (12)	0.0655 (18)	0.0441 (13)	0.0267 (12)	0.0134 (10)	0.0039 (12)

Table A4*. Bond Lengths for *7

Ru1-N1	2.1579(16)	C13-C14	1.377(4)
Ru1-C4	2.159(2)	C13-H13	0.9500
Ru1-C1	2.1742(19)	C14-C15	1.377(5)
Ru1-C5	2.1794(17)	C14-H14	0.9500
Ru1-C2	2.196(2)	C15-C16	1.379(4)
Ru1-C3	2.203(2)	C15-H15	0.9500
Ru1-P1	2.2862(7)	C16-H16	0.9500
Ru1-Cl1	2.4444(7)	C17-C18	1.483(3)
P1-C11	1.818(2)	C17-H17	0.9500
P1-C27	1.835(2)	C18-C20	1.540(4)
P1-C21	1.8394(18)	C18-C19	1.541(3)
N1-C17	1.292(2)	C18-H18	1.0000
N1-C12	1.441(3)	C19-H19A	0.9800
C1-C5	1.439(3)	C19-H19B	0.9800
C1-C2	1.440(3)	C19-H19C	0.9800
C1-C6	1.500(3)	C20-H20A	0.9800
C2-C3	1.411(4)	C20-H20B	0.9800
C2-C7	1.493(4)	C20-H20C	0.9800
C3-C4	1.454(4)	C21-C26	1.386(3)
C3-C8	1.503(3)	C21-C22	1.395(3)
C4-C5	1.421(3)	C22-C23	1.394(3)
C4-C9	1.498(4)	C22-H22	0.9500
C5-C10	1.503(3)	C23-C24	1.378(3)
C6-H6A	0.9800	C23-H23	0.9500
C6-H6B	0.9800	C24-C25	1.372(3)
C6-H6C	0.9800	C24-H24	0.9500
C7-H7A	0.9800	C25-C26	1.396(3)
C7-H7B	0.9800	C25-H25	0.9500
C7-H7C	0.9800	C26-H26	0.9500
C8-H8A	0.9800	C27-C32	1.394(4)
C8-H8B	0.9800	C27-C28	1.394(3)
C8-H8C	0.9800	C28-C29	1.417(4)

C9-H9A	0.9800	C28-H28	0.9500
C9-H9B	0.9800	C29-C30	1.374(6)
C9-H9C	0.9800	C29-H29	0.9500
C10-H10A	0.9800	C30-C31	1.339(6)
C10-H10B	0.9800	C30-H30	0.9500
C10-H10C	0.9800	C31-C32	1.392(4)
C11-C12	1.393(3)	C31-H31	0.9500
C11-C16	1.396(3)	C32-H32	0.9500
C12-C13	1.395(3)		

Table A5*. Bond Angles for *7

N1-Ru1-C4	154.47(9)	C4-C9-H9B	109.5
N1-Ru1-C1	108.80(7)	H9A-C9-H9B	109.5
C4-Ru1-C1	64.75(9)	C4-C9-H9C	109.5
N1-Ru1-C5	146.45(8)	H9A-C9-H9C	109.5
C4-Ru1-C5	38.22(8)	H9B-C9-H9C	109.5
C1-Ru1-C5	38.59(8)	C5-C10-H10A	109.5
N1-Ru1-C2	94.93(8)	C5-C10-H10B	109.5
C4-Ru1-C2	64.26(10)	H10A-C10-H10B	109.5
C1-Ru1-C2	38.46(7)	C5-C10-H10C	109.5
C5-Ru1-C2	63.95(8)	H10A-C10-H10C	109.5
N1-Ru1-C3	115.56(8)	H10B-C10-H10C	109.5
C4-Ru1-C3	38.92(10)	C12-C11-C16	119.4(2)
C1-Ru1-C3	63.91(8)	C12-C11-P1	114.66(16)
C5-Ru1-C3	63.90(8)	C16-C11-P1	125.79(18)
C2-Ru1-C3	37.42(10)	C11-C12-C13	119.6(2)
N1-Ru1-P1	79.83(5)	C11-C12-N1	117.67(18)
C4-Ru1-P1	125.54(7)	C13-C12-N1	122.7(2)
C1-Ru1-P1	105.96(6)	C14-C13-C12	119.6(3)
C5-Ru1-P1	99.67(6)	C14-C13-H13	120.2
C2-Ru1-P1	140.34(6)	C12-C13-H13	120.2
C3-Ru1-P1	163.21(6)	C13-C14-C15	121.2(2)
N1-Ru1-Cl1	88.68(5)	C13-C14-H14	119.4
C4-Ru1-Cl1	92.21(7)	C15-C14-H14	119.4
C1-Ru1-Cl1	155.79(6)	C14-C15-C16	119.5(3)
C5-Ru1-Cl1	124.68(6)	C14-C15-H15	120.2
C2-Ru1-Cl1	126.11(6)	C16-C15-H15	120.2
C3-Ru1-Cl1	93.76(7)	C15-C16-C11	120.5(3)
P1-Ru1-Cl1	93.26(2)	C15-C16-H16	119.7
C11-P1-C27	105.84(11)	C11-C16-H16	119.7
C11-P1-C21	102.38(9)	N1-C17-C18	127.83(19)
C27-P1-C21	100.74(9)	N1-C17-H17	116.1
C11-P1-Ru1	102.02(8)	C18-C17-H17	116.1

C27-P1-Ru1	122.90(8)	C17-C18-C20	108.7(2)
C21-P1-Ru1	120.47(7)	C17-C18-C19	108.8(2)
C17-N1-C12	115.38(17)	C20-C18-C19	109.55(18)
C17-N1-Ru1	129.10(15)	C17-C18-H18	109.9
C12-N1-Ru1	115.40(11)	C20-C18-H18	109.9
C5-C1-C2	107.23(19)	C19-C18-H18	109.9
C5-C1-C6	127.26(17)	C18-C19-H19A	109.5
C2-C1-C6	124.6(2)	C18-C19-H19B	109.5
C5-C1-Ru1	70.90(11)	H19A-C19-H19B	109.5
C2-C1-Ru1	71.60(11)	C18-C19-H19C	109.5
C6-C1-Ru1	131.42(15)	H19A-C19-H19C	109.5
C3-C2-C1	108.7(2)	H19B-C19-H19C	109.5
C3-C2-C7	127.9(2)	C18-C20-H20A	109.5
C1-C2-C7	123.2(2)	C18-C20-H20B	109.5
C3-C2-Ru1	71.54(14)	H20A-C20-H20B	109.5
C1-C2-Ru1	69.94(12)	C18-C20-H20C	109.5
C7-C2-Ru1	127.52(16)	H20A-C20-H20C	109.5
C2-C3-C4	107.92(19)	H20B-C20-H20C	109.5
C2-C3-C8	128.1(3)	C26-C21-C22	118.41(16)
C4-C3-C8	123.9(3)	C26-C21-P1	120.78(15)
C2-C3-Ru1	71.04(13)	C22-C21-P1	120.54(15)
C4-C3-Ru1	68.93(13)	C23-C22-C21	120.37(19)
C8-C3-Ru1	127.89(17)	C23-C22-H22	119.8
C5-C4-C3	107.5(2)	C21-C22-H22	119.8
C5-C4-C9	126.5(2)	C24-C23-C22	120.3(2)
C3-C4-C9	125.7(2)	C24-C23-H23	119.9
C5-C4-Ru1	71.65(12)	C22-C23-H23	119.9
C3-C4-Ru1	72.15(12)	C25-C24-C23	119.99(18)
C9-C4-Ru1	126.0(2)	C25-C24-H24	120.0
C4-C5-C1	108.49(19)	C23-C24-H24	120.0
C4-C5-C10	124.9(2)	C24-C25-C26	120.0(2)
C1-C5-C10	126.10(19)	C24-C25-H25	120.0
C4-C5-Ru1	70.13(11)	C26-C25-H25	120.0
C1-C5-Ru1	70.51(10)	C21-C26-C25	120.9(2)

C10-C5-Ru1	131.83(16)	C21-C26-H26	119.5
C1-C6-H6A	109.5	C25-C26-H26	119.5
C1-C6-H6B	109.5	C32-C27-C28	119.2(2)
H6A-C6-H6B	109.5	C32-C27-P1	117.70(19)
C1-C6-H6C	109.5	C28-C27-P1	123.1(2)
H6A-C6-H6C	109.5	C27-C28-C29	118.8(3)
H6B-C6-H6C	109.5	C27-C28-H28	120.6
C2-C7-H7A	109.5	C29-C28-H28	120.6
C2-C7-H7B	109.5	C30-C29-C28	120.4(3)
H7A-C7-H7B	109.5	C30-C29-H29	119.8
C2-C7-H7C	109.5	C28-C29-H29	119.8
H7A-C7-H7C	109.5	C31-C30-C29	120.4(3)
H7B-C7-H7C	109.5	C31-C30-H30	119.8
C3-C8-H8A	109.5	C29-C30-H30	119.8
C3-C8-H8B	109.5	C30-C31-C32	121.3(4)
H8A-C8-H8B	109.5	C30-C31-H31	119.4
C3-C8-H8C	109.5	C32-C31-H31	119.4
H8A-C8-H8C	109.5	C31-C32-C27	120.0(3)
H8B-C8-H8C	109.5	C31-C32-H32	120.0
C4-C9-H9A	109.5	C27-C32-H32	120.0

Table A6. Torsion Angels for 7

C5-C1-C2-C3	1.0(2)	P1-C11-C12-C13	-170.61(16)
C6-C1-C2-C3	170.53(19)	C16-C11-C12-N1	-176.52(19)
Ru1-C1-C2-C3	-61.34(15)	P1-C11-C12-N1	8.2(2)
C5-C1-C2-C7	-175.26(19)	C17-N1-C12-C11	145.65(19)
C6-C1-C2-C7	-5.7(3)	Ru1-N1-C12-C11	-30.7(2)
Ru1-C1-C2-C7	122.4(2)	C17-N1-C12-C13	-35.6(3)
C5-C1-C2-Ru1	62.34(13)	Ru1-N1-C12-C13	148.10(16)
C6-C1-C2-Ru1	-128.1(2)	C11-C12-C13-C14	-4.2(3)
C1-C2-C3-C4	1.0(2)	N1-C12-C13-C14	177.0(2)
C7-C2-C3-C4	177.1(2)	C12-C13-C14-C15	0.8(4)
Ru1-C2-C3-C4	-59.30(16)	C13-C14-C15-C16	2.1(4)
C1-C2-C3-C8	-175.9(2)	C14-C15-C16-C11	-1.6(4)
C7-C2-C3-C8	0.1(4)	C12-C11-C16-C15	-1.8(3)
Ru1-C2-C3-C8	123.8(2)	P1-C11-C16-C15	172.94(19)
C1-C2-C3-Ru1	60.34(14)	C12-N1-C17-C18	179.1(2)
C7-C2-C3-Ru1	-123.6(2)	Ru1-N1-C17-C18	-5.2(3)
C2-C3-C4-C5	-2.7(2)	N1-C17-C18-C20	-122.4(2)
C8-C3-C4-C5	174.4(2)	N1-C17-C18-C19	118.3(2)
Ru1-C3-C4-	-63.34(15)	C11-P1-C21-	148.99(18)

C5		C26	
C2-C3-C4-C9	-177.5(2)	C27-P1-C21-C26	40.0(2)
C8-C3-C4-C9	-0.4(4)	Ru1-P1-C21-C26	-98.89(17)
Ru1-C3-C4-C9	121.9(3)	C11-P1-C21-C22	-37.13(19)
C2-C3-C4-Ru1	60.63(15)	C27-P1-C21-C22	-146.16(17)
C8-C3-C4-Ru1	-122.3(2)	Ru1-P1-C21-C22	74.98(18)
C3-C4-C5-C1	3.3(2)	C26-C21-C22-C23	1.2(3)
C9-C4-C5-C1	178.1(2)	P1-C21-C22-C23	-172.82(16)
Ru1-C4-C5-C1	-60.33(14)	C21-C22-C23-C24	0.4(3)
C3-C4-C5-C10	-168.6(2)	C22-C23-C24-C25	-1.8(4)
C9-C4-C5-C10	6.2(4)	C23-C24-C25-C26	1.5(4)
Ru1-C4-C5-C10	127.8(2)	C22-C21-C26-C25	-1.5(3)
C3-C4-C5-Ru1	63.67(15)	P1-C21-C26-C25	172.50(19)
C9-C4-C5-Ru1	-121.6(3)	C24-C25-C26-C21	0.2(4)
C2-C1-C5-C4	-2.7(2)	C11-P1-C27-C32	163.45(17)
C6-C1-C5-C4	-171.9(2)	C21-P1-C27-C32	-90.25(18)
Ru1-C1-C5-C4	60.10(15)	Ru1-P1-C27-C32	47.26(19)
C2-C1-C5-C10	169.1(2)	C11-P1-C27-C28	-19.5(2)
C6-C1-C5-C10	-0.1(3)	C21-P1-C27-C28	86.82(18)
Ru1-C1-C5-	-128.1(2)	Ru1-P1-C27-	-135.66(15)

C10		C28	
C2-C1-C5-Ru1	-62.80(13)	C32-C27-C28-C29	0.9(3)
C6-C1-C5-Ru1	128.0(2)	P1-C27-C28-C29	-176.14(16)
C27-P1-C11-C12	-114.73(16)	C27-C28-C29-C30	0.9(3)
C21-P1-C11-C12	140.17(15)	C28-C29-C30-C31	-1.4(4)
Ru1-P1-C11-C12	14.89(15)	C29-C30-C31-C32	0.1(5)
C27-P1-C11-C16	70.3(2)	C30-C31-C32-C27	1.7(4)
C21-P1-C11-C16	-34.8(2)	C28-C27-C32-C31	-2.2(3)
Ru1-P1-C11-C16	-160.05(19)	P1-C27-C32-C31	175.00(19)
C16-C11-C12-C13	4.7(3)		

7.2 Appendix Figures

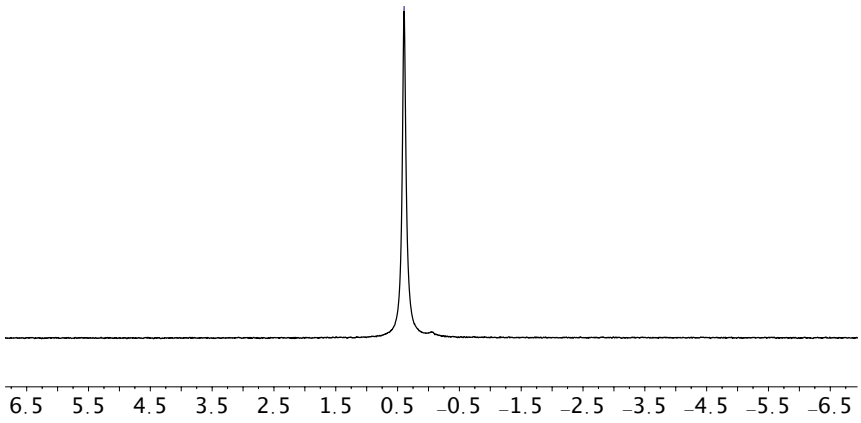

Figure A1: ^{11}B NMR spectrum (192 MHz, C_6D_6) of authentic BF_3 etherate.

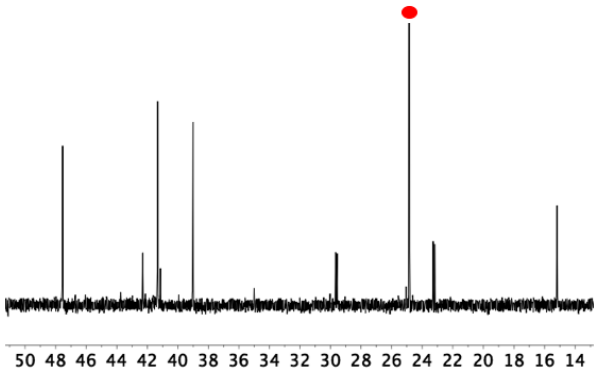

Figure A2: $^{31}P\{^1H\}$ NMR spectrum (243 MHz, C_6D_6) 24 h after of one equivalent MeOH was added to **1** (43.7 ppm) at room temperature. Signal identified: • $OPPh_3$

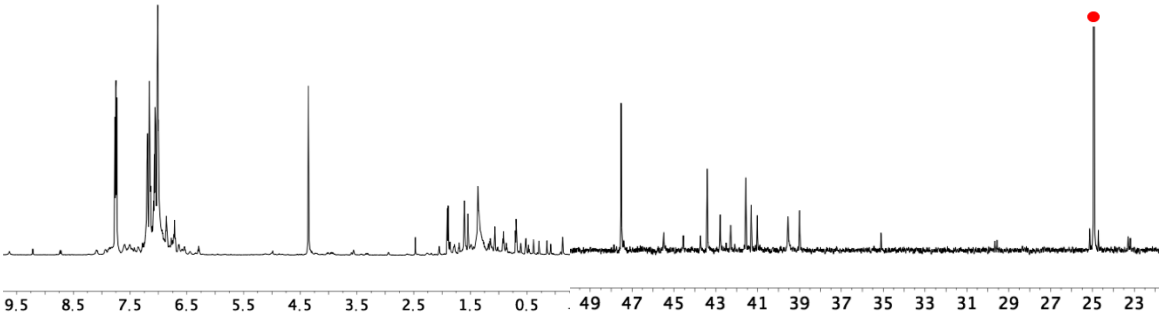

Figure A3: ^1H (600 MHz) and $^{31}P\{^1H\}$ (243 MHz) NMR spectrum 24 h after one equivalent BnOH was added to **1** (43.7 ppm) at room temperature in C_6D_6. Signal identified: • $OPPh_3$

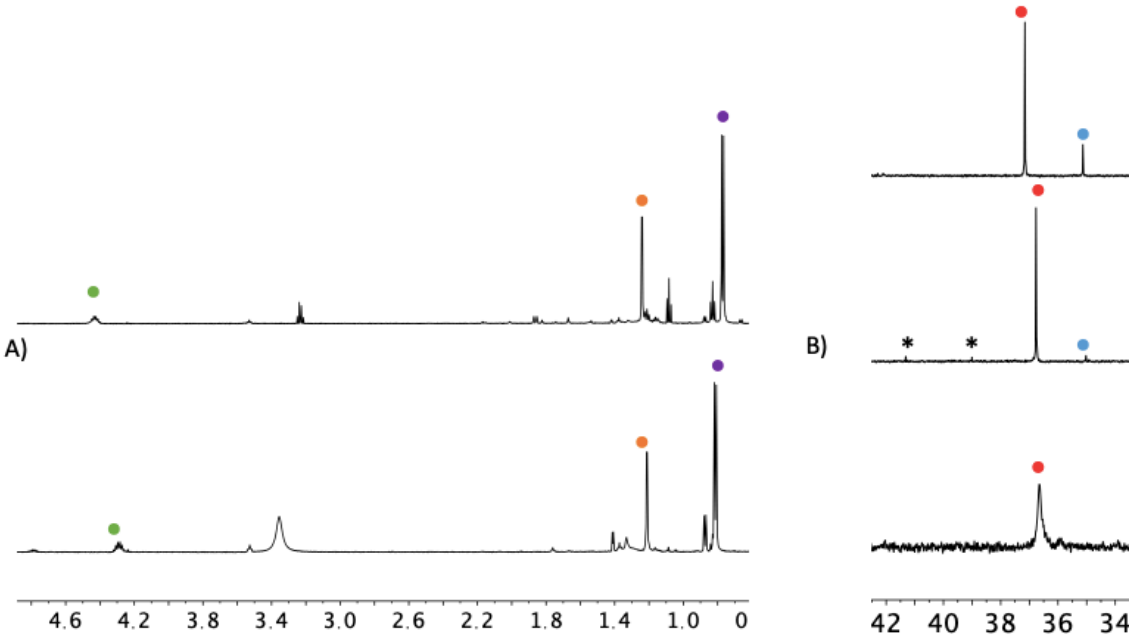

Figure A4: A) Section of the ^{1}H NMR spectra (600 MHz; C_6D_6) after the addition of two equivalents of phenol (top; **12a**) or 4-methoxyphenol (**12c**; bottom) to **1** (43.7 ppm). Signals Indicated: • Methine *H*, • Pd-C*H*$_3$, • Isopropyl-C*H*$_3$ B) ^{31}P{^{1}H} NMR Spectra (243 MHz; C_6D_6) after the addition of two equivalents of 4-methoxyphenol (top, C_6D_6), phenol (middle, C_6D_6), or [DMFH]OTf (bottom, THF) to **1**. Note: the ^{1}H NMR of **12b** was not acquired as THF was required to observe a ^{31}P{^{1}H} NMR spectrum and only THF-h_8 was utilised.

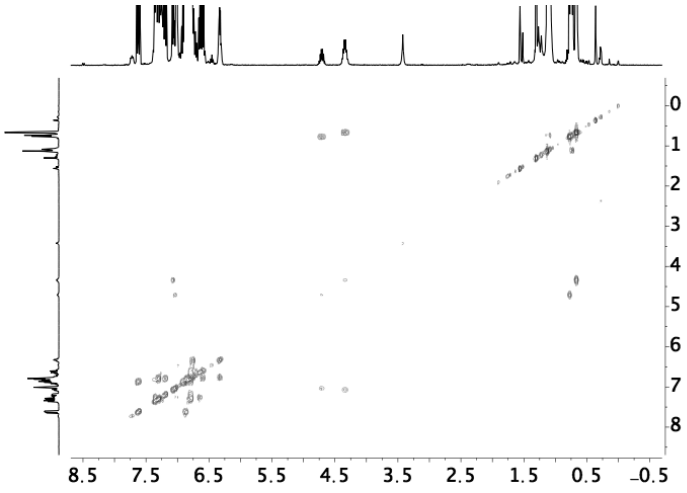

Figure A5: ^{1}H-^{1}H COSY (400 MHz, C_6D_6) spectrum after the addition of K[OPh] to **9** to yield **12a** in THF at room temperature.

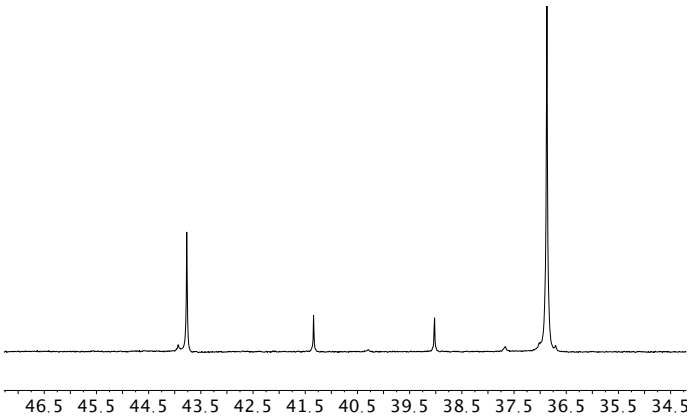

Figure A6: $^{31}P\{^{1}H\}$ NMR spectrum (123 MHz, C_6D_6) after the addition of a phenoxide base to **9** (35 ppm) in C_6D_6 to generate **12c** (major product at 36.6 ppm) and other minor impurities.

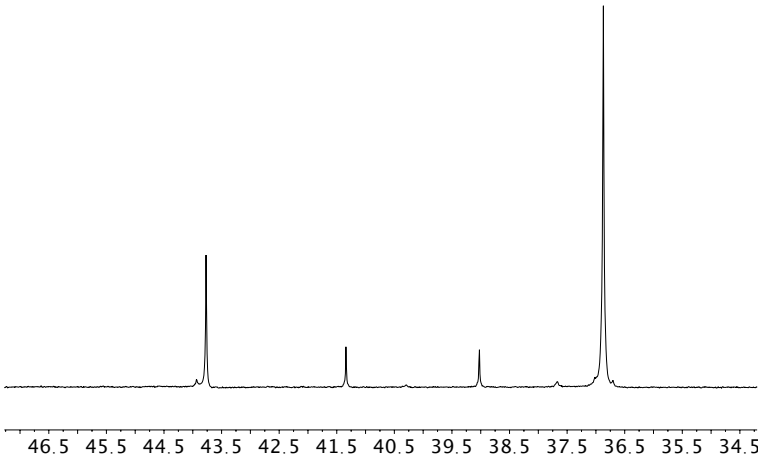

Figure A7: $^{31}P\{^{1}H\}$ NMR spectrum (123 MHz, C_6D_6) after the addition of a phenoxide base to **9** (35 ppm) in C_6D_6 to generate **12e** (major product at 36.6 ppm) and other minor impurities.

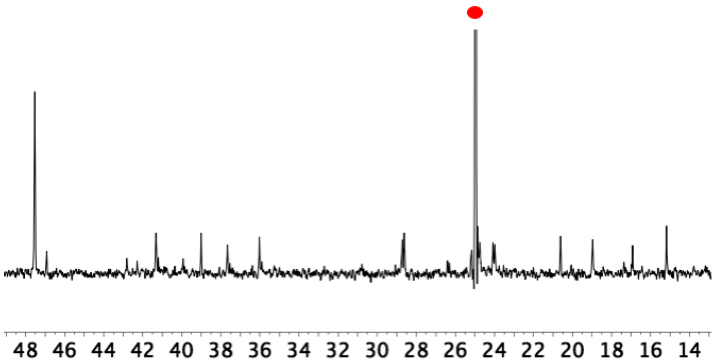

Figure A8: $^{31}P\{^{1}H\}$ NMR spectrum (243 MHz, C_6D_6) of a solution of **1** (43.7 ppm) after being exposed to 1 atm H_2 (30 s) and heated at 38ºC for 24 h. Signal identified: • $OPPh_3$

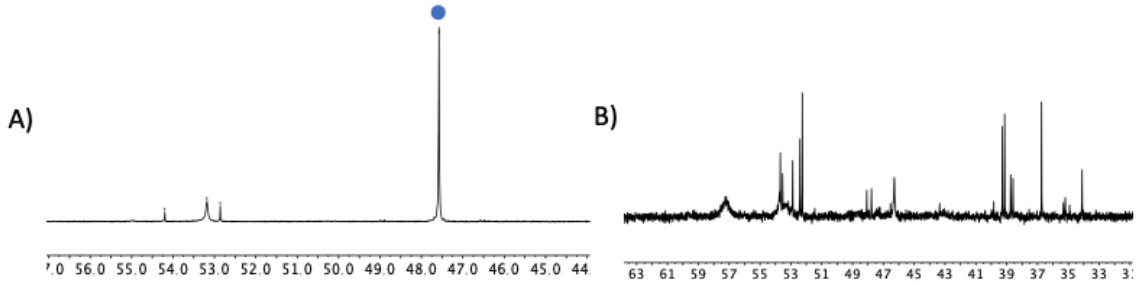

Figure A9: $^{31}P\{^{1}H\}$ NMR spectrum (243 MHz) of the addition of K[**L1**] (–15 ppm) to **13** (no P atom) where reaction solvent was C_6D_6 (A), THF or THF – 20 ºC (B) Signal identified: • **4**

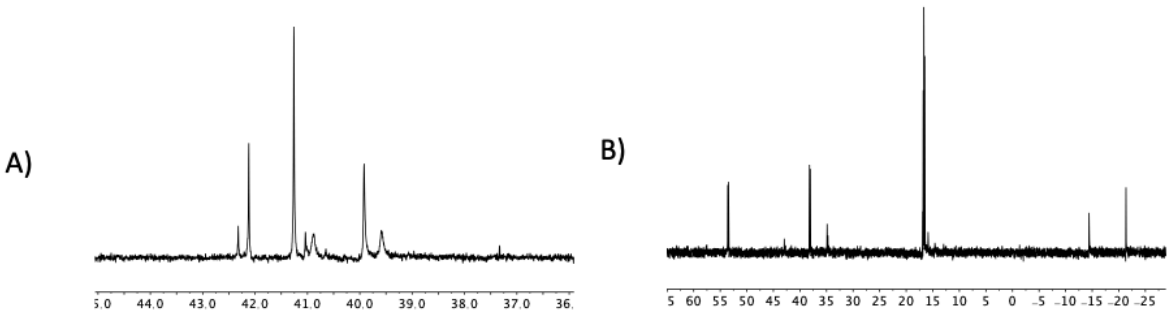

Figure A10: $^{31}P\{^{1}H\}$ NMR spectrum (243 MHz, C_6D_6) of the addition of H[**L1**] (–15 ppm) to **13** (no P atom) where reaction solvent was C_6D_6 (A), THF (B)

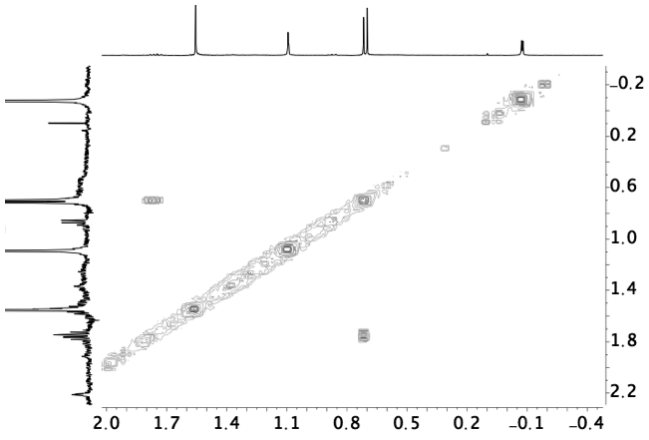

Figure A11: A section of the ^{1}H-^{1}H COSY (600 MHz, C_6D_6) of **16a**/**16b** demonstrating the only correlation in the alkyl region only suggesting the presence of an isopropyl group. The isopropyl group was deemed to an isobutlyramide from **16b**

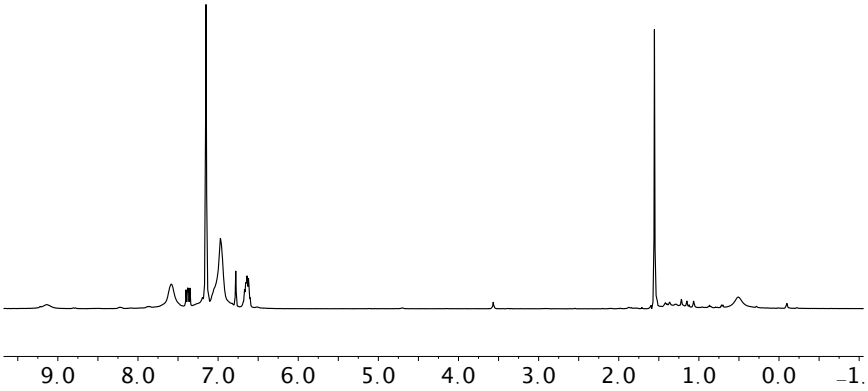

Figure A12: The ^{1}H NMR spectrum (400 MHz, C_6D_6) 48 h after the addition of O_2 to **1** in the presence of TEMPO·. The large singlet in the alkyl region is at 1.55 ppm was proposed to be acetone

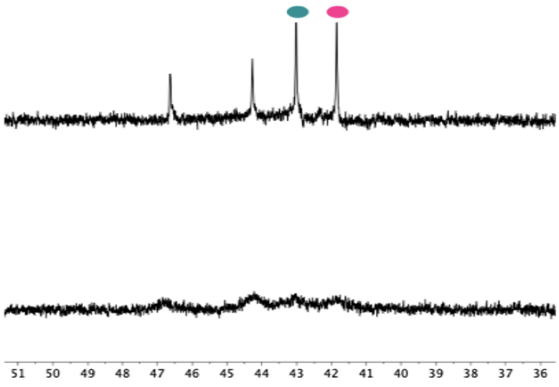

Figure A13: $^{31}P\{^{1}H\}$ NMR spectrum (243 MHz, C_6D_6) of the addition of H_2O to **16a (•)/16b (•**; top) and 24 h later (bottom).

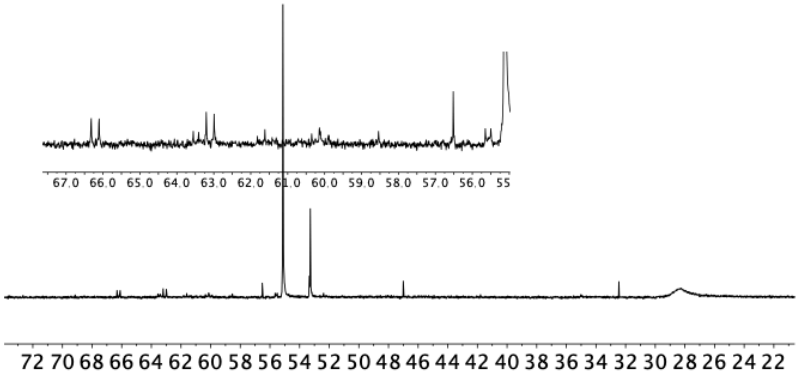

Figure A14: $^{31}P\{^{1}H\}$ NMR spectrum (163 MHz, C_6D_6) of removed unknown green solid that contained multiple unknown products and some **7**. This unknown green solid was removed via benzene/pentane precipitations before and after a $MgCl_2$ treatment in toluene to remove $O{=}PPh_3$ by-product from synthesis of **7.**

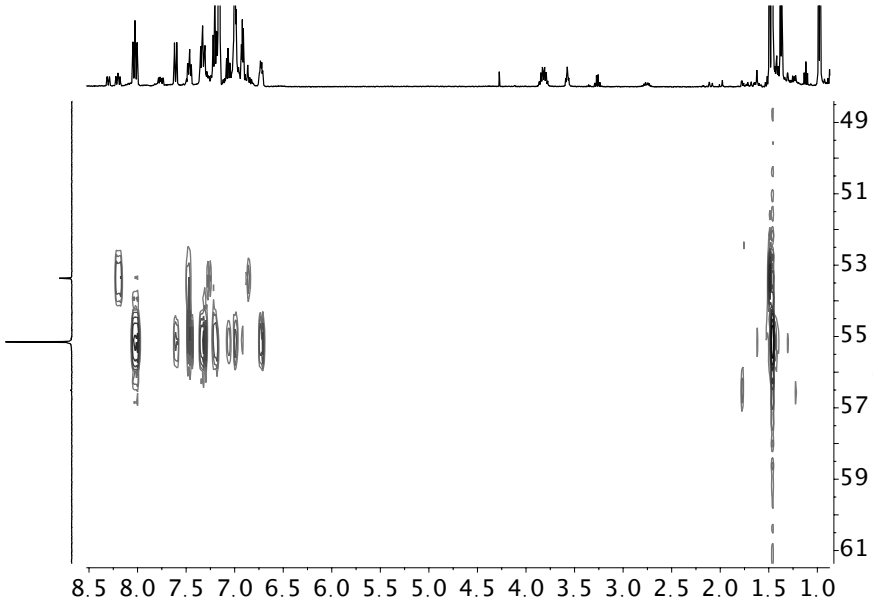

Figure A15: ^{1}H-^{31}P HMBC (400 & 163 MHz, C_6D_6) 2D-NMR experiment of **7** in C_6D_6

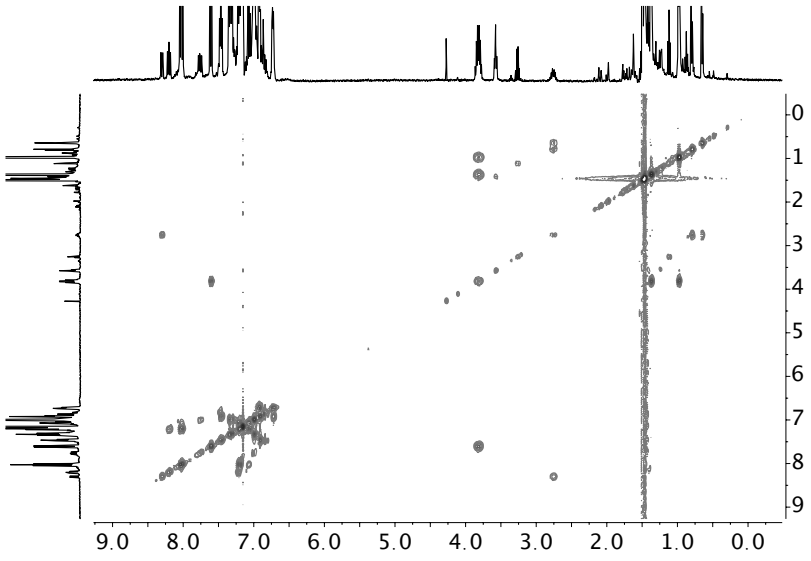

Figure A16: ^{1}H-^{1}H COSY (400 MHz, C_6D_6) 2D-NMR experiment of **7**

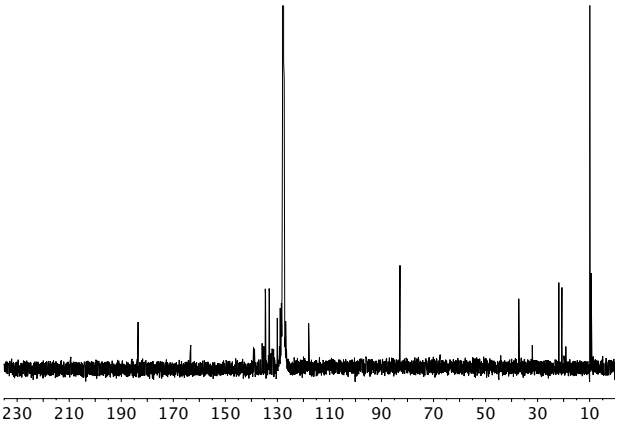

Figure A17: ^{13}C{^{1}H} NMR Spectrum of **7** (C_6D_6; 101 MHz). Major Signal at 130 ppm is C_6D_6.

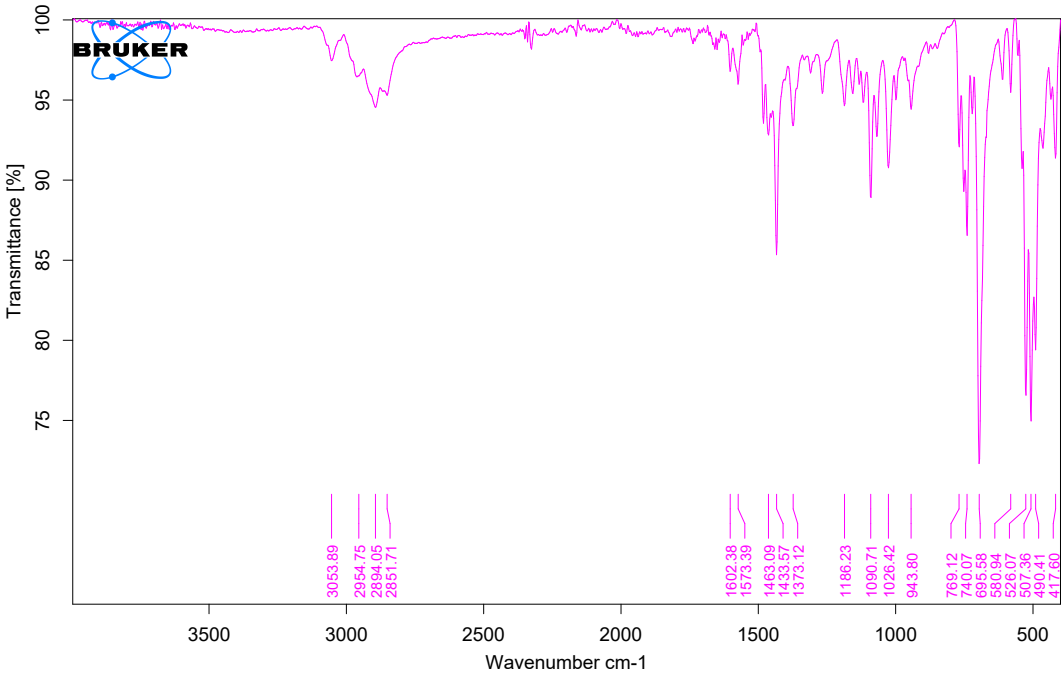

Figure A18: ATR-IR spectrum of a solid sample of **7**

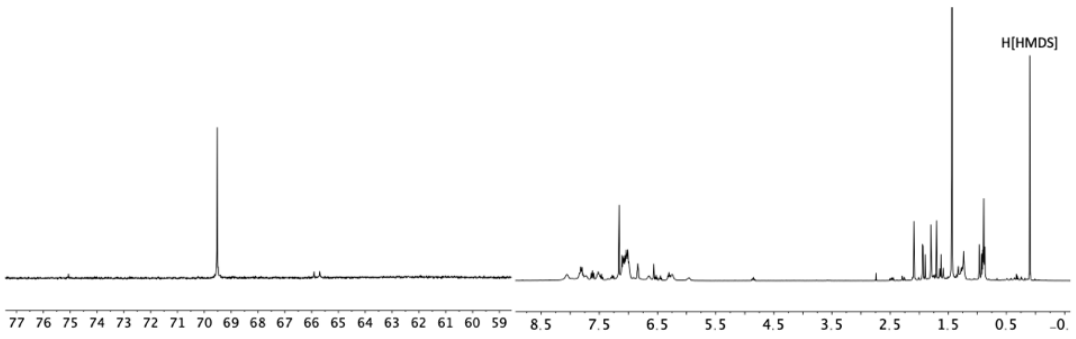

Figure A19: $^{31}P\{^{1}H\}$ (163 MHz) (left) and ^{1}H (400 MHz) NMR spectra of unknown impurity in synthesis of **8**/**5** with by-product H[HMDS] in C_6D_6.

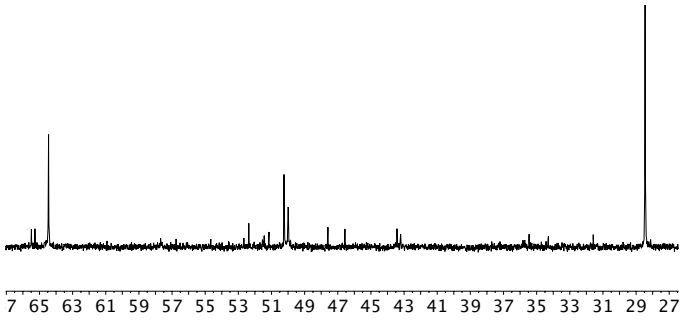

Figure A20: $^{31}P\{^{1}H\}$ (163 MHz) NMR spectrum after dissolving **5** in CD_3CN

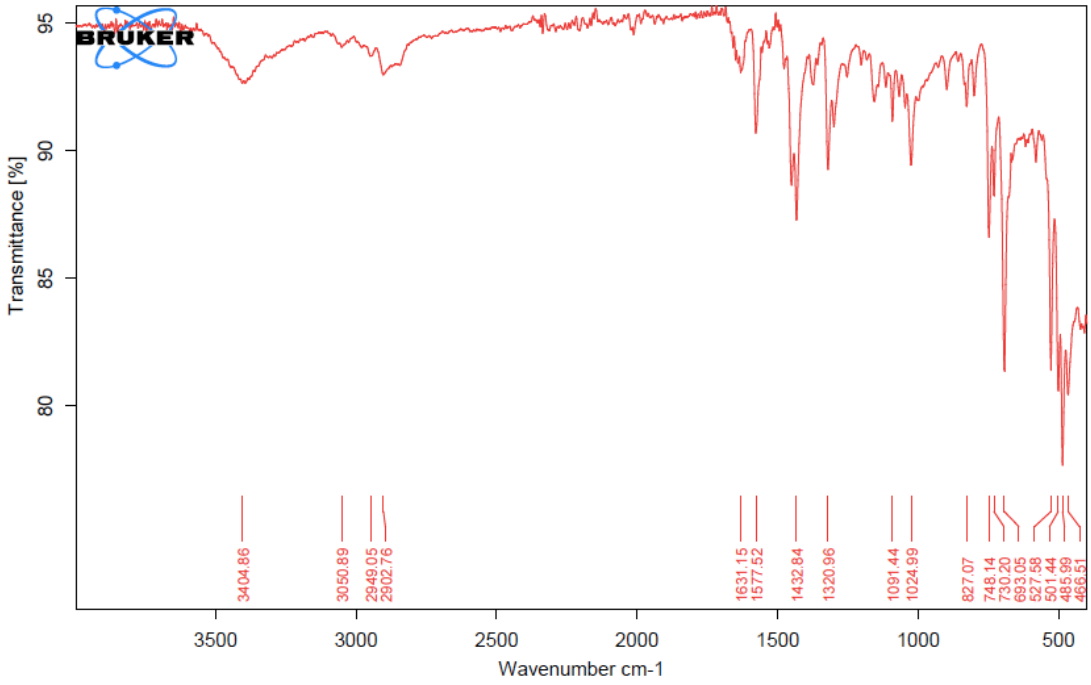

Figure A21: IR spectrum of solid state **5**

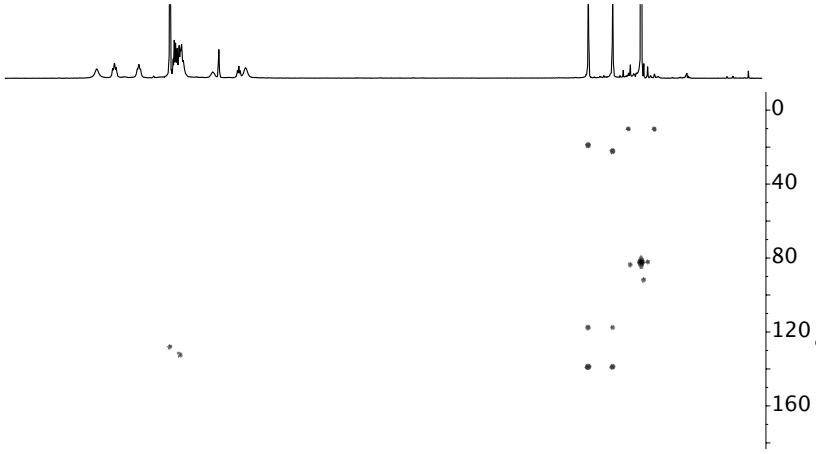

Figure A22: ^{1}H-^{13}C HMBC (400 and 101 MHz) of **5** at RT in C_6D_6

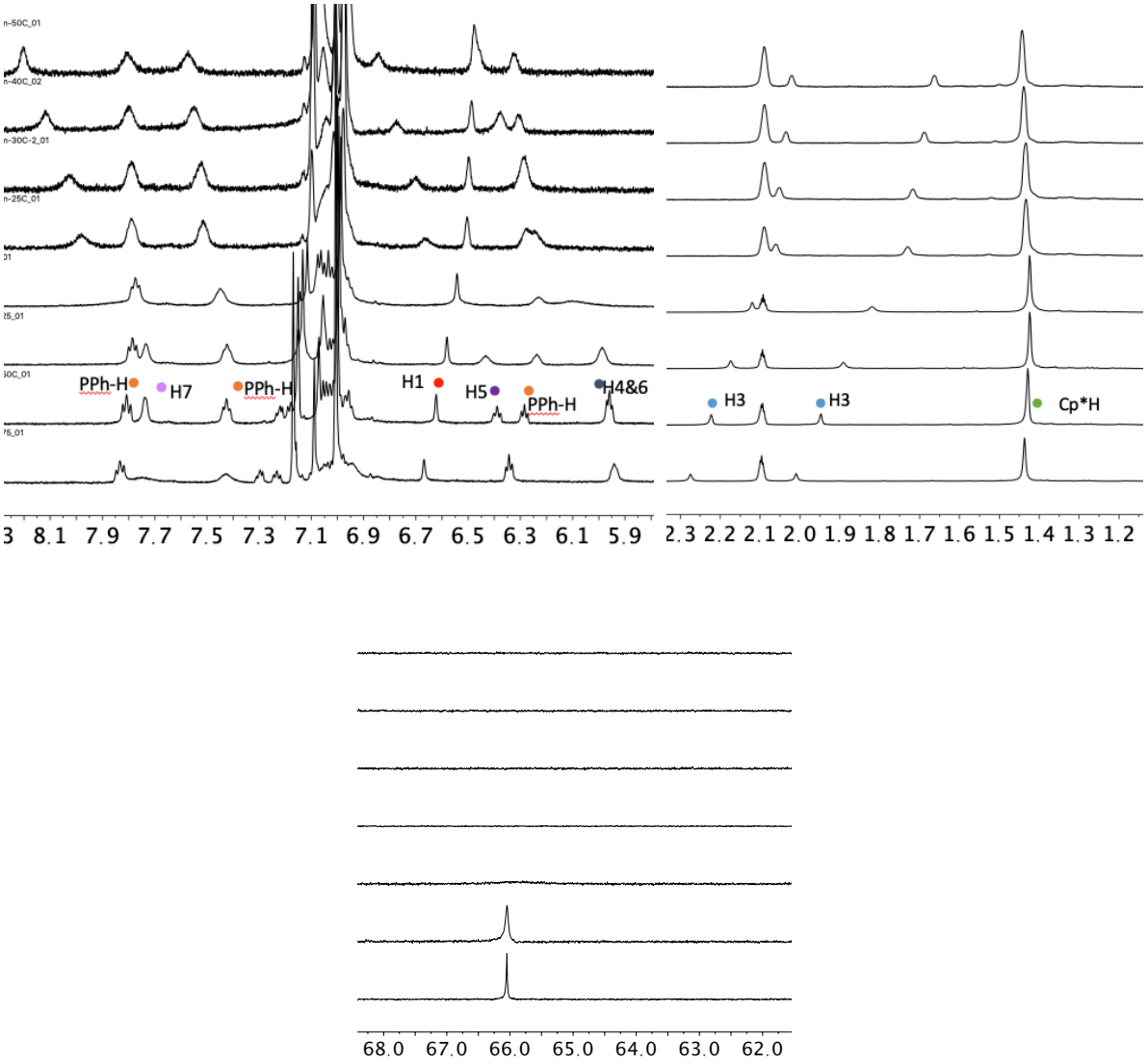

Figure A23: VT ^{1}H (top; 400 MHz) and ^{31}P{^{1}H} (bottom; 243 mHz) NMR spectra of **5** from 50 (top) to –50 (^{31}P{^{1}H} stack plot) or –75 ºC (^{1}H stack plot; bottom) in toluene-*d*$_{8}$*;* Temperatures from top to bottom: 50, 40, 30, 25, 0, –25, –50, and –75 ºC.

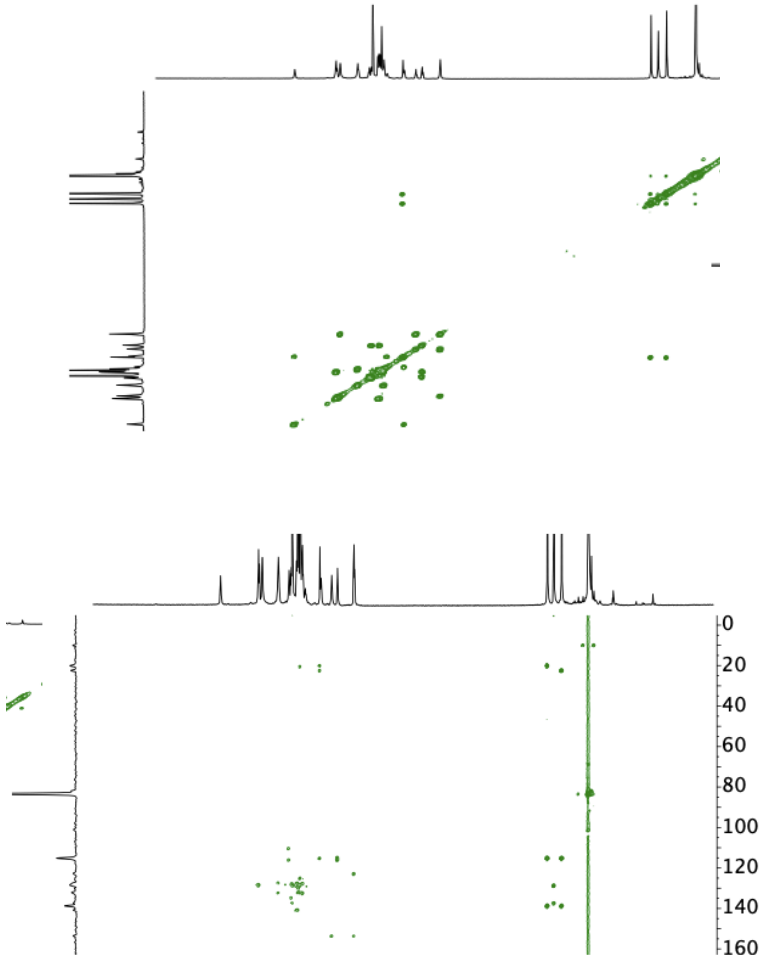

Figure A24: ^{1}H-^{1}H COSY (600 MHz; top) and ^{1}H-^{13}C HMBC (600 and 151 MHz; bottom) of **5** cooled to −50 °C in toluene-d_8 at the NMR spectrometer to yield proposed dimer **18**.

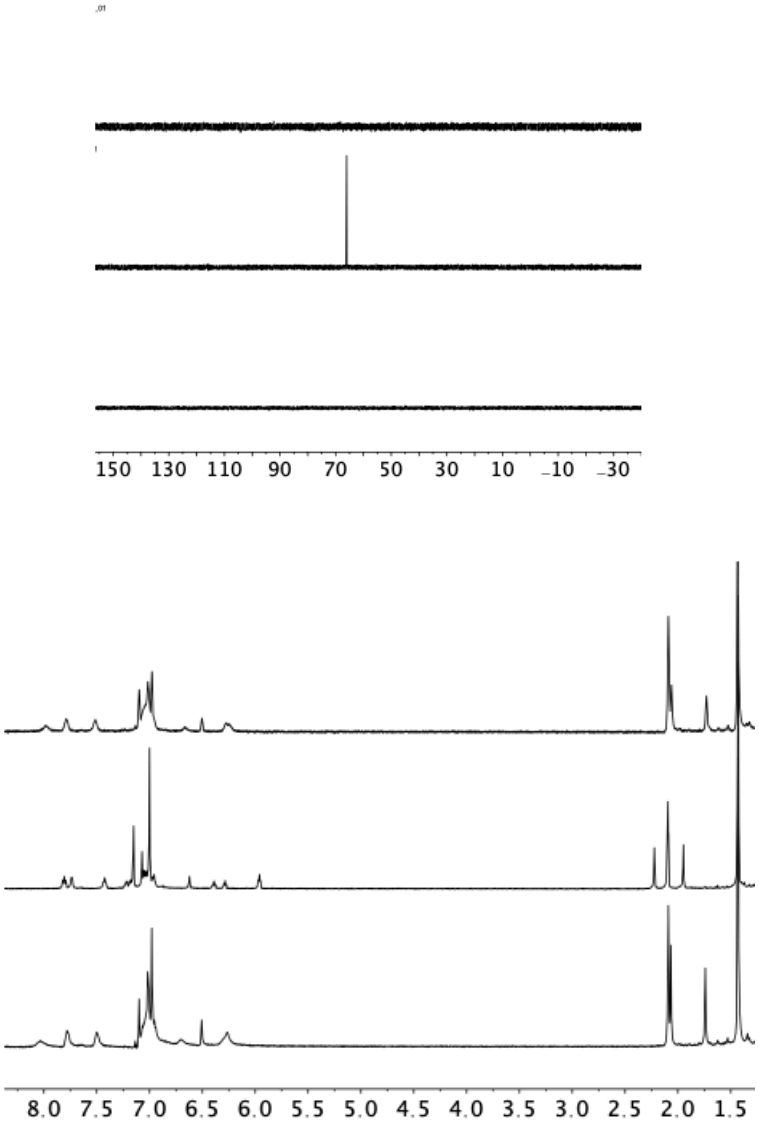

Figure A25: NMR analysis ($^{31}P\{^{1}H\}$ (243 MHz): top three spectra and ^{1}H (600 MHz): bottom three spectra) of **5** at 25 (top), – 50 ºC (middle) and re-warming to 25 ºC (bottom)

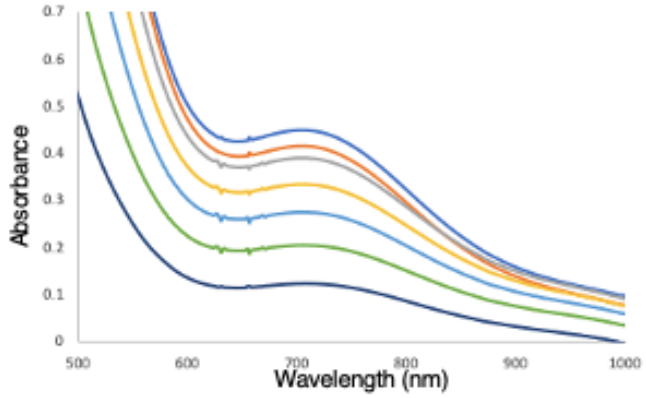
Absorbance
0.7
0.6
0.5
0.4
0.3
0.2
0.1
0
500
600
700
800
900
1000
Wavelength (nm)

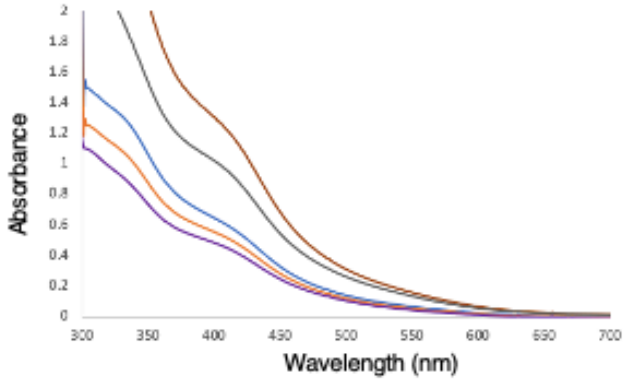
Absorbance
2
1.8
1.6
1.4
1.2
1
0.8
0.6
0.4
0.2
0
300
350
400
450
500
550
600
650
700
Wavelength (nm)

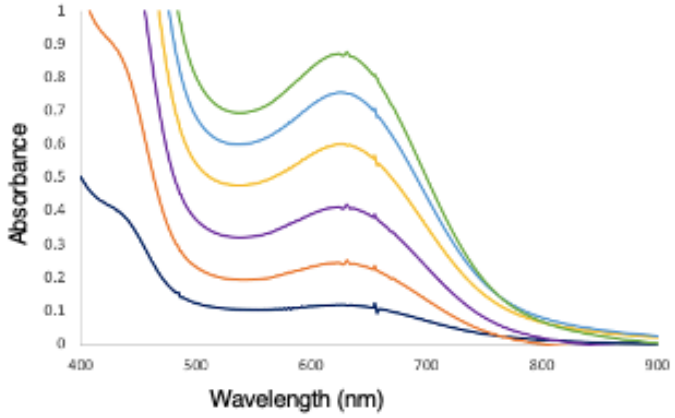
Absorbance
1
0.9
0.8
0.7
0.6
0.5
0.4
0.3
0.2
0.1
0
400
500
600
700
800
900
Wavelength (nm)

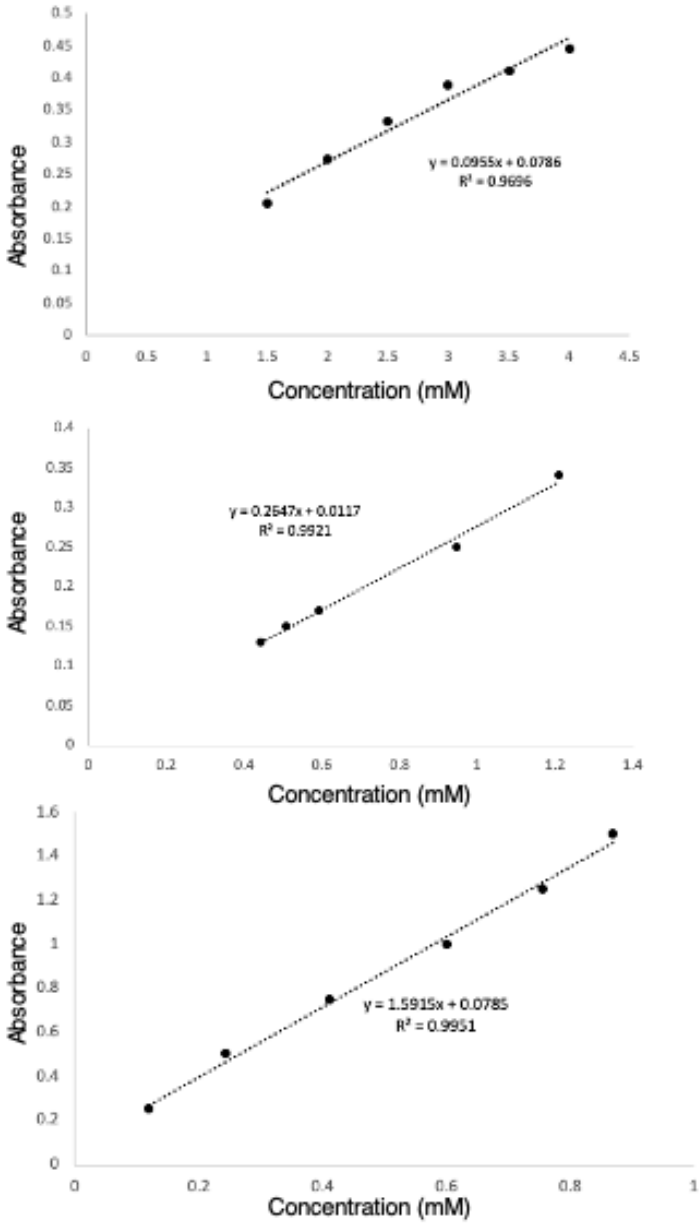

Figure A26: UV-Vis spectra (top coloured spectra) of **7** (top), **8** (middle), **5** (bottom) at various concentrations and corresponding Beer-Lambert plots (bottom).

$$K_{eq} = \frac{[\mathbf{8}]}{[\mathbf{5}][\boldsymbol{py}]} \quad (1)$$

Equation 1: K_{eq} equation describing the reaction of **5** to **8** upon addition of Lewis Base pyridine. Concentrations are in units of mol L^{-1}

$$K_{eq} = \frac{\left(\frac{A}{\varepsilon l}\right)}{[\mathbf{5}][\boldsymbol{py}]} \quad (2)$$

Equation 2: K_{eq} equation describing the reaction of **5** to **8** upon addition of Lewis Base pyridine. Where Beer-Lambert's law (A = εcl) was substituted into [**8**] for a K_{eq} value at 650 nm.[111] Concentrations (c and []) are in units of mol L^{-1}, length (l) is in units of cm, and ε is in units of L mol^{-1} cm^{-1}

$$K_{eq} = \frac{\left(\frac{A}{\varepsilon l}\right)}{\left([\mathbf{5}]_{initial} - \left(\frac{A}{\varepsilon l}\right)\right) * \left([\boldsymbol{py}]_{initial} - \left(\frac{A}{\varepsilon l}\right)\right)} \quad (3)$$

Equation 3: K_{eq} equation describing the reaction of **5** to **8** upon addition of Lewis Base pyridine. Where the equilibrium relationship $[\text{Reactant}]_{eq} = [\text{Reactant}]_{initial} - [\text{Product}]_{eq}$ was substituted into the equation for both $[\mathbf{5}]_{eq}$ and $[\mathbf{8}]_{eq}$.[111] Concentrations (c and []) are in units of mol L^{-1}, length (l) is in units of cm, and ε is in units of L mol^{-1} cm^{-1}.

$$\frac{\text{A}}{[\mathbf{5}]_{initial} * [\boldsymbol{py}]_{initial}} = \frac{A * ([\mathbf{5}]_{initial} + [\boldsymbol{py}]_{initial}) * K_{eq}}{[\mathbf{5}]_{initial} * [\boldsymbol{py}]_{initial}} \quad (4)$$

Equation 4: Equation 3 can be rearranged as shown by Frank Oswalt to equation 4 which can be plotted to give a linear relationship and the slope is the desired K_{eq}.[117] Concentrations (c and []) are in units of mol L^{-1}, length (l) is in units of cm, and ε is in units of L mol^{-1} cm^{-1}.

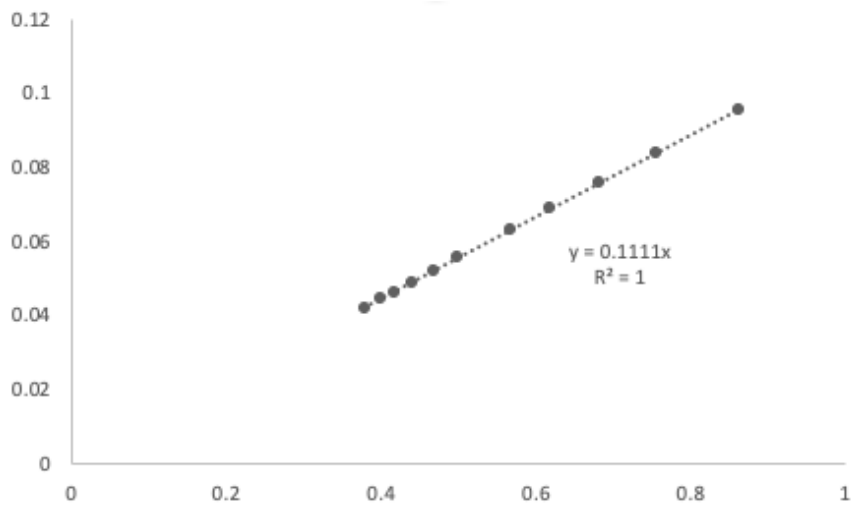

Figure A27: Plot used to calculate K_{eq} of the reaction of **5** with five equivalents of pyridine (**py**) to synthesis **8**. Where the y-axis was defined by y = (A)/([**5**]$_{initial}$ *[**py**]$_{initial}$) and x = ((A)*([**5**]$_{initial}$ + [**py**]$_{initial}$))/([**5**]$_{initial}$ *[**py**]$_{initial}$).[117]Where: A is the absorbance at various equivalents of pyridine used from aquired UV-vis titration data; [**5**]$_{initial}$ = 1.5 mM; [**py**] = 7.5 mM

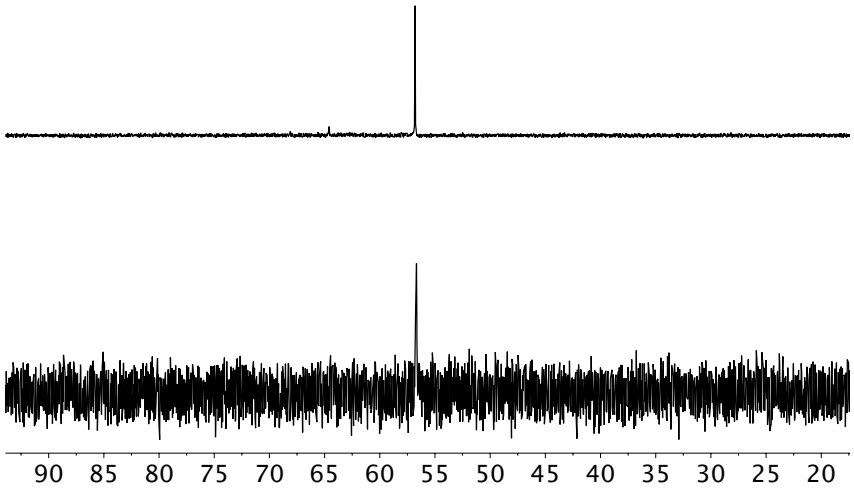

Figure A28: $^{31}P\{^{1}H\}$ NMR spectra (243 MHz) after the addition of phenylacetylene to **5** at room temperature (top) and 60 ºC (bottom) in C_6D_6

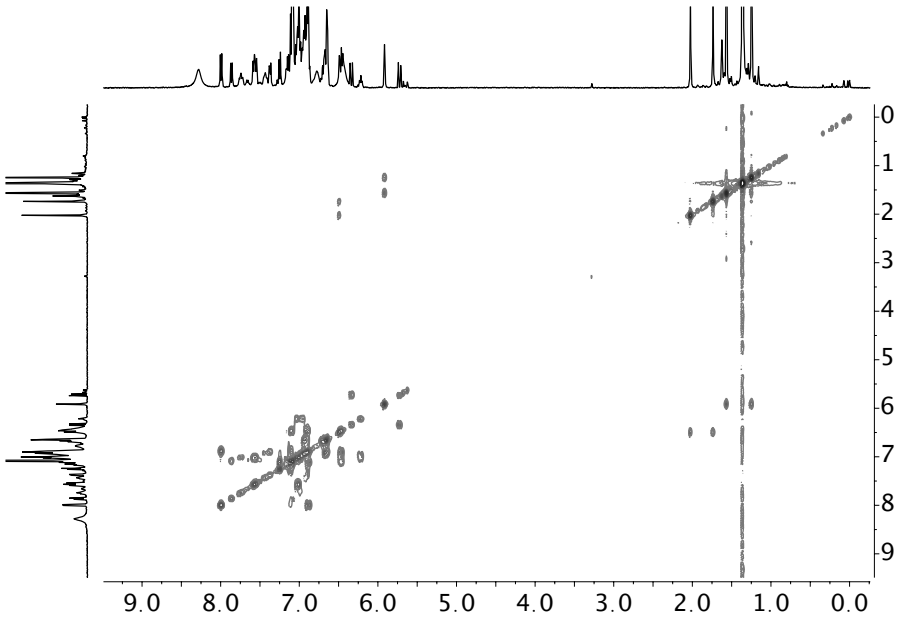

Figure A29: ^{1}H-^{1}H COSY spectrum (400 MHz) after the addition of phenylacetylene to **5** at room temperature in C_6D_6

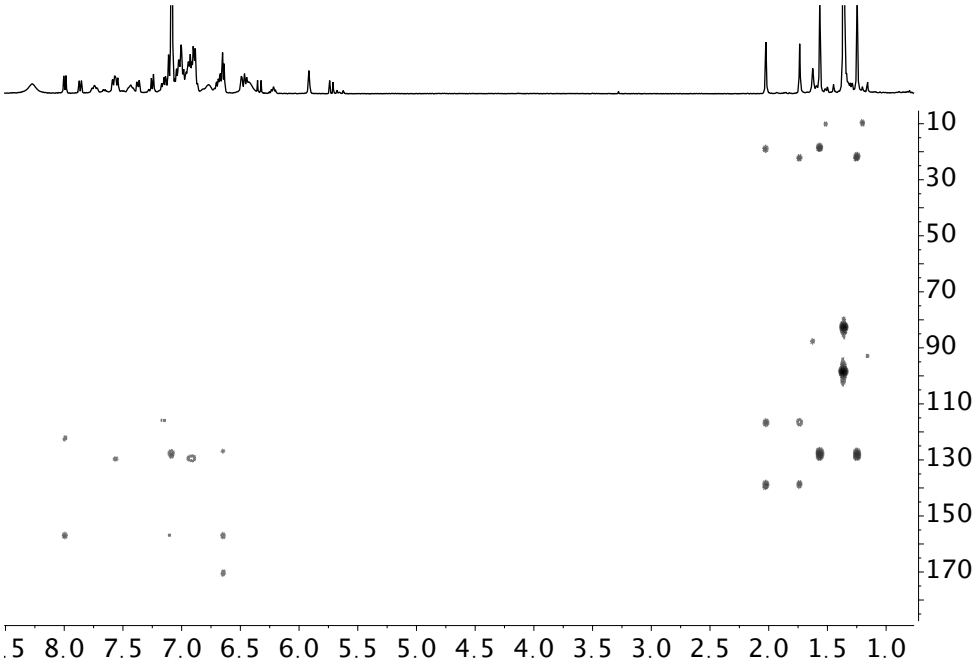

Figure A30: ^{1}H-^{13}C HMBC experiment (400 & 101 MHz) after the addition of phenylacetylene to **5** at room temperature in C_6D_6

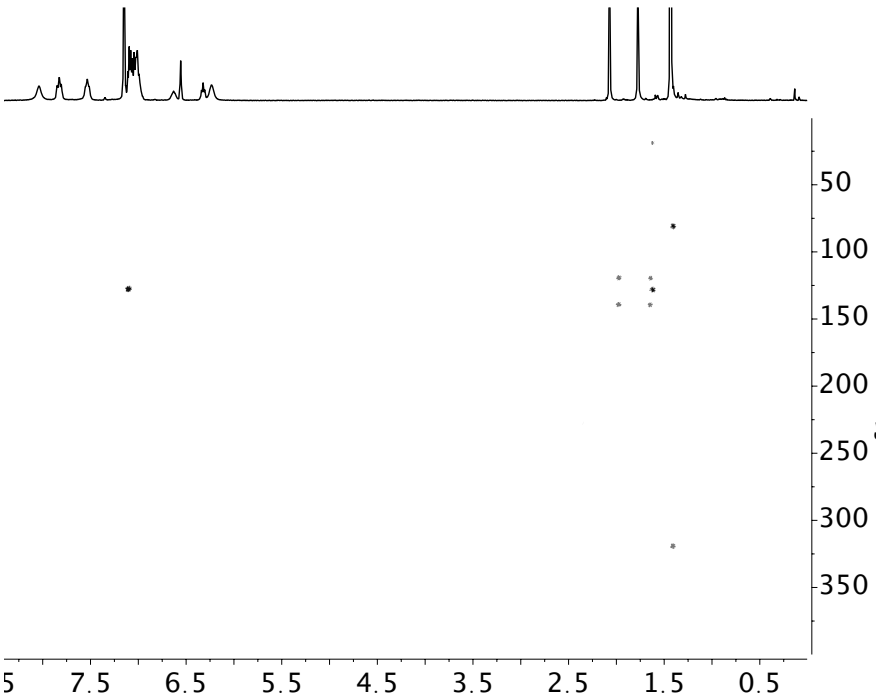

Figure A31: ^{1}H-^{13}C HMBC (600 & 151 MHz) and experiment after the addition of phenylacetylene to **5** at 60 ºC in C_6D_6

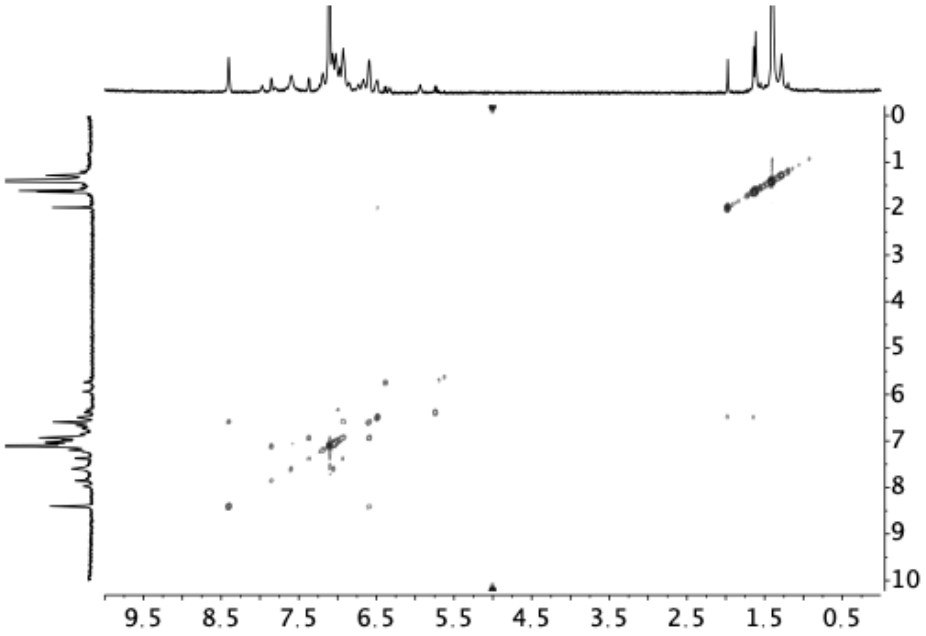

Figure A32: ^{1}H-^{1}H COSY (600 MHz; right) experiment after the addition of phenylacetylene to **5** at 60 ºC in C_6D_6

8 References

1. Hartwig, J.F.; *Organotransition Metal Chemistry: From Bonding to Catalysis.* University Science Books: Sausalito, Calif., 2010; p 539
2. Crabtree, R.H.; *The Organometallic Chemistry of the Transition Metals.* 5th ed.; Wiley: Hoboken, N.J., **2009**; p 225
3. Dach, R.; Song, J. J.; Roschangar, F.; Samstag, W.; Senanayake, C. H., *Org. Process Res. Dev.* **2012**, *16*, 1697
4. Copéret, C.; Chabanas, M.; Petroff Saint-Arroman, R.; Basset, J.-M., *Angew. Chem. Int. Ed.* **2003**, *42*, 156
5. Magano, J.; Dunetz, J. R., *Chem. Rev.* **2011**, *111*, 2177.
6. Grubbs, R. H., *Angew. Chem., Int. Ed.* **2006**, *45*, 3760
7. Vougioukalakis, G.C.; Grubbs, R.H. *Chem. Rev.* **2010**, *110*, 1746.
8. Milani, B.; Licini, G.; Clot, E. Albrecht, M. *Dalton Trans.* **2016**, *45*, 14419.
9. Petersen, A.R.; Taylor, R.A.; Vicente-Hernández, I.; Mallender, P.R.; Olley, H.; White, A.J.P.; Britovsek, G.J.P. *J. Am. Chem. Soc.* **2014**, *136*, 14089.
10. Kärkas, M.D.; Åkermark, B. *Dalton Trans.* **2016**, *45*, 14421.
11. Siemeling, U. *Aust. J. Chem.* **2011**, *64*, 1109.
12. Zhang, W.; Lai, W.; Cao, R. *Chem. Rev.* **2017**, *117*, 3717.
13. Yadav, S.; Saham, S.; Sen, S.S. *ChemCatChem* **2016**, *8*, 486.
14. Boisvert, L.; Goldberg, K.I. *Acc. Chem. Res.* **2012**, *45*, 899.
15. Keith, J.M.; Goddard III, W.A.; *Organometallics* **2012**, *31*, 545.
16. Stahl, S.S. *Angew. Chem.* **2004**, *43*, 3400.
17. Gligorich, K.M.; Sigman, M.S. *Chem. Commun.* **2009**, 3854.
18. Boisvert, L.; Denney, M.C. Hanson, S.K.; Goldberg, K.I. *J. Am. Chem. Soc.* **2009**, *131*, 15802.
19. Zhang, T.; Shen, H.-C.; Xu, J.-C.; Fan, T.; Han, Z.-Y.; Gong, L.-Z; *Org. Lett.* **2009**, *21*, 2048.
20. Toledo, A.; Funes-Ardoiz, I.; Maseras, F.; Albéniz, A.C. *ACS Catal.* **2018**, *8*, 7495.
21. Wang, D.; Weinstein, A.B.; White, P.B.; Stahl, S.S *Chem. Rev.* **2018**, *118*, 2636.
22. Sberegaeva, A.V.; Zavalij, P.Y.; Vedernikov, A.N. *J. Am. Chem. Soc.* **2016**, *138*, 1446.
23. Khunsnutdinova, J.R.; Rath, N.P.; Mirica, L.M. *J. Am. Chem. Soc.* **2012**, *134*, 2414.
24. Taylor, R.A.; Law, D.J.; Sunley, G.J.; White, A.J.P.' Britovsek, G.J.P. *Angew. Chem. Int. Ed.* **2009**, *48*, 5900.
25. Scheuermann, M.L.; Goldberg, K.I. *Chem. Eur. J.* **2014**, *20*, 14556.
26. Zeitler, H.E.; Kamisky, W.A.; Goldberg, K.I. *Organometallics* **2018**, *37*, 3644.
27. Ghorai, D.; Finger, L.H.; Zanoni, G.; Ackermann, L. *ACS Catal.* **2018**, *8*, 11657.
28. Siedschlag, R.B.; Bernales, V.; Vogiatzis, K.D.; Planas, N.; Clouston, L.J.; Bill, E.; Gagliardi, L.; Lu, C.C. *J. Am. Chem. Soc.* **2015**, *137*, 4638.
29. Jiang, X.-F.; Huang, H.; Chai, Y.-F.; Lohr, T.L.; Yu, S.-Y.; Lai, W.; Pan, Y.-J.; Delferro, M.; Marks, T.J. *Nature Chem.* **2017**, *9*, 188.
30. Uyeda, C.; Peters, J.C. *J. Am. Chem. Soc.* **2013**, *135*, 12023.
31. Chuang, G.J.; Wang, W.; Lee, E.; Ritter, T. *J. Am. Chem. Soc*. **2011**, 133, 1760.
32. Haines, B.E.; Berry, J.F.; Yu, J.-Q.; Musaev, D.G. *ACS Catal.* **2016**, *6*, 829.
33. Pye, D.R.; Mankad, N.P. *Chem. Sci.* **2017**, *8*, 1705.
34. Aullón, G.; Ujaque, G.; Lledós, A.; Alvarez, S. *Chem. Eur. J.* **1999**, *5*, 1391.

35. Kubas, G.J. *Chem. Rev.* **2007**, *107*, 4152.
36. Li, Y.; Hou, C.; Jiang, J.; Zhang, Z.; Zhao, C.; Page, A.J.; Ke. Z. *ACS Catal.* **2016**, *6*, 1655.
37. Bartmess, J.E.; Scott, J.A.; McIver Jr., R.T. *J. Am. Chem. Soc.* **1976**, *101*, 6046.
38. Li, Y.; Liu, J.; Huang, X.; Qu, L.-B.; Zhao, C.; Langer, R.; Ke, Z. *Chem. Eur. J.* **2019**, *25*, 13785.
39. Costa, M.; Pelagatti, P.; Pelizzi, C.; Rogolino, D. *J. Mol. Catal. A: Chem.* **2002**, *178*, 21.
40. Strukul, G.; Carturan, G. *J. Organomet. Chem.* **1978**, *157*, 475.
41. Bailey, W.D.; Phearman, A.S.; Luconi, L.; Rossin, A.; Yakhvarov, D.G.; D'Accolti, L.; Flowers, S.E.; Kaminsky, W.; Kemp, R.A.; Giambastiani, G.; Goldberg, K.I. *Chem. Eur. J.* **2019**, *25*, 1.
42. Tshabalala, T.A.; Ojwach, S.O. *J. Organomet. Chem.* **2018**, *873*, 35.
43. Ojwach, S.O.; Ogweno, A.O.; Akerman, M.P. *Catal. Sci. Technol.* **2016**, *6*, 5069.
44. Voronova, K.; Purgel, M.; Udvardy, A.; Bényei, A.C.; Kathó, Á. *Organometallics* **2013**, *32*, 4391.
45. Anastas, P.; Eghbali, N. *Chem. Soc. Rev.* **2010**, *39,* 301.
46. Crabtree, R. H. Multifunctional Ligands In Transition Metal Catalysis. *New J. Chem.* **2011**, *35*, 18.
47. Dobereiner, G. E.; Crabtree, R. H. *Chem. Rev.* **2010**, *110*, 681.
48. Cook, S. A.; Borovik, A. S., *Acc. Chem. Res.* **2015**, *48*, 2407.
49. Khunsnutdinova, J.R.; Milstein, D. *Angew. Chem. Int. Ed.* **2015**, *42*, 12236.
50. DuBois, D. L.; Bullock, R. M., *Eur. J. Inorg. Chem.* **2011**, *2011*, 1017.
51. Bullock, R. M.; Appel, A. M.; Helm, M. L., *Chem. Commun.* **2014**, *50*, 3125.
52. Grotjahn, D. B., *Top. Catal.* **2010**, *53*, 1009.
53. Grotjahn, D. B.; Incarvito, C. D.; Rheingold, A. L., *Angew. Chem. Int. Ed.* **2001**, *40*, 3884.
54. Sues, P. E.; Demmans, K. Z.; Morris, R. H., *Dalton Trans.* **2014**, *43*, 7650.
55. Camara, J.M.; Rauchfuss, T.B. *Nat. Chem.,* **2012**, *4*, 26.
56. Housecroft, C.E.; Sharpe, A.G. *Inorganic Chemistry*; Pearson: Harlow, **2012**. pgs: 231,887
57. Braunstein, P.; Naud, F. *Angew. Chem. Int. Ed.* **2001**, *40*, 680.
58. Trost, B.M.; Ryan, M.C. *Angew. Chem. Int. Ed.* **2017**, *56*, 2862.
59. Davies, D.L.; Macgregor, S.A.; McMullin, C.L. *Chem. Rev.* **2017**, *117*, 8649.
60. Annibale, V.T.; Song, D. *RSC Advances* **2013**, *3*, 11432.
61. Fulmer, G.R.; Kaminsky, W.; Kemp, R.A.; Goldberg, K.I. *Organometallics* **2011**, *30*, 1627.
62. Materne, K.; Braun-Cula, B.; Herwig, C.; Frank, N.; Limberg, C. *Chem .Eur. J.* **2017**, *23*, 11797.
63. Kang, Q.-K.; Lin, Y.; Li, Y.; Shi, H. *J. Am. Chem. Soc.* **2020**, *142*, 3706.
64. Paulson, E.R.; Moore, C.E.; Rheingold, A.L.; Pullman, D.P.; Sindewald, R.W.; Cooksy, A.L.; Grotjahn, D.B. *ACS Catal.* **2019**, *9*, 7217.
65. Larsen, C.R.; Erdogan, G.; Grotjahn, D.B. *J. Am. Chem. Soc.* **2014**, *136*, 1226.
66. Caro, C.F.; Lappert, M.F.; Merle, P.G. *Coord. Chem. Rev,* **2001**, *219-221*, 605.
67. Avent, A.G.; Hitchcook, P.B.; Lappert, M.F.; Sablong, R.; Severn, J.R. *Organometallics* **2004**, *23*, 2591.
68. Adams, G.M.; Weller, A.S.; *Coord. Chem. Rev.* **2018**, *355*, 150.

69. Grüzmacher, H. *Angew. Chem. Int. Ed.* **2008**, *47*, 1814.
70. Jackman, K.M.K.; Fogh, A.A.; Stubbs, J.M.; Blacquiere, J.M. *J. Organomet. Chem.* **2019**, *880*, 56.
71. Jackman, K.M.K.; Bridge, B.J.; Sauvé, E.R.; Rowley, C.N.; Zheng, C.H.M.; Stubbs, J.M.; Boyle, P.D.; Blacquiere, J.M. *Organometallics* **2019**, *38*, 1677.
72. Stubbs, J.M.; Firth, K.F.; Bridge, B.J.; Berger, K.J.; Hazlehurst, R.J.; Boyle, P.D.; Blacquiere, J.M. *Dalton Trans.* **2017**, *46*, 647.
73. Lim, L. Synthesis of a "Low Coordinate" Ruthenium Catalyst. 4491 Thesis, Western University, London, ON, **2019**.
74. Boudier, A.; Breuil, P.-A.,R. *J. Organomet. Chem.* **2012**, *718*, 31.
75. Prathihar, S.; Pegu, R.; Guha, A.K.; Sarma, B. *Dalton Trans*. **2014**, *43*, 17136.
76. Byers, P.K.; Canty, A.J.; Jin, H.; Kruis, D.; Markies, B.A.; Boersma, J.; Van Koten, G. *Inorganic Syntheses* **1998**, *32*, 162.
77. Salo, E.V.; Guan, Z. *Inorg. Chem*. **2003**, *22*, 5033.
78. Jones, I. C. *Magn. Reson. Chem.* **2005**, *43*, 497.
79. Chénard, E.; Sutrisno, A.; Zhu, L.; Assary, S.R.; Kowalski, J.A.; Barton, J.L.; Bertke, J.A.; Gray, D.L.; Brushett, F.R; Curtiss, L.A.; Moore, J.S. *J. Phys. Chem. C* **2016**, *120*, 8461.
80. K. Izutsu, *Acid-Base Dissociation Constants in Dipolar Aprotic Solvents*, Blackwell Scientific, Oxford, UK, 1990.
81. Broadwell, F.G. McCallum, R.J.; Olmstead, W.N. *J. Org. Chem.* **1984**, *45*, 1424.
82. *Reagent chemicals: specifications and procedures for reagents and standard-grade reference materials*; Part 4; American Chemical Society: Washington, DC, 2017.
83. Costa, M.; Pelagatti, P.; Pelizzi, C.; Rogolino, D. *J. Mol. Catal. A: Chem.* **2002**, *178*, 21.
84. Strukul, G.; Carturan, G. *J. Organomet. Chem.* **1978**, *157*, 475.
85. Bailey, W.D.; Phearman, A.S.; Luconi, L.; Rossin, A.; Yakhvarov, D.G.; D'Accolti, L.; Flowers, S.E.; Kaminsky, W.; Kemp, R.A.; Giambastiani, G.; Goldberg, K.I. *Chem. Eur. J.* **2019**, *25*, 1.
86. Tshabalala, T.A.; Ojwach, S.O. *J. Organomet. Chem.* **2018**, *873*, 35.
87. Ojwach, S.O.; Ogweno, A.O.; Akerman, M.P. *Catal. Sci. Technol.* **2016**, *6*, 5069.
88. Voronova, K.; Purgel, M.; Udvardy, A.; Bényei, A.C.; Kathó, Á. *Organometallics* **2013**, *32*, 4391.
89. Morokuma, K.; Koga, N. *J. Am. Chem. Soc.* **1985**, *107*, 7230.
90. Lemenovskii, D.A.; Babin, Y.V.; Simonyan, V.V.; Gloriozov, I.P.; Mamaev, V.M. *Mendeleev Commun.* **2000**, *10*, 155.
91. Su, M.-D.; Chu, S.-Y. *Inorg. Chem.* **1998**, *37*, 3400.
92. Denney, M.C.; Smythe, N.A.; Cetto, K.L.; Kemp, R.A.; Goldberg, K.I. *J. Am. Chem. Soc.* **2006**, *128*, 2508.
93. Decharin, N.; Stahl, S.S. *J. Am. Chem. Soc.* **2011**, *133*, 5732.
94. Wasserman, H.H.; Han, W.T. *Tetrahedron Lett.* **1984**, *25*, 3747.
95. Wasserman, H.H.; Ives, J.L. *J. Am. Chem. Soc.* **1976**, *98*, 7868.
96. Wasserman, H.H.; Ives, J.L. *J. Org. Chem.* **1978**, *43*, 3238.
97. Wasserman, H.H.; Han, W.T. *Tetrahedron Lett.* **1984**, *25*, 3238.
98. Wasserman, H.H.; Terao,S. *Tetrahedron Lett.* **1975**, *21*, 1735.
99. Zhou, X.; :Lau, K.-C.; Petro, B.J.; Jordan, R.F. *Organometallics* **2014**, *33*, 7209.
100. Contrella, N.D.; Sampson, J.R.; Jordan, R.F.; *Organometallics* **2014**, *33*, 3546.

101. Kochi, T.; Noda, S.; Yoshimura, K.; Nozaki, K. *J. Am. Chem. Soc.* **2007**, *129*, 8948.
102. Huacuja, R.; Graham, D.J.; Fafard, C.M.; Chen, C.-H.; Foxman, B.M.; Herbert, D.E.; Alliger, G.; Thomas, C.M.; Ozerov, O.V. *J. Am. Chem. Soc.* **2011**, *133*, 3820.
103. Smoll, K.A.; Kaminsky, W.; Goldberg, K.I. *Organometallics* **2017**, *36*, 1213.
104. Lukin, K.; Kishore, V; Gordon, T. *Org. Process Res. Dev.* **2013**, *17*, 666.
105. Nascimento, D.L.; Fogg, D.E.; Davy, E.C. *Catal*. *Sci. Technol.*, **2018**, *8*, 1535.
106. Lipshutz, B.H.; Blomgren, P.A. *Org. Lett.* **2001**, *3*, 1869.
107. Patiny, L.; Borel, A. *J. Chem. Inf. Model.* **2013**, *53*, 1223.
108. Pregosin, P.S. *NMR in Organometallic Chemistry*: Wiley-VCH: Weinham, Germany, 2012; pp 280.
109. Atkins, P.W.; Paula, J.D. *Atkins Physical Chemistry*, 10th Ed.: Oxford University Press: Oxford UK, 2014; pp 256.
110. Meek, S.J.; Pitman, C.L.; Miller, A.J.M. *J. Chem. Educ.* **2016**, *93*, 275.
111. Friedrich, A.; Drees, M.; Käss, M.; Herdtweck, E.; Schneider, S. *Inorg. Chem.* **2010**, *49*, 5482.
112. Avent, A. G.; Hitchcock, P. B.; Lappert, M. F.; Sablong, R.; Severn, J. R. *Organometallics* **2004**, *23*, 2591.
113. Wambach, T. C.; Fryzuk, M. D. *Inorg. Chem.* **2015**, *54*, 5888.
114. Fogler, E.; Garg, J. A.; Hu, P.; Leitus, G.; Shimon, L. J. W.; Milstein, D. *Chem. Eur. J.* **2014**, *20*, 15727.
115. B. Hitchcock, P.; F. Lappert, M.; Layh, M. *J. Chem. Soc.*, *Dalton Trans.* **1998**, 1619.
116. Weller, M. T.; Young, N.A. *Characterisation Methods in Inorganic Chemistry*: Oxford University Press: Oxford UK, 2017; pp 164.
117. Frank, H.S.; Oswalt, R.L. *J. Am. Chem. Soc.* **1947**, *69*, 1321.
118. Chang, R.; Goldsby, K.A. *Chemistry* 11th edition: MgGraw-Hill Companies: New York US, 2013
119. Lamberti, M; Forman, G.C.; Poater, A.; Broggi, J.; Slawin, A.M.Z.; Cavallo, L.; Nolan, S.P. *Organometallics* **2012**, *31*, 756.
120. Ríos, I. d.l.; Tenorio, M.J.; Puerta, C.; Valerga, P. *J. Am. Chem. Soc.* **1997**, *119*, 6529.
121. Zeng, M.; Herzon, S.B. *J. Am. Chem. Soc.* **2004**, *136*, 7058.
122. Pati, K.; Liu, R.-S. *Chem. Commun.* **2009**, *35*, 5233.
123. Scherer, A.; Mukherjee, T.; Hampel, F.; Gladysz, J.A.; *Organometallics* **2014**, *33*, 6709.
124. Jasper Jr., S.A.; Jones, R.B.; Mattern, J.; Huffman, J. C.; Todd, L.J. *Inorg. Chem.* **1994**, *33*, 5620.
125. Boudier, A.; Breuil, P.-A.,R. J. *Organomet. Chem.* **2012**, *718*, 31.
126. Bruker-AXS, SAINT version 2013.8, **2013**, Bruker-AXS, Madison, WI 53711, USA
127. Bruker-AXS, SADABS version 2012.1, **2012**, Bruker-AXS, Madison, WI 53711, USA
128. Sheldrick, G. M., *Acta Cryst.* **2015**, *A71*, 3.
129. Sheldrick, G. M., *Acta Cryst.* **2015**, *C71*, 3.

130. Macrae, C. F.; Bruno, I. J.; Chisholm, J. A.; Edington, P. R.; McCabe, P.; Pidcock, E.; Rodriguez-Monge, L.; Taylor, R.; van de Streek, J. and Wood, P. A. *J. Appl. Cryst.*, **2008**, *41*, 466.

9 CV

Meagan B. Kindervater

Education

Mount Allison University Sackville, NB
Bachelor of Science in Chemistry
First Class Honours with Distinction January 2015 – May 2018

Honours and Awards

NSERC Undergraduate Summer Research Award	2018
Mount Allison University Dean's List	2018
Teaching Assistant of the Month at Mount Allison University	2018
ISRG Undergraduate Summer Research Award	2017
Swadon Award	2016 - 2017
Mount Allison University Dean's List	2016 - 2017

Research Experience

Organic/Organometallic Synthesis

- ***Graduate Student, Supervisor: J.M. Blacquiere*** September 2018 – 2020
  - Conducted experimental research investigating the coordination chemistry of a structurally responsive phosphine 1-azaallyl ligand to Ru and Pd for small-molecule activation and potential catalytic applications.
  - Conducted preliminary reactivity studies of a Pd(II) dimer with small molecules (O_2, H_2, and various E-H compounds).
  - Synthesized and characterised a Ru-phosphine imine and a Ru-phosphine 1-azaallyl complex. Initial reaction studies with Ru-phosphine 1-azaallyl complex and phenylacetylene were performed.

- ***Research Assistant, Supervisor: SA Westcott*** October 2016 – August 2018
  - Conducted experimental research investigating the synthesis and biological reactivity of novel Schiff-base compounds derived from ortho-vanillin and sulfachloropyridazine.
  - Investigated the synthesis of novel 3-hydroxy-4-pyridinone ligands (derived from maltol/ethyl-maltol and 4/5-ASA) and their corresponding gallium(III) complexes to test their biological reactivity.
  - Investigated the synthesis of phosphinoborylated amibiphilic ligands (derived from heteroatom-containing aldehydes or aldimines and Ph_2PBpin) and explored their coordination to various transition metals (Pt and Pd).

- ***Research Assistant, Supervisor: G Briand*** January – April 2018
  - Conducted experimental research investigating the synthesis of a polydentate ONS carboxylate-thiolate ligand derived from sarcosine methyl ester hydrochloride and ethylene sulfide for coordination to bismuth.

Publications

- Kindervater, M.B.; Binder, J.F.; Baird, S.R.; Vogels, C.M.; Geier, S.J.; Macdonald, C.L.B.; Westcott, S.A. *J. Organomet. Chem.* **2019**, *880*, 378-385.

Conference Abstracts and Presentations

Presentations delivered by underlined author.
PP= Poster Presentation, OP= Oral Presentation

1(PP). 'Synthesis of Novel 3,4-Hydroxypyridinones From 4-Aminosalicylic Acid and Their Corresponding Gallium Complexes' Meagan B. Kindervater, Christopher M. Vogels, Stephen A. Westcott. 43rd Annual Science Atlantic/CIC Student Chemistry Conference, Halifax, NS, June 2018.

2(PP). 'Reactivity of a Pd(II) Phosphine-Azaallyl Complex' Meagan B. Kindervater and Johanna M. Blacquiere. 102nd Canadian Chemistry Conference and Exhibition, Quebec City, QC, June 2019.

Employment

Teaching Assistant – Western University September 2018 – April 2020

- In-Lab TA – Organic for Life Sciences I and Introductory Chemistry II
- Resource Room TA – Introductory Chemistry II

Teaching Assistant – Mount Allison University September 2016 – April 2018

- In-Lab TA –Introductory Chemistry I, Analytical I, and Intermediate Organic Chemistry
- Resource Room TA – Introductory Chemistry I

Volunteer Experience

Laboratory Assistant – Western University September 2018 – April 2020
Supervised laboratory activities for multiple outreach events: 78 high school students who performed an equilibrium experiment; 40 high school students who performed an electrochemistry experiment; and assisted 30 grade school students to make slime.